Geometric singular perturbation analysis of systems with friction

Bossolini, Elena

Publication date:
2018

Document Version
Publisher's PDF, also known as Version of record

Geometric singular perturbation analysis of systems with friction

Elena Bossolini

Kongens Lyngby 2017
14 October

Technical University of Denmark
Department of Applied Mathematics and Computer Science
Richard Petersens Plads, building 324,
2800 Kongens Lyngby, Denmark
Phone +45 4525 3031
compute@compute.dtu.dk
www.compute.dtu.dk

Summary

This thesis is concerned with the application of geometric singular perturbation theory to mechanical systems with friction. The mathematical background on geometric singular perturbation theory, on the blow-up method, on non-smooth dynamical systems and on regularization is presented. Thereafter, two mechanical problems with two different formulations of the friction force are introduced and analysed.

The first mechanical problem is a one-dimensional spring-block model describing earthquake faulting. The dynamics of earthquakes is naturally a multiple timescale problem: the timescale of earthquake ruptures is very short, when compared to the time interval between two consecutive ruptures. We identify a small parameter ε that describes the separation between the timescales, so that $\varepsilon = 0$ idealises the complete timescale separation. Earthquake faulting problems also have multiple spatial scales. The action of friction is generally explained as the loss and restoration of linkages between the surface asperities at the molecular scale. However, the consequences of friction are noticeable at much larger scales, like hundreds of kilometers.
By using geometric singular perturbation theory and the blow-up method, we provide a detailed description of the periodicity of the earthquake episodes. In particular, we show that attracting limit cycles arise from a degenerate Hopf bifurcation, whose degeneracy is due to an underlying Hamiltonian structure that leads to large amplitude oscillations. We use a Poincaré compactification to study the system near infinity. At infinity, the critical manifold loses hyperbolicity with an exponential rate. We use an adaptation of the blow-up method to recover the hyperbolicity. This enables the identification of a new attracting manifold, that organises the dynamics at infinity for $\varepsilon = 0$. This in turn leads to the formulation of a conjecture on the behaviour of the limit cycles as the

timescale separation increases for $0 < \varepsilon \ll 1$. We illustrate our findings with numerics, and outline the proof of the conjecture. We also discuss how our results can be used to study a similar class of problems.

The second mechanical problem is a friction oscillator subject to stiction. The vector field of this discontinuous model does not follow the Filippov convention, and the concept of Filippov solutions cannot be used. Furthermore, some Carathéodory solutions are unphysical. Therefore, we introduce the concept of stiction solutions: these are the Carathéodory solutions that are physically relevant, i.e. the ones that follow the stiction law. However, we find that some of the stiction solutions are forward nonunique in subregions of the slip onset. We call these solutions singular, in contrast to the regular stiction solutions that are forward unique. In order to further the understanding of the nonunique dynamics, we introduce a regularization of the model. This gives a singularly perturbed problem that captures the main features of the original discontinuous problem. We identify a repelling slow manifold that separates the forward slipping to forward sticking solutions, leading to a high sensitivity to the initial conditions. On this slow manifold we find canard trajectories, that have the physical interpretation of delaying the slip onset. We show numerically that the regularized problem has a family of periodic orbits interacting with the canards. We observe that this family is unstable of saddle type and that it connects, in the rigid body limit, the two regular, slip-stick branches of the discontinuous problem, that were otherwise disconnected.

Resumé

I denne afhandling anvendes geometrisk singulær perturbationsteori til at studere mekaniske systemer med friktion. Den nødvendige matematiske baggrund inden for geometrisk singulær perturbationsteori, blow-up metoden, ikke-glatte dynamiske systemer samt regularisering bliver gennemgået. Herefter bliver to mekaniske problemer med forskellige modeller for friktionskraften introduceret og analyseret.

Det første mekaniske system er en en-dimensional fjeder-masse model, der beskriver dynamikken af forkastninger under et jordskælv. Dynamikken af jordskælv har naturligt to tidsskalaer: tidsskalaen for bevægelsen under jordskælvet er meget kort sammenlignet med tidsskalaen mellem jordskælv. Desuden har jordskælv multiple rumlige skalaer: mens forkastingen kan være hundrede af kilometer lang, skyldes jordskælvet brud på bindinger mellem de ru overflader på en molekulær skala. Vi identificerer en lille parameter ε som beskriver separationen mellem tidsskalaerne, så $\varepsilon = 0$ idealiserer deres fuldstændige separation. Ved hjælp af geometrisk singulær perturbationsteori og blow-up metoden giver vi en detaljeret beskrivelse af den periodiske dynamik af jordskælvsepisoder. Vi viser, at tiltrækkende grænsecykler opstår i en degenereret Hopf bifurkation, hvor degenerationen skyldes en underliggende Hamiltonstruktur, der giver anledning til svingninger med stor amplitude. Vi benytter en Poincaré kompaktifikation til at studere systemet i nærheden af uendelig. I det uendelige mister den kritiske mangfoldighed hyperbolicitet med en eksponentiel rate. Vi benytter en tilpasning af blow-up metoden til at genvinde hyperbolicitet. Dette muliggør bestemmelsen af en ny tiltrækkende mangfoldighed som organiserer dynamikken i uendelig for $\varepsilon = 0$. Dette leder til formuleringen af en formodning om opførslen af grænsecyklerne når tidsskala-separation forøges for $0 < \varepsilon \ll 1$. Vi illustrerer resultaterne numerisk, og opridser et bevis for formodningen. Endvidere disku-

terer vi hvordan vore resultater kan bruges til at studere en lignende klasse af modeller.

Det andet mekaniske problem er en friktionsoscillator modelleret med 'stiction' friktion. Vektorfeltet for denne diskontinuerte model følger ikke Fillipovkonventionen, og begrebet Fillipovløsning kan ikke anvendes. Desuden er visse Carathéodoryløsninger ufysiske. Derfor indfører vi begrebet stiction-løsning: dette er de Carathéodoryløsninger, der er fysisk relevante, dvs. dem der følger stictionforskriften. Vi finder, at nogle af stiction-løsningerne ikke er entydige i forlæns tid i visse områder hvor slippet begynder. Vi kalder disse løsninger singulære, i modsætning til de regulære løsninger, der er entydige i forlæns tid. For bedre at forstå den flertydige dynamik indfører vi en regularisering af modellen. Dette giver et singulært perturbationsproblem, der fanger de væsentligste egenskaber af den oprindelige diskontinuerte model. Vi identificerer en frastødende langsom mangfoldighed som separerer de løsninger der i forlæns tid hæfter, fra dem der slipper, og denne giver anledning til stor følsomhed på begyndelsesbetingelserne. På den langsomme mangfoldighed finder vi canard-løsninger, hvis fysiske fortolkning er en forsinkelse af slip. Vi viser numerisk at det regulariserede problem har en familie af periodiske løsninger som vekselvirker med canard-løsningerne. Vi observerer at denne familie er ustabil af sadeltype, og at den forbinder de to regulære grene af løsninger med både hæftning og slip i den diskontinuerte model, der elles var uforbundne.

Preface

This thesis was prepared at the Department of Mathematics and Computer Science (DTU Compute) of the Technical University of Denmark in fulfilment of the requirements for acquiring a Ph.D. degree. The research described herein was conducted under the supervision of Professor Morten Brøns and Associate Professor Kristian Uldall Kristiansen at DTU Compute, between October 2014 and October 2017. The work is to the best of my knowledge original, except where acknowledgments and references are made to previous work.

Part of this work has been presented in the following publications:
– E. Bossolini, M. Brøns, and K. U. Kristiansen. Singular limit analysis of a model for earthquake faulting. *Nonlinearity*, 30(7):2805-2834, 2017.
– E. Bossolini, M. Brøns, and K. U. Kristiansen. Canards in stiction: On solutions of a friction oscillator by regularization. *SIAM Journal on Applied Dynamical Systems*, 16(4):2233-2258, 2017.

My participation to the Intensive Research Program in Non-smooth Dynamical Systems in Barcelona has been partially supported by the Idella foundation and by the Intensive Research Program itself. My participation to SIAM DS15 and SIAM DS17 has been partially supported by the Otto Mønsted foundation and by the SIAM Student Travel Award, respectively.

Lyngby, 14 October-2017

Elena Bossolini

Acknowledgements

Considerate la vostra semenza:
fatti non foste a vivere come bruti,
ma per seguir virtute e canoscenza.

Call to mind from whence ye sprang:
Ye were not form'd to live the life of brutes,
But virtue to pursue and knowledge high.

– Dante Alighieri, canto xxvi 118-120

This thesis would not be here without the support of my two supervisors: Morten Brøns and Kristian Uldall Kristiansen, who taught me the rigour, the precision and the logic that is necessary to have, in order to solve difficult problems analytically. Thanks to you, I have learnt the basics of the profession of the dynamicist. I thank you for motivating and encouraging me, and for your patience when I did not understand things at the first or second time. I particularly thank you Kristian, for the passion that you have put in supervising me.
I am grateful to have met many special people during the last three years, who have inspired my work.
I thank Mike R. Jeffrey, Tomás Lázaro, Josep M. Olm, Alessandro Colombo, Paul Glendinning and Gerard O. Tost for taking care of me during the Intensive Research Program on Non-smooth Dynamical Systems in Barcelona. Seeing you in the action of understanding new and complicated problems has been a great source of inspiration. I thank Simon Webber and Eoghan Staunton for the beers and the discussions that we have had during this period.
I thank Thibaut Putelat for introducing me to his point of view on rate-and-state friction models, and for helping me with my computations in AUTO while in Barcelona. I also thank the Danish company Roulunds Braking for showing us the problem of the one-dimensional spring-block problem, that has turned out to be the main focus of my research.

These three years at DTU Compute have been an unforgettable experience. I have been sharing the office with two special girls, Nürdagul and Marzieh. I thank you Nürdagul, for bringing happiness and energy in our office everyday. You are an example of perseverance and motivation in mathematics. Marzieh, I am glad that we have met each other, you are a good friend and I have really enjoyed talking to you during our coffee breaks. I also thank Dimitri, Morten and Zeinab for the many coffees, cakes and chats that we have been having during these three years.
Our section of Mathematics is blessed for having one of the best secretaries of the whole university, Dorthe. Thank you Dorthe for all the support that you have given me, and for always having a nice word for me.
Having a cancelled flight can be a lucky event, if in such occasion one gets to meet another Ph.D. student from DTU, who will turn out to be a very good friend, and who will present you three other special people. I am talking about Nicola, Andrea, Michele and Chiara. Thank you guys for all the lunch breaks and dinners that we had together. The last year at DTU would have not been the same without you. I look forward to keep our friendship in the future.
To my friends Amrei and Antoine, thank you for all the "not laundries but breakfasts" that we had. I thank you our nice conversations and for the support that you have shown me in these three years. Thank you Amrei for proofreading the introduction of this thesis.
I thank Susanne and Kim for their support in the last two years and for inviting Sebastian and me over for dinner during the last weeks before the hand-in.
To my dearest friend Marco, with whom I have been having uncountably many Facetime conversations in the last three years. Thank you for your great friendship. I am glad that despite the distance, we manage to find ways to talk and see each other.
There are two girls that I have know for more than 25 years and that are very special to me. Thank you Maria and Giulia, you are a great example that friendship does not diminish with distance or time. As Giulia says, every time we see each other, it feels like we have always been together.
To my family, thank you for your love, for supporting me and for believing in me. I appreciate that every time I come home, you try to spend as much time as possible with me. Thank you for all your visits here, and for bringing pieces of Mantova to Copenhagen.
During the first year of the Ph.D., I have participated to a DCAMM Symposium, where researchers from the Danish universities in applied mathematics and mechanics got to meet each other. I thank my Ph.D. education, because here I have met my boyfriend Sebastian.
To my beloved Sebastian, thank you for your love, your support and for making me dream of a future together. I look forward to discover what our next experience is going to be.

Contents

Chapter 1

Introduction

La meccanica è il paradiso
della matematica,
perché qui
se ne possono cogliere i frutti.

Mechanics is the paradise
of mathematical science,
because here we come
to the fruits of mathematics.

– Leonardo da Vinci

Often we come to notice friction in the drastic instances when friction is lacking, such as when we slip on a polished floor or on an icy road. At a closer look, we can realise that friction plays an important role in our everyday life, and that it is a key way of loosing energy in mechanics. Sometimes, the desire is to maximise the energy dissipated by friction, as in the case of car brakes [CCM+09], while other times the wish is to minimise the dissipation, as when we use bearings or lubricants. Often, we can hear the action of friction. Friction induced vibrations cause the sound of string instruments [Sch73], some sounds from nature, like the stridulation of crickets and cicadas [Aka02], and they are even linked to the booming of sand dunes [FGHP98, And12]. There are other types of noise that are induced by friction, and that are less desirable. Among these, the squeaking of the chalk on a blackboard, the creaking of doors, the squealing of train wheels and the chattering of machine tools [Ibr94, FGHP98, HA00, Aka02]. Friction is also considered to play an important role in earthquake faulting and in the periodicity of the earthquake episodes [Sho02, EBL08, ZN12, BBK17b].

Understanding the mechanisms of friction is key to the understanding of many mechanical processes. However, in spite of all the experimental and theoretical efforts, there is still no comprehensive understanding of the physical processes and no universal friction model exists [OACdW+98, FGHP98, Mar98b, WPM15]. It is recognised that friction is a force resulting from multiple processes and that it acts on different scales: the timescale can vary from seconds to millennia while the spatial scale can range from microns to hundreds of kilometers [Har04, ABS08].
There have been several attempts in modelling friction. The simplest models follow directly from the early experiments of Leondardo da Vinci, Amontons and Coulomb [OACdW+98, FGHP98]. These basic models are all based on the evidence that friction acts opposite to the direction of motion and changes abruptly when the motion changes in direction. The basic Coulomb model states that friction is independent of the magnitude of velocity. Improvements to this model may consist in the addition of the Stribeck effect, or of the maximum static friction force, as in the *stiction* model [OACdW+98]. During the second half of the last century, new models have appeared with the aim to improve the original ideas of Coulomb. These have been initiated by the work of Burridge and Knopoff [BK67] where the interaction between surfaces has been modelled by multiple spring-blocks. The subsequent experiments on rocks by Dieterich [Die72, Die78, Die79] and Rice and Ruina [RR83, GRRT84, RT86], initiated the so-called *rate-and-state* friction models. These models assume the friction force not only to be velocity dependent, but also to be *state* dependent, so that there is some memory in the system. The more recent spinodal law [PWD08, PD15, CPW16] is a further generalization of the rate-and-state models. To date, there is no general agreement on the physical meaning of the state, and on how many states friction has.

The classical way of modelling mechanical processes, is by using *ordinary differential equations (ODEs)*. These ODEs have the general form

$$\frac{\mathrm{d}z}{\mathrm{d}t} = Z(z), \tag{1.1}$$

where $z \in \mathbb{R}^k$ is a vector of variables and $Z(z)$ is a nonlinear vector field describing the underlying mechanical processes. The properties of the solution $z(t)$ of (1.1), strongly depend on Z. For instance, classical results of existence and uniqueness of solutions, are obtainable when Z is locally Lipschitz continuous in z, that means

$$||Z(x) - Z(y)|| \leq K||x - y||, \qquad x, y \in U, \tag{1.2}$$

for some constant $K > 0$ and $U \subset \mathbb{R}^k$ open. Rate-and-state friction models can be modelled by ODEs like (1.1), where in particular multiple timescales appear. This means that some of the variables x in z evolve on a timescale τ that is

faster than the timescale t along which the remaining variables y in z evolve. For this reason we call τ the *fast* timescale and t the *slow* timescale and we define by $\varepsilon = t/\tau$ the small parameter that expresses the ratio between the two. Therefore, for multiple timescales problems (1.1) can be rewritten as

$$\begin{aligned} x' &= f(x, y, \varepsilon), \\ y' &= \varepsilon g(x, y, \varepsilon), \end{aligned} \tag{1.3}$$

where $(x, y) \in \mathbb{R}^m \times \mathbb{R}^n$ so that $m + n = k$ and the prime has the meaning of differentiation with respect to the fast time τ. The *fast system* (1.3) is equivalent to the *slow system*

$$\begin{aligned} \varepsilon \dot{x} &= f(x, y, \varepsilon), \\ \dot{y} &= g(x, y, \varepsilon), \end{aligned} \tag{1.4}$$

for $\varepsilon > 0$, where the dot now has the meaning of differentiation with respect to the slow time t. In the phase plane, solutions of (1.3) coincide with the ones of (1.4), and the only difference lies in the speed with which the trajectories are swept.

It is rather difficult to do numerical simulations of (1.4) for ε small, because numerics are often not sufficiently accurate for singularly perturbed problems. Traditionally, analytical results have been obtained with the method of matched asymptotic expansion [vGKS05, Hol13]. Methods from non-standard analysis have also been used to study such type of systems [DD95]. More recently, a geometric approach has proven to be rather successful in treating slow-fast problems of the type (1.3). This theory, that is based on Fenichel's seminal work [Fen74, Fen79] is called *geometric singular perturbation theory (GSPT)*. The idea is to consider the *singular limit* $\varepsilon = 0$ of the fast and slow systems (1.3) – (1.4) so that we obtain the *layer problem*

$$\begin{aligned} x' &= f(x, y, 0), \\ y' &= 0, \end{aligned} \tag{1.5}$$

and the *reduced problem*

$$\begin{aligned} 0 &= f(x, y, 0), \\ \dot{y} &= g(x, y, 0), \end{aligned} \tag{1.6}$$

respectively. We call the set $(x, y) : f(x, y, 0) = 0$ the *critical manifold* C_0. This is the set of equilibrium points of the layer problem (1.5) and it is also the set along which the solutions of the reduced problem (1.6) are constrained to. The layer and the reduced problems are simpler to study than (1.3). Firstly, both systems have a smaller dimension than (1.3): system (1.5) has in fact $m < k$ equations while (1.6) has $n < k$ equations. Secondly, each system has only one leading timescale, that is either the fast or the slow one. C_0 is said to be *normally hyperbolic* if the Jacobian $f_x(x, y, 0)|_{C_0}$ has all the eigenvalues bounded away from the imaginary axis.

Fenichel's results guarantee that for $\varepsilon > 0$ sufficiently small, a compact normally hyperbolic subset $S_0 \subset C_0$, perturbs smoothly into a local invariant *slow manifold* S_ε. The solutions of the singularly perturbed problem (1.3) can be obtained, under certain assumptions, as $\mathrm{O}(\varepsilon)$ perturbation of the singular trajectories constructed by piecing together segments of the layer and of the reduced problem, respectively.

Geometric singular perturbation theory has found application in several fields, among those chemistry [GS09, MSLG98, Shc05], neurology [Moe06, RW07] and electrical circuits [DR96, DMD06]. For problems with more than two timescales we refer to [KPK08, KPKR08] and [Kue15, §13.8].

As mentioned above, the results of Fenichel are valid for C_0 normally hyperbolic. In points where this assumption is lost, interesting new behaviour can occur. A classical example of the loss of normal hyperbolicity is when the vector field of the reduced problem is tangent to the vector field of the layer problem, so that it is not possible to separate the two timescales. The *blow-up method* is a geometrical method that has been first used to deal with the loss of normal hyperbolicity by Dumortier and Roussaire [DR96]. We consider the modern formulation of the method in the context of geometric singular perturbation theory, introduced by Szmolyan and collaborators [KS01a, KS01b, KS01c, SW01]. This method has proven to be successful in explaining canard solutions and canard explosions [DMD06, DKO08, Wec12], describing the mechanisms of relaxation oscillations [SW04, KPK08, GS09, KS11], and bursting [VKK16].

While rate-and-state friction models can be written in a slow-fast formulation like (1.3), this is not possible for the Coulomb-type models. These indeed are systems with a discontinuous right-hand side, so that (1.1) can be written as

$$\frac{\mathrm{d}z}{\mathrm{d}t} = \begin{cases} Z^+(z), & h(z) > 0, \\ Z^-(z), & h(z) < 0, \end{cases} \tag{1.7}$$

for some $h(z) : \mathbb{R}^k \to \mathbb{R}$. The set $\Sigma : h(z) = 0$ is called the *switching manifold*, and it is the set along which the vector field Z changes discontinuously. We suppose that $Z^\pm$ are sufficiently smooth in their respective region of definition, so that solutions are well defined in their respective interiors. On Σ, the Lipschitz condition (1.2) is not satisfied and we need to discuss how to define a solution through a discontinuous set and also when this solution exists and when it is unique. Once a notion of solution is introduced, this may be forward nonunique, and furthermore, it can be difficult to define what we mean by perturbation of a non-smooth system and study its bifurcations.
The work of Filippov [Fil88] has been fundamental to solve a class of problems that we call of Filippov-type. For this class of problems, the vector field within Σ and the computation of the forward solutions depend by the vector fields

$Z^{\pm}$ only. This has proven effective in many cases [Fil88, DBBCK08, GHS10], but may bring inconsistencies as in the case of the two-fold singularity, where nonunique forward solutions may appear [CJ11, KH15a, KH15b]. For systems not of Filippov-type more care is needed, as standard results are not always applicable.

Given all the problems related to non-smooth systems, it makes sense to consider a smoothed version of (1.7). In this way we obtain a smooth system that can be studied with the standard theory of smooth dynamical systems, and that looses its smooth properties at the non-smooth limit. *Regularization* turns out to be an effective smoothing method [ST96]. This means to consider the 1-parameter family of vector fields

$$Z_\varepsilon(z) := \frac{1}{2}Z^+(z)\left(1+\phi\left(\varepsilon^{-1}h(z)\right)\right)+\frac{1}{2}Z^-(z)\left(1-\phi\left(\varepsilon^{-1}h(z)\right)\right), \tag{1.8}$$

for $\varepsilon > 0$ sufficiently small and ϕ a smooth function with some special properties. In particular it is desired that for $\varepsilon \to 0$ then $Z_\varepsilon \to Z^{\pm}$ for $h(z) \neq 0$. Interestingly, the vector field (1.8) is singular for $\varepsilon \to 0$ on $h(z) = 0$ and it can be rewritten as a multiple timescale problem of the form (1.3) using a blow-up of $h(z) = 0$. If ϕ is chosen properly, then the layer and reduced problem of (1.3) are equivalent to the vector field $Z^{\pm}$ and the one within Σ respectively. Thus, this is a new way of using Fenichel's results: *instead of studying the $\varepsilon = 0$ case, to obtain information about the behaviour of solutions for $\varepsilon > 0$, in this circumstance we study the singularly perturbed problem to construct solutions of the original discontinuous system.*

This thesis is about the application of geometric singular perturbation theory to two different friction models: one of the rate-and-state class, and one of the Coulomb-type class. The application of GSPT in rate-and-state models is a novelty, as the existing results were obtained by using the method of the matched asymptotic expansions [PWD08, PB11] or with theory for standard dynamical systems [GRRT84]. Regularization of friction models has already been introduced, as in [Ste00, Jef15, BRMS16], either by considering a vector field like (1.8) or by introducing hidden terms [Jef14]. However regularization of non-Filippov type systems, is still quite new. We now briefly describe the specific problems considered and we summarise our main results.

The first problem that we study is the one-dimensional spring-block model with Ruina rate-and-state friction law, that is often used for describing earthquake faulting. We want to show that this model has periodic solutions of relaxation oscillation type, where each period is composed of an earthquake rupture phase and a subsequent healing phase. To begin with, we identify a small parameter ε that gives the separation between the slow and the fast timescales. Hence, we aim to use standard techniques from GSPT to show the existence and stability

of the periodic solutions. However, the critical manifold C_0 is unbounded, and even though it is attracting everywhere, it loses normal hyperbolicity with an exponential rate at infinity. Furthermore, orbits lying on C_0 reach infinity in finite time. It turns out that the understanding of the behaviour of solutions at infinity is crucial, but in this regime the dynamics is very non-hyperbolic. By repeatedly using the blow-up method around infinity, we find a centre manifold that guides the dynamics in this region. We then construct a singular orbit for $\varepsilon = 0$ and we conjecture that the relaxation oscillation cycles are perturbations of this orbit for $\varepsilon > 0$.
Furthermore, we show that the periodic solutions of our system also describe travelling wave solutions of a more complicated model for earthquake faulting.

The second problem that we consider is the one of a mass-spring oscillator that is subject to stiction friction. This friction law is discontinuous, so that the problem is of the form (1.7). Furthermore, the stiction law defines naturally a vector field along the switching manifold, so that the system turns out not to be of Filippov-type. We introduce the notion of *stiction solutions*: those are the solutions of the system that are physically meaningful. However, some of these solutions are forward nonunique, and in order to solve the nonuniqueness, we introduce a regularization of the type (1.8). In this way, we obtain a slow-fast system like (1.3). The corresponding critical manifold is a surface with two fold lines. Along the fold lines there are some special points where canard solutions of saddle type appear. These canards evolve along the attracting side of the critical manifold, pass through the canard point and stay close to the repelling side of the critical manifold for some time, before leaving it by following a fast fibre. We show that the canard solutions are related to some of the nonunique stiction solutions of the original non-smooth system.

There are further mathematical motivations, apart from the physical interest, for the study of the two models. The first problem is an example of the use of the blow-up method in the context of non-trivial problems. In order to obtain a geometric desingularization of the vector field, the blow-up needs to be applied several times, and we show how to follow a solution through the many blow-ups. Furthermore, we will introduce an example of a non-standard blow-up transformation.
The first problem also shows an interesting example of a *flat slow manifold* in the context of non-trivial applications. This is a case where the critical manifold is everywhere attracting, but it loses hyperbolicity with an exponential rate at infinity. To solve this problem, we apply a technique that has recently been developed by Kristiansen [Kri17].
The second problem can be seen as an introduction to regularization in non-trivial applications. Finally, this second problem highlights a modelling issue that sometimes may not be noticed. We show that the choice of using a smooth or a non-smooth vector field to model the same phenomenon can lead to very

different results, even though the difference between the two models is minimal. We leave open the question on how friction should be modelled, and whether there exists a global model that can describe all the observable behaviours that are induced by friction.

The thesis consists of four chapters. Chapter 2 presents the mathematical preliminaries, of both singularly perturbed and discontinuous dynamical systems. The blow-up and the regularization methods are introduced, and we give a short introduction to canard solutions. In chapter 3 we present the problem of the one-dimensional spring-block model subject to the Ruina rate-and-state friction law, while chapter 4 presents the problem of the mass-spring oscillator subject to stiction friction. The results of chapter 3, regarding the analysis at the singular limit, are published in [BBK17b], while the ones of chapter 4 are published in [BBK17a].

Chapter 2

Mathematical preliminaries

This chapter introduces some recent mathematical results that will be used later in chapter 3 and 4. The chapter is subdivided as follows. Section 2.1 presents geometric singular perturbation theory and the fundamental results of Fenichel. The blow-up method of section 2.2 can be used to extend geometric singular perturbation theory to non-hyperbolic points, that are points where Fenichel's results are not valid. Canard solutions are a special type of solutions appearing in slow-fast systems, and these are presented in 2.3. Then, 2.4 introduces non-smooth dynamical systems, and discusses existence and uniqueness of forward solutions for this type of systems. Finally, 2.5 introduces the regularization method of Sotomayor and Teixeira.

2.1 Geometric singular perturbation theory

Geometric singular perturbation theory has been developed to study ordinary differential equations (ODEs) with multiple timescales. These are problems where the derivative of a subset of variables, has a larger magnitude than that of the remaining variables. The simplest case is when there are only two timescales, so that we can call some variables fast, while the other are slow. We refer to [KPK08, KPKR08, DGK+12] for examples of problems with three or more

timescales. The definitions and theorems of this section are based on [Fen74, Fen79, Jon95, Kap99, Kos12] and [Kue15, §3].

We call a *fast-slow dynamical system* a system of differential equations of the type

$$\begin{aligned} x' &= f(x, y, \varepsilon), \\ y' &= \varepsilon g(x, y, \varepsilon), \end{aligned} \tag{2.1}$$

where $f : \mathbb{R}^{m+n+1} \to \mathbb{R}^m$ and $g : \mathbb{R}^{m+n+1} \to \mathbb{R}^n$ are smooth functions, $0 < \varepsilon \ll 1$ and the prime has the meaning of differentiation with respect to the *fast time* τ. The time evolution of the variables $x \in \mathbb{R}^m$ in (2.1) is *fast* when compared to the one of the *slow* variables $y \in \mathbb{R}^n$, since the latter in general have a derivative of order of $\varepsilon \ll 1$. By introducing the time rescale $t = \tau\varepsilon$ we rewrite (2.2) as the *slow system*

$$\begin{aligned} \varepsilon \dot{x} &= f(x, y, \varepsilon), \\ \dot{y} &= g(x, y, \varepsilon), \end{aligned} \tag{2.2}$$

where the dot has the meaning of differentiation with respect to the *slow time* t. The orbits of the *fast system* (2.1) have a one-to-one correspondence with the orbits of the slow system (2.2) for $\varepsilon > 0$. The two systems differ in the time it takes to move along a same trajectory. The parameter ε describes the separation between the two scales and it is often referred to as the *timescale parameter*.
The idea is to study the fast and the slow processes separately, and for this reason we consider the *singular limit* $\varepsilon = 0$, where (2.1) limits to the *layer problem*

$$\begin{aligned} x' &= f(x, y, 0), \\ y' &= 0, \end{aligned} \tag{2.3}$$

and (2.2) limits to the *reduced problem*

$$\begin{aligned} 0 &= f(x, y, 0), \\ \dot{y} &= g(x, y, 0). \end{aligned} \tag{2.4}$$

The layer problem (2.3) describes the evolution of the fast variables x, while the remaining y variables are constants of motion. For this reason, the analysis of (2.3) is similar to a bifurcation analysis, where we study the solutions of (2.3) while varying the y-variables as bifurcation parameters. We define the *critical manifold* C_0 as the set of equilibrium points of (2.3), this is the set of points that satisfy $f(x, y, 0) = 0$. Furthermore, we say that the critical manifold is *normally hyperbolic* in $S_0 \subset C_0$, if the $m \times m$ matrix $f_x(x, y, 0)$ of partial derivatives with respect to the fast variables x has no eigenvalues with zero real part for all $(x, y) \in S_0$. A compact, normally hyperbolic subset $S_0 \subset C_0$ is called *attracting*, if the eigenvalues of $f_x(x, y, 0)$ have all negative real part, it is

called *repelling* if the eigenvalues of $f_x(x, y, 0)$ have all positive real part and it is called of *saddle type* otherwise.

The critical manifold also plays an important role in the analysis of the reduced problem: this is the set to which the solutions of (2.4) are constrained. Around points $p \in C_0$ where $f_x(x, y, 0)$ is non-singular, by using the Implicit Function Theorem we can explicit the condition $f(x, y, 0)$ as $x = h(y)$. Thus, the differential algebraic equation (2.4) becomes

$$\dot{y} = g(h(y), y, 0), \tag{2.5}$$

and solutions of (2.5) describe the phase space within C_0.

At the singular limit $\varepsilon = 0$, we have obtained a way to describe the phase space of the problem (2.1) in separate regions, that means within and outside of the critical manifold C_0. We expect that when $\varepsilon > 0$ is sufficiently small, solutions of (2.1) will be a perturbation of the singular solutions that we have found. Fenichel's theorems [Fen74, Fen79] describe when this is possible.

Theorem 2.1 ([Fen79]) *Suppose that S_0 is a compact normally hyperbolic subset of the critical manifold C_0 and that $f, g \in C^r(1 \leq r < \infty)$. Then for $\varepsilon > 0$ sufficiently small, there exists a locally invariant C^r-smooth manifold S_ε that is diffeomorphic to S_0 and that has Hausdorff distance $\mathrm{O}(\varepsilon)$ (as $\varepsilon \to 0$) from S_0. Furthermore the flow on S_ε converges to the slow flow as $\varepsilon \to 0$.*

The local invariance of S_ε means that trajectories can enter or leave S_ε only through its boundaries. The fact that S_ε is diffeomorphic to S_0 means that, if we can write S_0 as $x = h(y) \in C^r$ for $\varepsilon = 0$, then for $\varepsilon > 0$ there exists a function h_ε such that S_ε can be written as the graph $x = h_\varepsilon(y)$ and $h_\varepsilon \to h$ as $\varepsilon \to 0$. The dynamics on S_ε is then described by

$$\dot{y} = g(h_\varepsilon(y), y, \varepsilon),$$

and for this reason S_ε is also called the *slow manifold*.
Suppose that a point $p = (x, y) \in S_0 \subset C_0$ is a hyperbolic equilibrium point of the layer problem (2.3) and that has m^s eigenvalues with negative real part and m^u eigenvalues with positive real part. This produces the m^s-dimensional local stable manifold $W^s_{\mathrm{loc}}(p)$ and the m^u-dimensional local unstable manifold $W^u_{\mathrm{loc}}(p)$ at the point p, respectively. By considering all $p \in S_0$, we can construct two manifolds $W^s_{\mathrm{loc}}(S_0)$ and $W^u_{\mathrm{loc}}(S_0)$ of the layer problem (2.3) that intersect in S_0, that is

$$W^s_{\mathrm{loc}}(S_0) = \bigcup_{p \in S_0} W^s_{\mathrm{loc}}(p), \qquad W^u_{\mathrm{loc}}(S_0) = \bigcup_{p \in S_0} W^u_{\mathrm{loc}}(p).$$

These manifolds also persist for $\varepsilon > 0$ sufficiently small and their characterization is given in the following theorem.

Theorem 2.2 ([Fen79]) *Consider the same assumptions as in Theorem 2.1. Then for $\varepsilon > 0$ sufficiently small, there exists families of $(n+m^s)$- and $(n+m^u)$-dimensional local stable and unstable C^r-manifolds $W^s_{loc}(S_\varepsilon)$ and $W^u_{loc}(S_\varepsilon)$, which are both locally invariant and C^r-close to $W^s_{loc}(S_0)$ and $W^u_{loc}(S_0)$. Furthermore the dynamics within $W^s_{loc}(S_\varepsilon)$ and $W^u_{loc}(S_\varepsilon)$ is described by C^r-invariant foliations $\mathcal{F}^s_\varepsilon$ and $\mathcal{F}^u_\varepsilon$ such that the distance between orbits starting within the same leaf decays or grows exponentially fast.*

It follows that the slow manifold S_ε has the same stability properties of S_0, with respect to the fast variables. Thus an attracting subset $S_a \subset C_0$ perturbs smoothly into a locally invariant attracting manifold $S_{a,\varepsilon}$ for $\varepsilon > 0$ sufficiently small. Similarly for a repelling subset $S_r \subset C_0$. For a proof of Theorems 2.1 and 2.2, we refer to the seminal papers of Fenichel [Fen74, Fen79] or to [Jon95]. Fenichel's results require normal hyperbolicity in the subset $S_0 \subset C_0$, and they are not valid in points $(x, y) \in C_0$ where the kernel of $f_x(x, y, 0) = 0$ is non-empty. It is important to find a way to study the behaviour of the solutions of the slow-fast problem (2.1) around non-hyperbolic points, and the blow-up method of section 2.2 aims to do this.

2.2 The blow-up method

This section presents the blow-up method, that has proven to be successful in extending the results of geometric singular perturbation theory to points where the critical manifold looses normal hyperbolicity. The technique is based on the pioneering work of Dumortier and Roussarie, who have shown it usefulness in the study of the relaxation oscillation cycles of the Van der Pol oscillator [DR96]. The blow-up method has found several applications in the last two decades, and in this section, we describe the blow-up of a non-hyperbolic point in the planar case, following the description of [SW01, Kos12] and [Kue15, §7]. In subsection 2.2.1 we show an adaptation of the method by Kristiansen [Kri17] that is useful to desingularize flat slow manifolds.

Suppose that the origin of system (2.1) is such that

$$f(0, 0, 0) = 0, \quad f_x(0, 0, 0) = 0, \tag{2.6}$$

that means, in the origin the critical manifold C_0 is not normally hyperbolic. The blow-up method desingularizes the dynamics around the degenerate equilibrium point by using a geometric transformation. Firstly, we rewrite (2.1) as

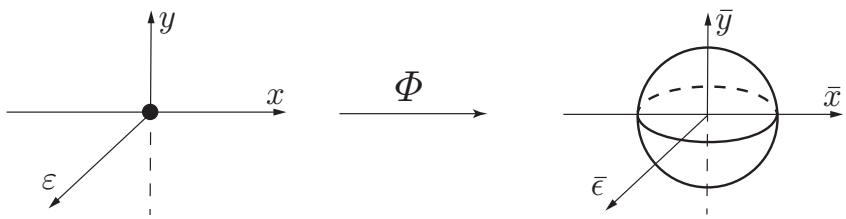

Figure 2.1: Blow-up of a point to a sphere.

the extended system

$$\begin{aligned} x' &= f(x, y, \varepsilon), \\ y' &= \varepsilon g(x, y, \varepsilon), \\ \varepsilon' &= 0, \end{aligned} \tag{2.7}$$

where we treat ε as a dynamic variable. We call Z the extended vector field defined by (2.7). By virtue of (2.6), system (2.7) has an equilibrium in the origin with triple zero eigenvalue. Then, we define $B = S^2 \times [0, r_0]$ with $r_0 > 0$ and introduce the *blow-up* transformation $\Phi : B \to \mathbb{R}^3$

$$x = \bar{r}^a \bar{x}, \quad y = \bar{r}^b \bar{y}, \quad \varepsilon = \bar{r}^c \bar{\epsilon}, \tag{2.8}$$

with $(a, b, c) \in \mathbb{Z}^3$ and $S^2 := \{(\bar{x}, \bar{y}, \bar{\epsilon}) \mid \bar{x}^2 + \bar{y}^2 + \bar{\epsilon}^2 = 1\}$.

In the subset $r > 0$, the map Φ is a diffeomorphism, and in this set we can define a vector field $\bar{Z}$ that is conjugated to Z for $0 < r < r_0$, so that no information on Z is lost by considering $\bar{Z}$. On the other hand, Φ is singular for $r = 0$, as it maps a sphere to the origin. Since the origin was an equilibrium point of the original vector field (2.7), on the surface of the sphere $r = 0$ the blown-up vector field $\bar{Z}$ vanishes. A non-degenerate vector field on the sphere is obtained by dividing $\bar{Z}$ by a suitable power of the radius $\bar{r}$. Formally this is done by introducing a time transformation, and we will show this in more detail in chapter 3.

The basic idea of the blow-up method is to find a singular segment contracting to the sphere for $\varepsilon = 0$, connect it to a singular orbit moving along the sphere, and then follow the motion away from the sphere, where each singular segment has hyperbolic or algebraic behaviour. When $\varepsilon > 0$, we can use standard methods for regularly perturbed systems, to detect the distance of the perturbed solution from the singular trajectory. Figure 2.2 illustrates the results obtained by the blow-up method in the case of the singularly perturbed planar fold.

To study the blown-up vector field $\bar{Z}$, one could use spherical coordinates, but this may lead to lengthy computations. Instead, the natural way of studying $\bar{Z}$ is to introduce charts that give a local description on the dynamics along

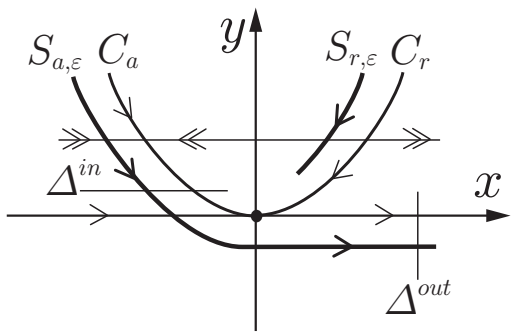

Figure 2.2: The singularly perturbed planar fold [KS01a]. The vector field of the figure satisfies conditions (2.6) together with $f_{xx}(0,0,0) \neq 0, f_y(0,0,0) \neq 0$ and $g(0,0,0) \neq 0$. C_0 is locally quadratic around the origin, and it is not normally hyperbolic at this point. We assume the left branch of C_0 to be attracting, and the right branch to be repelling. $\Delta^{in}, \Delta^{out}$ are two sections. By using the blow-up method, Krupa and Szmolyan [KS01a] could continue the slow attracting manifold $S_{a,\varepsilon}$ from Δ^{in} – where it is $O(\varepsilon)$-close to C_a for $0 < \varepsilon \ll 1$ – to Δ^{out}, showing furthermore that at Δ^{out} $S_{a,\varepsilon}$ is $O(\varepsilon^{2/3})$-close to the x-axis.

the sphere. This is done by setting one of the variables of S^2 equal to ± 1, so that each chart is perpendicular to one of the axes. It turns out that a very important chart is the one for $\bar{\epsilon} = 1$, that is usually referred to as chart K_2. This chart is sometimes called the *family rescaling chart* or *classical chart* [DR96, KH15b]. The importance of chart K_2 lies in the fact that when $\bar{\epsilon} = 1$, then $\bar{r}^c = \varepsilon$ from (2.8), and therefore, the space is foliated by invariant planes $\bar{r} = const$, since $\varepsilon' = 0$. However in the other charts, $\bar{r}$ is not a constant, but one needs to remember that for $\varepsilon > 0$ solutions are foliated on invariant manifolds $\bar{r}^c\bar{\epsilon} = const$. These other charts are needed to connect the dynamics outside of the sphere to the one on the sphere.

One of the difficult parts of the blow-up method is in finding the correct weights (a, b, c) for the map (2.8). There is no general method to find them, but sometimes the theory of Newton polyhedra for polynomial vector fields can turn out to be useful. We say that a blow-up is *homogeneous* if $a = b = c$, while we say that it is *quasi-homogeneous* if the weights differ in value.
If in one of the blown-up charts there is a degenerate equilibrium point with all zero eigenvalues, it is necessary to introduce a new blow-up map at this point and repeat the procedure. This is the case of multiple blow-ups.
Sometimes, a system may have a higher dimensional geometrical structure that is not hyperbolic, like a line or a plane. For example, if the line $x = 0$ of (2.7)

is non-hyperbolic, in order to blow-it up we need to set $a = 0$ in (2.8), so that $x = 0$ is blown-up to a cylinder. For examples of higher dimensional blow-ups, we refer to [KS11, KS16] as well as the problem presented in chapter 3.
In some cases, a blow-up transformation of a polynomial type like (2.8) is not sufficient and adaptations of the method are needed. For instance, in chapter 3 we present a blow-up transformation of the type

$$x = \bar{r}\bar{x}, \qquad y = \frac{\mathrm{e}^{-1/\bar{r}}}{\bar{r}}\bar{y},$$

for $(\bar{x}, \bar{y}) \in S^1$ and $\bar{r} \geq 0$, so that one of the terms in the blow-up has an expression with an exponential function of the radius. The following subsection 2.2.1 presents a method to resolve the case of exponential terms appearing in the vector field.

2.2.1 Background on flat slow manifolds

In this subsection we present some results from [Kri17] on *flat* slow manifolds. This means that we wish to consider a problem of the type (2.1) where the critical manifold has one eigenvalue λ that decays exponentially as $x \to 0$. A simple planar example of such a system is given in [Kri17] and has the form

$$\begin{aligned} x' &= x^2(y - \mathrm{e}^{-1/x}), \\ y' &= \varepsilon\mu\, \mathrm{e}^{-1/x}, \end{aligned} \tag{2.9}$$

with $0 < \varepsilon \ll 1$, $\mu \neq 0, (x, y) \in \mathbb{R}^2$ and $x \geq 0$. The critical manifold of (2.9) is $C_0 = S_a \cup S_c$, where S_a is attracting $S_a := \{(x, y) \in \mathbb{R}^2 \mid y = \mathrm{e}^{-1/x}\}$ while S_c is not normally hyperbolic $S_c := \{(x, y) \in \mathbb{R}^2 \mid x = 0\}$. However, the computation of the linear stability along S_a gives

$$f_x(x, y, \varepsilon)\Big|_{S_a} = -\mathrm{e}^{-1/x},$$

so that S_a looses hyperbolicity exponentially fast as $x \to 0$. The blow-up in the formulation (2.8) requires homogeneity in the leading order terms, and this is not the case when there are exponential terms as in (2.9). The idea of Kristiansen [Kri17] is to apply the blow-up transformation to an extended vector field, where we not only consider ε as a dynamical variable, but we introduce an auxiliary variable

$$q = \mathrm{e}^{-1/x}, \tag{2.10}$$

whose differentiation with respect to the fast time τ gives, by the chain rule,

$$q' = \mathrm{e}^{-1/x}\,\frac{x'}{x^2} = q\frac{x'}{x^2}.$$

Thus the extended vector field (2.9), augmented by q and ε, becomes

$$\begin{aligned} x' &= x^2(y-q), \\ y' &= \varepsilon\mu q, \\ q' &= q(y-q), \\ \varepsilon' &= 0, \end{aligned} \tag{2.11}$$

where the right-hand side of (2.11) has now only polynomial terms. By construction, q is slaved by x by virtue of (2.10), but this is not explicit in (2.11). The set of equilibria of (2.11) is now

$$\{(x,y,q,\varepsilon) \mid y = q, \varepsilon = 0\} \cup \{(x,y,q,\varepsilon) \mid x = q = 0\},$$

and the set $y = q, \varepsilon = 0$ corresponds to S_a. The linearization of (2.11) on S_a has $-q$ as eigenvalue, so that S_a is normally hyperbolic and attracting for $q > 0$, and it looses normal hyperbolicity for $q = 0$ with an algebraic rate instead than exponential as before. Thus, the blow-up method can be invoked for the analysis of (2.11). The proper blow-up transformation in this case is

$$x = x, \quad y = r\bar{y}, \quad q = r\bar{q}, \quad \varepsilon = r\bar{\epsilon}. \tag{2.12}$$

Thanks to this transformation, we gain hyperbolicity of S_a on the blown-up cylinder. We refer to [Kri17] for the details of the analysis. Notice that $\bar{\epsilon} = 1$ in (2.12) gives $q = \varepsilon\bar{q}$, and by (2.10) we have $x = \ln^{-1}(\varepsilon^{-1})$ in the regime $\bar{q} = \mathrm{O}(1)$. A non-trivial example of a flat slow manifold is presented in chapter 3. We will show that the regime where q is sufficiently small and comparable with ε, is the right regime to find an attracting centre manifold that guides the dynamics at infinity.

2.3 Canard solutions

Canards solutions are a generic feature of slow-fast systems with one fast and $m \geq 2$ slow variables, whose discovery dates back to the pioneering work of Benoit et al. [BCDD81, Ben83]. They appear for example in the Van der Pol oscillator [DR96], in a model for aircraft ground dynamics [RDKL11], in a model for stellar wind [CKW17] and in the regularization of some non-smooth systems [KH15a]. The results in this section are based on [SW01] and [Kue15, §8.5]. We consider a system with one fast and two slow variables of the type

$$\begin{aligned} \varepsilon\dot{x} &= f(x, y_1, y_2, \varepsilon), \\ \dot{y}_1 &= g_1(x, y_1, y_2, \varepsilon), \\ \dot{y}_2 &= g_2(x, y_1, y_2, \varepsilon). \end{aligned} \tag{2.13}$$

The critical manifold $C_0 = \{(x, y_1, y_2) : f(x, y_1, y_2, 0) = 0\}$ is generically a surface, and the condition $f_x(x, y_1, y_2, 0) = 0$ is generically a one-dimensional curve L within C_0. Hence, along L the manifold C_0 is non-hyperbolic. Without loss of generality, we assume that the origin $(0, 0, 0, 0) := 0$ lies in L and furthermore

$$f(0) = 0, \quad f_x(0) = 0, \tag{2.14}$$

together with

$$f_{y_2}(0) \neq 0, \quad f_{xx}(0) \neq 0. \tag{2.15}$$

In an interval I containing the origin, and under assumptions (2.14) and (2.15), L can be parametrized by y_2 as

$$L = \{(\theta(y_2), \psi(y_2), y_2) \in \mathbb{R}^3 : y_2 \in I\}.$$

We define the *transversality condition*

$$l(y_2) := (f_{y_1} g_1 + f_{y_2} g_2)|_{(\theta(y_2), \psi(y_2), y_2, 0)}.$$

It turns out that the existence of canard solutions depends crucially on the value of $l(y_2)$. Specifically, canards appear when $l(0) = 0$ that is, when the reduced flow projected onto the (y_1, y_2)-plane is tangent to the fold line L at the origin.

It is possible to show that under assumptions (2.14) and (2.15), there exists a coordinate change that allows to rewrite system (2.13) near the origin as

$$\begin{aligned} \varepsilon \dot{x} &= y_1 + x^2 + \mathrm{O}(\varepsilon x, \varepsilon y_1, \varepsilon y_2, \varepsilon^2, y_1^2 x, x^3, \varepsilon y_1 y_2), \\ \dot{y}_1 &= b y_2 + c x + \mathrm{O}(y_1, \varepsilon, y_2^2, x y_2 x^2), \\ \dot{y}_2 &= a + \mathrm{O}(x, y_1, y_2, \varepsilon), \end{aligned} \tag{2.16}$$

with computable constants $(a, b, c) \in \mathbb{R}^3$. The critical manifold around the origin is $C_0 = \{y_1(x, y_2) = -x^2(1 + \mathrm{O}(x, y_2))\}$. In this way, the critical manifold has an attracting region C_a for $x < 0$ and a repelling region C_r for $x > 0$, that are separated by the fold line $L : \{x = 0, y_1 = 0\}$, that corresponds to the y_2-axis. The reduced problem is obtained by differentiating the function $y_1(x, y_2)$ with respect to time, and by substituting it for $\dot{y}_1$ in (2.16), so to obtain

$$\begin{aligned} -2x(1 + \mathrm{O}(x, y_2))\dot{x} &= b y_2 + c x + \mathrm{O}(y_2^2, x y_2, x^2), \\ \dot{y}_2 &= a + \mathrm{O}(x, y_2). \end{aligned} \tag{2.17}$$

Along the fold curve L, (2.17) is singular and solutions may approach this singular curve in finite forward or backward time. We introduce the time rescale

$$\mathrm{d}t = -2x(1 + \mathrm{O}(x, y_2))\mathrm{d}\tilde{t}, \tag{2.18}$$

where t is the original slow time of system (2.17). After the time rescale, the flow of (2.17) is given by

$$\begin{aligned} x' &= by_2 + cx + \mathrm{O}(y_2^2, xy_2, x^2), \\ y_2' &= -2ax + \mathrm{O}(x^2, xy_2), \end{aligned} \tag{2.19}$$

where the prime denotes the differentiation with respect to the new time $\tilde{t}$. System (2.19) is no more singular along the fold line L, and therefore we say it is *desingularized*. However, the removal of the singularity of (2.17) comes at the expense of changing the time direction of the solutions of (2.19) in the repelling region $x > 0$ by virtue of (2.18).
In (2.19), the origin is an equilibrium point, and its linear stability is identified by the real part of the eigenvalues of the Jacobian matrix: $\lambda_{1,2} = (c \pm \sqrt{c^2 - 8ab})/2$. The following lemma presents the possible stability properties that the origin of (2.19) may have.

Lemma 2.3 ([SW01]) *For $ab > 0$, the origin of (2.19) has the following non-degenerate types*

$$\begin{aligned} c > 0, 8ab < c^2 &\text{ unstable node}, \quad c > 0, c^2 < 8ab \text{ unstable focus}, \\ c < 0, 8ab < c^2 &\text{ stable node}, \quad c < 0, c^2 < 8ab \text{ stable focus}, \end{aligned}$$

while for $ab < 0$, the equilibrium is a saddle point. Furthermore, the origin has the following co-dimension one degenerate types for $c \neq 0$

$$\begin{aligned} ab = 0, a \neq 0 &\text{ saddle-node type I}, \\ ab = 0, b \neq 0 &\text{ saddle-node type I}, \\ 8ab = c^2 &\text{ degenerate node}. \end{aligned}$$

For $c = 0$ the only degenerate type occurs for $ab > 0$, and this is a centre.

Because of the time rescale (2.18), the non-desingularized system (2.17) has a *folded singularity* at the origin, that is either a folded node, folded focus, folded saddle, folded saddle-node or folded centre depending on the case considered in Lemma 2.3.

Definition 2.4 We say that a trajectory of the slow-flow is a *singular vrai canard*, if under the flow of (2.17) it moves from the attracting to the repelling side of the critical manifold. If instead it moves from the repelling to the attracting side, we say that it is a *singular faux canard*.

According to Definition 2.4, singular canard solutions exists for some of the folded singularities. A non-trivial example that shows singular canard solutions is given in chapter 4.

For $\varepsilon > 0$ sufficiently small, singular canard solutions of (2.17) persist in the original problem (2.16) [Ben83, Ben90]. An effective way to show their persistence is to consider the blow-up of (2.19), so that we can extend the flow of the attracting region C_a and of the repelling region C_r up to the fold line. In the blown-up space, we then consider an invariant subset identified by $\varepsilon = const.$ so that C_a and C_r perturb to the slow attracting $S_{a,\varepsilon}$ and slow repelling $S_{r,\varepsilon}$ manifolds, respectively [SW01]. The intersection of the two slow manifolds $S_{a,\varepsilon}$ and $S_{r,\varepsilon}$, extended to the fold line, determines an invariant line which corresponds to the perturbation of the singular canard solution for $0 < \varepsilon \ll 1$, and in some cases it is referred to as maximal canard. It follows that such solution flows along a repelling set for a time of O(1) in the slow timescale $t = \tau\varepsilon$, before leaving through an escaping fast fibre. Since the slow manifolds $S_{a,\varepsilon}$ and $S_{r,\varepsilon}$ are nonunique, but there are infinitely many of them in an interval $\mathrm{O}(exp(-c/\varepsilon))$ with c some positive constant, then there are infinitely many canard solutions that stay close to the maximal canard on the repelling set for a finite time before escaping.

2.4 Non-smooth dynamical systems

Non-smooth systems are systems of the form

$$\dot{z} = Z(z), \qquad z(0) = z_0, \tag{2.20}$$

where $Z : \mathbb{R}^n \to \mathbb{R}^n$ is discontinuous on a set[1] $\Sigma := \{z \in \mathbb{R}^n \mid h(z) = 0\}$ for some $h : \mathbb{R}^n \to \mathbb{R}$ such that $\nabla h(z)|_{z\in\Sigma} \neq 0$, and the dot has the meaning of differentiation with respect to the time t. The *discontinuity set* Σ subdivides the space $\mathbb{R}^n$ into the domains $G^+ : \{z \in \mathbb{R}^n \mid h(z) > 0\}$ and $G^- : \{z \in \mathbb{R}^n \mid h(z) < 0\}$, so that $Z(z)$ can be written as

$$Z(z) = \begin{cases} Z^+(z), & z \in G^+, \\ Z^-(z), & z \in G^-, \end{cases} \tag{2.21}$$

and we assume $Z^{\pm}(z)$ to be sufficiently smooth in the respective domains of definition. Furthermore, a third smooth vector field may be specified on Σ. Non-smooth dynamical systems are important in describing some engineering problems, such as power electronics voltage converters [dBBC01, FHS09], mechanical systems with impact [Nor91] or friction [HOP98, GB99], or hybrid systems in control dynamics [HB03].

[1] For the case of multiple surfaces of discontinuity, we refer to [Fil88, §23]. In this thesis we do not consider discontinuity in the solutions, also called solutions with jumps.

2.4.1 Forward solutions of a non-smooth system

Consider a trajectory with initial condition in $z_0 \in G^+$ (or G^-) that under the evolution (2.21) intersects the discontinuity set Σ in a point z. Classical results on the existence and uniqueness of solutions require Lipschitz continuity of the vector field, but this is lost at Σ, where $Z(z)$ is discontinuous. Hence, the question is how to continue the solution from z. It makes sense that the forward solution, if it exists, may depend on the local values of the vector fields $Z^{\pm}(z)$ around $z \in \Sigma$, as well as, on the vector field that may be defined on Σ.
In the following we introduce two different concepts of forward solution for a non-smooth system, and we show the difference between the two with an illustrative example. We do not consider solutions in backwards time since, as we shall see, the information of where the trajectory comes from, is easily lost at the discontinuity.

Carathéodory solutions A Carathéodory solution is the natural generalization of the concept of solution of a smooth system, to the case of a system with discontinuous right-hand side.
If the vector field $Z(z)$ was continuous everywhere, then its solution $z(t)$ would satisfy

$$z(t) = z_0 + \int_0^t Z(z(s))\,\mathrm{d}s, \quad t \in [0, T]. \tag{2.22}$$

An absolutely continuous function $z(t) : [0, T] \to \mathbb{R}^n$ is a Carathéodory solution of (2.20), if it satisfies (2.22) for almost all $t \in [0, T]$. Thus the integral in (2.22) is interpreted as a Lebesgue integral. In other words, the tangent vector of $z(t)$ can differ from the vector field $Z(z)$ only in a time set of measure zero.

We show with an example how to compute Carathéodory solutions in practice. Consider the system $\dot{z} = Z(z)$ of Figure 2.3(a), with $Z : \mathbb{R}^2 \to \mathbb{R}^2$ given by

$$Z(x, y) = \begin{cases} (1, x)^T, & y > 0, \\ (0, 1)^T, & y < 0, \end{cases} \tag{2.23}$$

and $z = (x, y)^T$. This system is discontinuous in $\Sigma = \{y = 0\}$, so that $\mathbb{R}^2$ is separated into the two domains $G^+ = \{y > 0\}$ and $G^- = \{y < 0\}$. Let $Z^{\pm}(x, y)$ be the vector field $Z(x, y)$ restricted to $G^{\pm}$ and extended continuously to its closure at $y = 0$.
The point $F = (0, 0) \in \Sigma$ is called a *fold point*, since the orbit $y = x^2/2$ of $Z^+(z)$ has a quadratic tangency with Σ at F, while $Z^-(F) \neq 0$ [GST11, Kri17]. The point F separates Σ into the half line

$$\Sigma^{cr} := \Sigma \cap \{x > 0\},$$

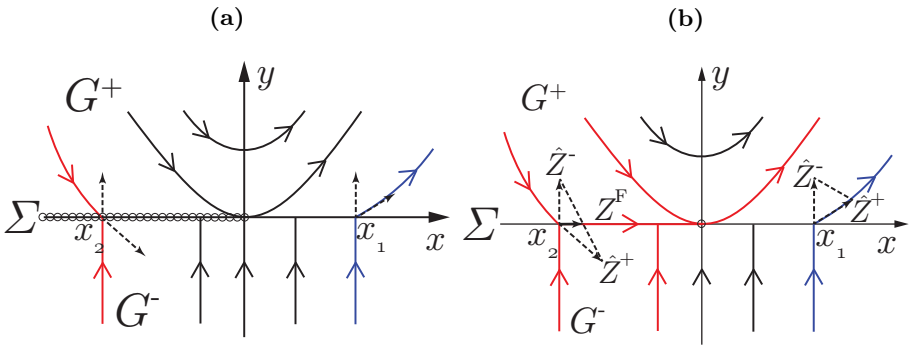

Figure 2.3: Solutions of (2.23) by using the Carathéodory definition of solution (a), and Filippov's convex method (b). In blue: a *crossing* trajectory. This is constructed in the same way for both definitions. In red: two trajectories that reach Σ in finite time. At $(x_2, 0)$ there is no forward Carathéodory solution but, according to Filippov's method, there is a *sliding* solution that escapes Σ at the point of singularity in the origin [Fil88, 2a. §19].

where both $Z^{\pm}(z)$ point into G^+ and the half line

$$\Sigma^{sl} := \Sigma \cap \{x < 0\},$$

where $Z^+(z)$ points towards G^- while $Z^-(z)$ points towards G^+, see Figure 2.3(a). In Σ^{sl}, neither Z^+ nor Z^- point towards their own region of definition, and we cannot make sense of (2.22) in this set. Hence, every orbit, that under the flow of (2.23) intersects Σ in Σ^{sl}, has no forward Carathéodory solution from Σ^{sl}, see the red orbits of Figure 2.3(a). On the other hand, Z^+ points towards its own region of definition in Σ^{cr}. Therefore the forward Carathéodory solution departing from a point $z_0 \in G^-$, that under the flow of (2.23) intersects Σ in Σ^{cr}, must follow the vector field Z^+ from there on, see the blue orbit in Figure 2.3(a).

This example shows that Carathéodory solutions are obtained by extending $Z^{\pm}(z)$ up to the closure of the respective region of definition, and then by gluing them together. If a further vector field was defined within Σ, there may have been subsets of Σ where forward solutions were nonunique. Systems with stiction friction show nonuniqueness at Σ, and this is discussed in chapter 4.

We have seen that sometimes forward Carathéodory solutions may not exist. To overcome this problem, one may decide to define a vector field within the region of discontinuity, in a way that depends on the local behaviour of $Z^{\pm}(z)$ around the discontinuity. This is the underlining idea of Filippov's method.

Filippov solutions Filippov's idea is to replace (2.21) by a differential inclusion of the form

$$\dot{z} \in \mathcal{Z}(z), \quad z(t_0) = z_0, \tag{2.24}$$

where $\mathcal{Z}(z)$ is constructed as follows. In points z where the function $Z(z)$ is continuous, the set $\mathcal{Z}(z)$ coincides with the function $Z(z)$ at this point. If some point z belongs to the set of discontinuity Σ, then $\mathcal{Z}(z)$ is constructed in some other way, and the simplest method is to use a linear convex combination of $Z^+(z)$ and $Z^-(z)$. We refer to [Fil88, §4] for a discussion of other methods for constructing $\mathcal{Z}(z)$ in Σ.

Filippov's convex method, defines the set $\mathcal{Z}(z)$ at the point $z \in \Sigma$ as the set of vectors belonging to the *convex combination* of $\hat{Z}^+(z)$ and $\hat{Z}^-(z)$, where

$$\hat{Z}^+(z) = \lim_{\substack{z^* \in G^+ \\ z^* \to z}} Z^+(z^*), \quad \hat{Z}^-(z) = \lim_{\substack{z^* \in G^- \\ z^* \to z}} Z^-(z^*).$$

Which vector field should we choose among the ones that belong to the set $\mathcal{Z}(z)$? We discuss two cases.
If $\mathcal{Z}(z)$ lies entirely on one side of Σ, say G^+, then any $Z(z) \in \mathcal{Z}(z)$ can be chosen. A solution departing from G^-, that under the forward flow of $Z^-(z)$ intersects Σ in such point z, *crosses* Σ in a time of measure zero, and then follows $Z^+(z)$, where the solution is interpreted in a Carathéodory sense.
If $\mathcal{Z}(z)$ intersects Σ, Filippov's method selects the vector $Z^{sl}(z) \in \mathcal{Z}(z)$, that is tangent to the discontinuity set Σ in z, that is

$$Z^{sl}(z) = \lambda Z^+(z) + (1-\lambda) Z^-(z), \tag{2.25}$$

where

$$\lambda = \frac{\nabla h(z) \cdot Z^-(z)}{\nabla h(z) \cdot (Z^-(z) - Z^+(z))}.$$

The solution $z(t)$ that satisfies $\dot{z} = Z^{sl}(z)$ is the solution of $\dot{z} = Z(z)$ by virtue of (2.24), and it is referred to as *sliding motion*. The sliding motion is stable (unstable) if both $Z^{\pm}$ point towards (away from) Σ^{sl}. If the motion is unstable, solutions may leave Σ^{sl} at any forward time, hence nonuniqueness appears.

Because of (2.25), we refer to Filippov's method as Filippov's *linear* convex combination, and the vector field is of *Filippov-type*. If a system does not follow Filippov's method at the discontinuity, we say that it is non-Filippov, and an example of such system is considered in chapter 4. The case where nonlinear terms in λ are added in (2.25) is mentioned in [Fil88, §4] and has been the subject of recent studies by Jeffrey [Jef14].

We recall example (2.23) and look to how the solutions of the system change by using Filippov's convention. In $z \in \Sigma^{cr}$ the set $\mathcal{Z}(z)$ lies entirely on G^+.

Therefore, the Filippov solution departing from G^- and intersecting Σ^{cr} at z, *crosses* Σ and continues on G^+ by following $Z^+(z)$.
At a point $z \in \Sigma^{sl}$ the set $\mathcal{Z}(z)$ intersects Σ. According to Filippov's method the solution $z(t)$ *slides* and satisfies $\dot{z} = Z^{sl}(z)$ where

$$Z^{sl} = \lambda(1,x)^T + (1-\lambda)(0,1)^T = \left(\frac{1}{1-x}, 0\right)^T,$$

and $\lambda = 1/(1-x)$. The sliding region Σ^{sl} is backwards nonunique: once the orbits land on Σ^{sl}, the information of when the orbit has landed is lost. Once $z(t)$ reaches the fold point $F = (0,0)$, it lifts off and follows $Z^+(z)$. According to Filippov's notation, $F = (0,0)$ is a point of singularity and not an equilibrium point [Fil88, 2a.§19].

Remark 2.5 *Solutions of a non-smooth system can be backwards nonunique, as in example (2.23), or forward nonunique, as in the case of the two-fold singularity [CJ11, KH15b], once they land on the discontinuity set. Slow-fast systems (2.1) also loose the information of where the solution comes from, at the singular limit $\varepsilon = 0$. In this case, the layer and the reduced problem are in fact disconnected and one constructs* candidate *solutions in forward time by piecing together segments of the layer problem with segments of the reduced problem [Ben90]. However for $0 < \varepsilon \ll 1$, solutions of (2.1) recover the uniqueness and they are everywhere well defined, but at the price of possibly being exponentially sensitive to the initial conditions.*

By comparing the Carathéodory and Filippov solutions of (2.23), we conclude that the two solutions coincide in regions of crossing. In contrast, Carathéodory solutions do not exist in sets where $Z^{\pm}$ point outside of their own regions of definition, while Filippov's method resolves the problem by introducing a sliding vector field. However Filippov's method does not take into account that a vector field may be pre-defined along Σ, and in such cases Carathéodory's notion may give a meaningful way of continuing solutions while Filippov's method may fail. A non trivial example of such case is considered in chapter 4.

2.5 Regularization of non-smooth vector fields

The previous section indicates that the analysis of non-smooth systems can be quite difficult, since even the notion of solution is not straightforward, and the existence and uniqueness of solutions is not guaranteed. Furthermore, it is challenging to understand perturbations of non-smooth systems, and to define what do we mean by a generic bifurcation in a non-smooth context [Kue15,

§19.3]. Therefore, it makes sense to consider a *smoothed* version of the problem, that means, we want to smoothen out the discontinuous vector field (2.20) in a small region of size $\mathrm{O}(\varepsilon)$, $0 < \varepsilon \ll 1$, around the discontinuity Σ. Regularization has been useful in the study of the fold singularity [BRMS16] and of the two-fold singularity [KH15a, KH15b] to name a few.

We consider the definition of *regularization* of the vector field $Z(z)$ (2.21) introduced by Sotomayor and Texeira [ST96]. This is a 1-parameter family $Z_\varepsilon(z)$ of smooth vector fields

$$Z_\varepsilon(z) := \frac{1}{2}Z^+(z)\left(1+\phi\left(\varepsilon^{-1}h(z)\right)\right) + \frac{1}{2}Z^-(z)\left(1-\phi\left(\varepsilon^{-1}h(z)\right)\right), \tag{2.26}$$

for $0 < \varepsilon \ll 1$. The function ϕ is called the *regularization function* and it can be constructed in different ways. In particular, ϕ is intrinsically related to the modelling, and thus the physics, of the original problem. A way to check whether ϕ is a good regularization function for the model considered, is to check if, given $z(t)$ a solution of the discontinuous problem (2.21), there exists a sequence of smooth solutions $z_\varepsilon(t)$ of $\dot{z}_\varepsilon = Z_\varepsilon(z)$ that is uniformly converging to $z(t)$ as $\varepsilon \to 0$ [LT97, Col17].

For systems of Filippov-type, the set C^k_{ST} of Sotomayor-Teixeira (ST) regularization functions $\phi \in C^k, k \geq 1$ is successful. These functions satisfy two conditions [Kri17], namely finite deformation

$$\phi(s) = \begin{cases} 1, & s \geq 1, \\ \in (-1,1), & s \in (-1,1), \\ -1, & s \leq -1, \end{cases} \tag{2.27}$$

and monotonicity

$$\phi_s(s) > 0 \quad \text{within} \quad s \in (-1,1).$$

Other classes of regularization functions can be considered instead of (2.27). In [GST11] the authors have used a piecewise linear function for ϕ. Otherwise, one may relax the condition $\phi(s) \in (-1,1)$ for $s \in (-1,1)$ of (2.27), as we do in chapter 4. Finally, analytic functions such that $\phi(s) \to \pm 1$ for $y \to \pm 1$ may also be used. In [Kri17], the author shows that regularizing the vector field either with an analytic or a C^k_{ST} function for ϕ, gives the same results. However, in the case of an analytic function the analysis is more complicated, as it is necessary to consider (2.26) as the vector field in chart K_2 of a blown-up space and the analysis of other two charts is needed to connect the dynamics to that of the discontinuous system outside of the region of regularization.

The *regularized problem* $\dot{z}_\varepsilon = Z_\varepsilon(z)$ is singular for $\varepsilon \to 0$ on $h(z) = 0$, because of (2.26). In certain cases, it is possible to rewrite the problem as a slow-fast system of the type (2.1) with small parameter ε, by using a blow-up of $h(z) = 0$ and

eventually some coordinate transformation. This has been shown in [BdST06] for the class of C^k_{ST} regularizations. Clearly, if we can rewrite the regularized problem as a slow-fast system, then the machinery of geometric singular perturbation theory turns useful into the study of the regularized problem. Most importantly, if ϕ is well chosen, then the layer problem describes the same dynamics of the vector fields $Z^{\pm}$, and the reduced problem describes the vector field within Σ. This observation motivates the study of the smooth, regularized problem, in order to understand the original non-smooth system. *The idea is indeed to study the regularized problem by using Fenichel's theory and the blow-up method in a setting where we have a well defined notion of solution, and in this way to construct solutions of the original discontinuous system for* $\varepsilon = 0$.

In chapter 4, we will show that the regularization of a non-Filippov problem of a mass-spring oscillator with stiction friction turns into a slow-fast problem of the type (2.1), for an appropriate choice of the regularization function ϕ. The original non-smooth system has forward nonunique Carathéodory solutions along two lines on Σ, and these lines correspond to two fold lines of the critical manifold for the regularized problem. We will show that along the fold lines there are some special points where canard solutions of saddle type appear, and that these canards are related to some of the nonunique solutions of the original non-smooth system.

Chapter 3

Slow-fast analysis of a model for earthquake faulting

In this chapter we consider a one-dimensional spring-block model with Ruina's state law describing earthquake faulting. By using geometric singular perturbation theory and the blow-up method, we provide a detailed description of the periodicity of the earthquake episodes. In particular, we show that the limit cycles arise from a degenerate Hopf bifurcation, whose degeneracy is due to an underlying Hamiltonian structure that leads to large amplitude oscillations. We use a Poincaré compactification to study the system near infinity. At infinity, the critical manifold loses hyperbolicity with an exponential rate. We use an adaptation of the blow-up method to recover the hyperbolicity. This enables the identification of a new attracting manifold, that organises the dynamics at infinity. This in turn leads to the formulation of a conjecture on the behaviour of the limit cycles as the timescale separation increases. We illustrate our findings with numerics, and suggest an outline of the proof of the conjecture.

3.1 Introduction

Earthquake events are a non-linear multi-scale phenomenon. Some of the non-linear occurrences are fracture healing, repeating behaviour and memory effects

[Rui83, Hea90, VECM94, Mar98b]. In this chapter we focus on the repeating behaviour of the earthquake cycles, where a cycle is defined as the combination of a rupture event with a following healing phase. An earthquake rupture consists of the instantaneous slipping of a fault side relative to the other side. The healing phase allows the fault to strengthen again, and this process evolves on a longer timescale than the rupture event [CL89, Mar98a].

The repetition of the earthquake events is significant for the predictability of earthquake hazards. The data collected in the Parkfield experiment in California show evidence of recurring micro-earthquakes [NM99, MVE95, Biz10, ZN12]. For large earthquakes it is harder to detect a repeating pattern from the data, even though recent works indicate the presence of recurring cycles [BZ08].

The one-dimensional spring-block model, together with the empirical Ruina friction law, is a fundamental model to describe earthquake dynamics [BK67, Rui83, RR83, GRRT84, RT86, CLST91, BB96, FXN+14]. Although the model does not represent all the non-linear phenomena of an earthquake rupture, it still reproduces the essential properties of the fault behaviour, as extrapolated from experiments on rocks. The dimensionless form of the model is

$$\begin{aligned} \dot{x} &= -\,\mathrm{e}^{z}\,(x + (1+\alpha)z)\,, \\ \dot{y} &= \mathrm{e}^{z} - 1, \\ \varepsilon\dot{z} &= -\,\mathrm{e}^{-z}\left(y + \frac{x+z}{\xi}\right), \end{aligned} \tag{3.1}$$

where x is related to the friction force, y is related to the displacement of the block, and z to its velocity. Numerically, it has been observed that (3.1) has periodic solutions corresponding to the recurrence of the earthquake episodes, as shown in Figure 3.1 for two different values of the parameter ε and $\alpha > \xi$ fixed. The steep growth of the y-coordinate corresponds to the earthquake rupture, while the slow decay corresponds to the healing phase. Hence, the periodic solutions of (3.1) have a multiple timescale dynamics. Furthermore, in Figure 3.1 we observe that the amplitude of the oscillations increases for decreasing values of the timescale separation ε. For these reasons extensive numerical simulations are difficult to perform in the relevant parameter range, that is $\varepsilon \in [10^{-24}, 10^{-8}]$ [RT86, CL89, MC96, LRBZZ00, EBL08, EBL11]. The numerical simulations of Erickson *et al* [EBL08] suggest that, for fixed $\varepsilon > 0$, the periodic solutions of (3.1) occur in a finite interval of values $\alpha > \xi$. If α is much larger than ξ, then chaotic dynamics may appear.
It is the purpose of the present chapter to initiate a rigorous mathematical study of (3.1) as a singular perturbation problem [Jon95, Kap99]. At the singular limit $\varepsilon = 0$, we find an unbounded *singular cycle* when $\alpha > \xi$. For $\varepsilon > 0$, we conjecture this cycle to perturb into a stable, finite amplitude limit cycle that explains the behaviour of Figure 3.1. In this way we can predict the periodic solutions of

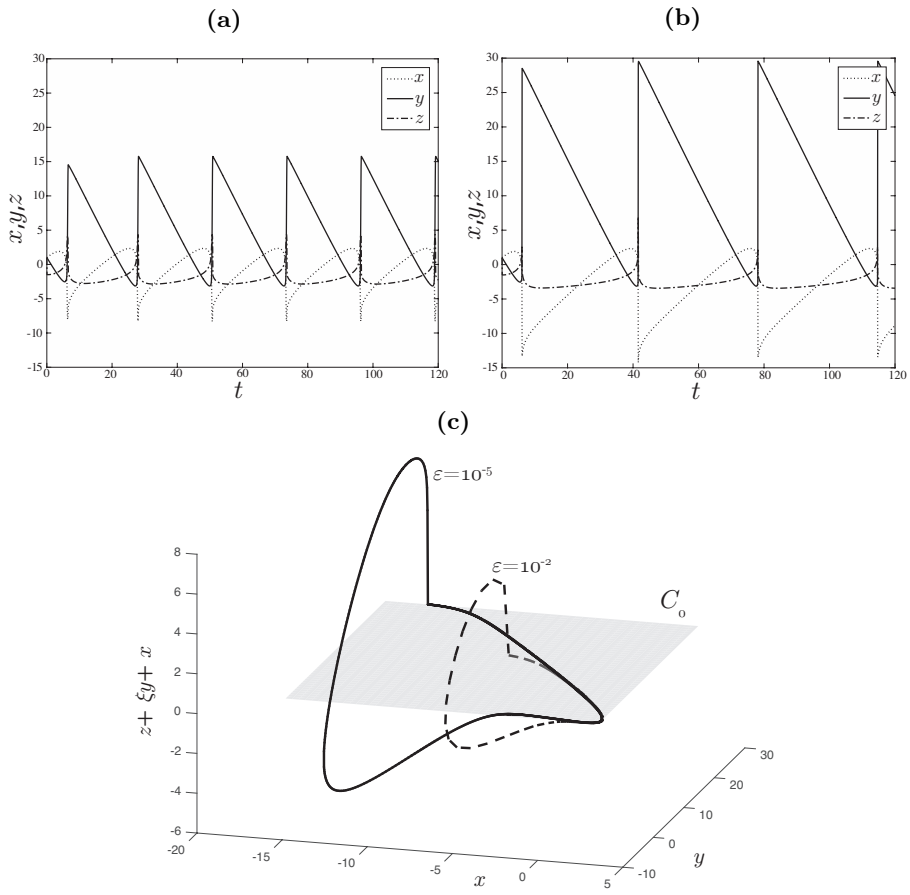

Figure 3.1: Numerical simulations of (3.1) for $\alpha = 0.9$ and $\xi = 0.5$. In (a): $\varepsilon = 10^{-2}$. In (b): $\varepsilon = 10^{-5}$. In (c): phase space of both simulations. The grey plane C_0 and the coordinate $z + \xi y + x$ are clarified in section 3.3.

(3.1) even in parameter regions that are not possible to explore numerically. We expect that the deeper understanding of (3.1) that we provide, together with the techniques that we introduce, can be of help to study the continuum formulation of the Burridge and Knopoff model, in particular regarding the analysis of the Heaton pulses [Hea90].

As we will see in section 3.3, in our analysis the critical manifold loses normal hyperbolicity at infinity with an exponential rate. This is a non-standard loss of hyperbolicity that also appears in other problems [RDKL11]. To deal with

this issue we will first introduce a compactification of the phase space with the Poincaré sphere [Chi06, §1.8] and repeatedly use the blow-up method of Dumortier and Roussarie [DR96] in the version of Krupa and Szmolyan [KS01a]. In particular we will use a technique that has recently been developed in [Kri17]. For an introduction to the blow-up method we refer to [Kue15, §7].

Another way to study system (3.1) when $\varepsilon \ll 1$ is by using the method of matched asymptotic expansions, see [Eck73] for an introduction. Putelat *et al* [PWD08] have matched the different timescales of (3.1) by using an energy conservation argument, while Pomeau and Berre [PB11] have found a condition that describes the intermediate phases between the two scales.

This chapter is structured as follows. In section 3.2 we briefly discuss the physics of system (3.1). In section 3.3 we set (3.1) in the formalism of geometric singular perturbation theory, and in section 3.4 we consider the analysis of the reduced problem for fixed ξ and $\varepsilon = 0$. Here, a degenerate Hopf bifurcation appears for $\alpha = \xi$, whose degeneracy is due to an underlying Hamiltonian structure that we identify. We derive a bifurcation diagram in section 3.5, after having introduced a compactification of the reduced problem. From this and from the analysis of section 3.6, we conclude that the limit cycles of Figure 3.1 cannot be described by the sole analysis of the reduced problem. In section 3.7 we define a candidate *singular cycle* Γ_0 for $\alpha > \xi$, that is used in our main result: Conjecture 3.16. This conjecture is on the existence of limit cycles $\Gamma_\varepsilon \to \Gamma_0$ for $\varepsilon \to 0$ and fixed α, where $\alpha > \xi$. The conjecture is supported by numerical simulations, but in section 3.8 we also lay out the foundation of a proof by using the blow-up method to gain hyperbolicity of Γ_0 at the singular limit. This analysis constitutes the foundation for the construction of the Poincaré map of section 3.9, that is needed to prove Conjecture 3.16. Finally, in section 3.10 we conclude and summarise the results of this chapter and in section 3.11 we outline possible future work directions by setting our problem in the larger context of rate-and-state friction laws.
Sections 3.2–3.7 and 3.10 are based on the results published in [BBK17b]. This is a manuscript focusing only on the singular limit analysis of the problem of earthquake faulting. Section 3.8 adds more detail to the analysis of [BBK17b] and sections 3.9 and 3.11 are new.

3.2 Model

The one-dimensional spring-block model is presented in Figure 3.2. We suppose that one fault side slides at a constant velocity v_0 and drags the other fault side of mass M through a spring of stiffness κ. The friction force $F_\mu = \sigma\mu$ acts

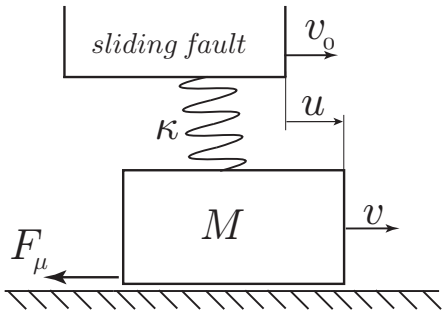

Figure 3.2: Spring-block model describing earthquake faulting.

against the motion. A common assumption is to suppose that the normal stress σ, i.e. the stress normal to the friction interface [Nak01], is constant: $\sigma = 1$. The friction coefficient μ is modelled with the Ruina rate-and-state friction law $\mu = \mu(v, \theta)$, with v the sliding velocity and θ the *state* variable. The state θ accounts for how long the two surfaces have been in contact [Rui83, Mar98b]. The equations of our model are

$$\begin{aligned} \theta' &= -\frac{v}{L}\left(\theta + b\ln\left(\frac{v}{v_0}\right)\right), \\ u' &= v - v_0, \\ Mv' &= -\kappa u - \left(\theta + a\ln\left(\frac{v}{v_0}\right)\right), \end{aligned} \tag{3.2}$$

where the variable u is the relative displacement between the two fault sides and the prime denotes the time derivative. The parameter L is the characteristic displacement that is needed to recover the contact between the two surfaces when the slip occurs, while a and b are empirical coefficients that depend on the material properties [Mar98b]. We introduce the dimensionless coordinates (x, y, w, t) into system (3.2), where $\theta = ax,\ u = Ly,\ v = v_0 w,\ \tilde{t} = (L/v_0)t$

$$\begin{aligned} \dot{x} &= -w\left(x + (1+\alpha)\ln(w)\right), \\ \dot{y} &= w - 1, \\ \varepsilon\dot{w} &= -y - \frac{x + \ln(w)}{\xi}. \end{aligned} \tag{3.3}$$

We notice that equation (3.3) has a singularity in $w = 0$, and to avoid it, we henceforth introduce the variable $z = \ln(w)$, so that we obtain the formulation presented in (3.1). In system (3.3) we have introduced the parameters: $\varepsilon = Mv_0^2/(\kappa L^2)$ such that $1/\sqrt{\varepsilon}$ is a non-dimensional frequency, $\xi = (\kappa L)/a$: the non-dimensional spring constant and $\alpha = (b-a)/a$: the sensitivity to the velocity relaxation [EBL08]. We consider the parameter values presented by Madariaga

[Mad98]: $\varepsilon \in [10^{-24}, 10^{-8}]$, $\xi = 0.5$, $\alpha > \xi$. An extensive reference to the parameter sets is in the work of Dieterich [Die72, Die78, Die79]. We choose to keep the parameter $\xi > 0$ fixed (selecting $\xi = 0.5$ in our computations) and we use α as the bifurcation parameter. With this choice, the study of (3.1) as a singular perturbation problem is simplified. Indeed, as we will see in section 3.3, the critical manifold of (3.1) is a surface that depends on ξ. The results of our analysis can be easily interpreted for the case of α fixed and ξ varying, that is the standard approach in the literature.

Extensions of the one-dimensional spring-block model The Burridge and Knopoff (B-K) model [BK67] idealises the fault as a chain of spring-blocks of the type of Figure 3.2. In particular, each block is connected to the sliding fault by a spring of stiffness κ_λ, while a spring of stiffness κ_μ connects two neighbouring blocks, that are Δs distant [EBL11], see Figure 3.3. It follows that (3.2) is the simplest version of the B-K model, when only one block is considered. By letting the number of blocks in the chain to infinity, and by letting $\Delta s\,, M \to 0$, we obtain the continuum formulation of the B-K model

$$\begin{aligned} \frac{\partial \Theta}{\partial t} &= -\left(\frac{\partial U}{\partial t} + 1\right)\left(\Theta + (1+\alpha)\ln\left(\frac{\partial U}{\partial t} + 1\right)\right), \\ \frac{\partial^2 U}{\partial t^2} &= c^2 \frac{\partial^2 U}{\partial s^2} - \gamma_\lambda^2 U - \frac{\gamma_\mu^2}{\xi}\left(\Theta + \mu_0 + \ln\left(\frac{\partial U}{\partial t} + 1\right)\right), \end{aligned} \tag{3.4}$$

where Θ accounts for the state of the friction, and U is associated to the fault displacement [EBL11]. The parameter c is the speed of sound in the material, μ_0 is the steady state friction coefficient for a fault sliding at the velocity of the driving plate, and $\gamma_{\lambda,\mu}$ are the non-dimensional frequencies of $\kappa_{\lambda,\mu}$ respectively. A travelling wave solution of (3.4)

$$\begin{aligned} \Theta(s,t) &= X(\eta(s,t)), \\ U(s,t) &= Y(\eta(s,t)) - \frac{\gamma_\mu^2}{\gamma_\lambda^2 \xi}\mu_0, \end{aligned}$$

with $\eta(s,t) = s + kt$, solves the ODE

$$\begin{aligned} kX' &= -(kY'+1)\left(X + (1+\alpha)\ln(kY'+1)\right), \\ k^2 Y'' &= c^2 Y'' - \gamma_\lambda^2 Y - \frac{\gamma_\mu^2}{\xi}\left(X + \ln(kY'+1)\right), \end{aligned}$$

where the prime denotes the differentiation with respect to η. By introducing the rescaling $W = kY' + 1$, $\hat{t} = \eta/k$, and $\hat{\varepsilon} = (k^2 - c^2)/k^2\gamma_\lambda^2$, $\hat{\xi} = \gamma_\lambda^2 \xi/\gamma_\mu^2$, we

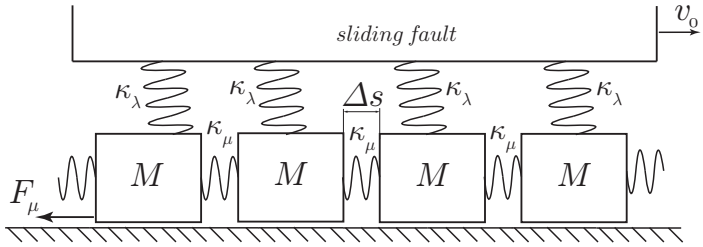

Figure 3.3: The Burridge and Knopoff model.

obtain a system of three first-order differential equations

$$\begin{aligned} \dot{X} &= -W\left(X + (1+\alpha)\ln(W)\right), \\ \dot{Y} &= W - 1, \\ \hat{\varepsilon}\dot{W} &= -Y - \frac{X + \ln(W)}{\hat{\xi}}, \end{aligned}$$

that has the same structure of (3.3), and where the dot has the meaning of differentiation with respect to the time $\hat{t}$. This result further motivates the study of the one-dimensional spring-block model: periodic solutions of (3.3) correspond to travelling wave train solutions of (3.4). These travelling wave train solutions may explain the traveling slip pulses of earthquake ruptures [Hea90].

3.3 Singular perturbation approach to the model

The positive constant $\varepsilon \ll 1$ in system (3.1) measures the separation of two timescales. In particular the variables (x, y) are slow, while z is fast. We call equation (3.1) the *slow problem*, and the dot refers to the differentiation with respect to the slow time t. We introduce the fast time $\tau = t/\varepsilon$ to obtain the *fast problem*

$$\begin{aligned} x' &= -\varepsilon\, \mathrm{e}^z (x + (1+\alpha)z), \\ y' &= \varepsilon\left(\mathrm{e}^z - 1\right), \\ z' &= -\,\mathrm{e}^{-z}\left(y + \frac{x+z}{\xi}\right), \end{aligned} \tag{3.5}$$

where the prime stands for differentiation with respect to τ. The two systems (3.1) and (3.5) are equivalent whenever $\varepsilon > 0$. In the singular analysis we consider two different limit systems. By setting $\varepsilon = 0$ in (3.1) we obtain the

reduced problem

$$\begin{aligned} \dot{x} &= -\mathrm{e}^{z}(x + (1+\alpha)z), \\ \dot{y} &= \mathrm{e}^{z} - 1, \\ 0 &= -\mathrm{e}^{-z}\left(y + \frac{x+z}{\xi}\right), \end{aligned} \tag{3.6}$$

that is also referred in the literature as the quasi-static slip motion (specifically $M \to 0$ in (3.2), [Rui83]). Setting $\varepsilon = 0$ in (3.5) gives the *layer problem*

$$z' = -\mathrm{e}^{-z}\left(y + \frac{x+z}{\xi}\right), \quad (x,y)(\tau) = (x^0, y^0). \tag{3.7}$$

System (3.7) has a plane of equilibrium points that we denote the *critical manifold*

$$C_0 := \left\{(x,y,z) \in \mathbb{R}^3 \,\middle|\, z = -x - \xi y\right\}.$$

This manifold, depicted in grey in Figure 3.1(c), is attracting

$$\left.\frac{\partial z'}{\partial z}\right|_{C_0} = -\xi^{-1}\,\mathrm{e}^{-z} < 0. \tag{3.8}$$

The results by Fenichel [Fen74, Fen79] guarantee that compact subsets of C_0 perturb into attracting (due to (3.8)) slow-manifolds S_ε, for ε sufficiently small. However we notice in (3.8) that C_0 loses its normal hyperbolicity at an exponential rate when $z \to +\infty$. This is a key complication: orbits leave a neighbourhood of the critical manifold even if it is formally attracting. This is a non-standard loss of hyperbolicity that appears also in other physical problems [RDKL11]. To our knowledge, [Kri17] is the first attempt on a theory of exponential loss of hyperbolicity. In section 3.8 we will apply the method described in [Kri17] to resolve the loss of hyperbolicity at infinity. In the case of loss of hyperbolicity at an algebraic rate, like in the autocatalator problem originally studied by Gucwa and Szmolyan [GS09], we refer to the work of Kuehn [Kue14].

The following analysis will show that the study of the singular perturbation problem (3.1) is further complicated by the presence of both the exponential and the linear term in z. In particular, the linear term corresponds in the physical variables to $z = \ln(w)$, where the logarithmic function is derived from the interpolation of data of real earthquakes [Mar98b].

Naïvely we notice that when $z \gg 1$, the dynamics of system (3.1) is driven by a new timescale, that is not related to its slow-fast structure. Assuming $z \gg \ln \varepsilon^{-1}$, we can rewrite (3.1) as

$$\begin{aligned} \dot{x} &= -x - (1+\alpha)z, \\ \dot{y} &= 1, \\ \dot{z} &= 0, \end{aligned} \tag{3.9}$$

where we have further rescaled the time by dividing the right-hand side by e^z and ignored the higher order terms. Hence in this regime there is a family of x-nullclines

$$x + (1 + \alpha)z = 0, \tag{3.10}$$

that are attracting since $\partial\dot{x}/\partial x = -1$. This naïve approach is similar to the one used by Rice and Tse [RT86] to describe the different timescales that appear in system (3.1).

3.4 Reduced problem

We write the reduced problem (3.6) as a vector field $f_0(y, z; \alpha)$, by eliminating x in (3.6)

$$f_0(y, z; \alpha) := \begin{cases} \dot{y} &= e^z - 1, \\ \dot{z} &= \xi + e^z (\alpha z - \xi y - \xi). \end{cases} \tag{3.11}$$

From now on we identify the (y, z)-plane of the reduced problem with C_0. The following proposition describes the degenerate Hopf bifurcation at the origin of (3.11) for $\alpha = \xi$.

Proposition 3.1 *The vector field (3.11) has an equilibrium point in $(y, z) = (0, 0)$, that undergoes a degenerate Hopf bifurcation for $\alpha = \xi$. In particular $f_0(y, z; \xi)$ is Hamiltonian, and it can be rewritten as*

$$f_0(y, z; \xi) = g(y, z) J \nabla H(y, z), \tag{3.12}$$

with

$$g(y, z) = \frac{e^{\xi y + z}}{\xi}, \tag{3.13a}$$

$$H(y, z) = -e^{-\xi y} \left(\xi y - \xi z + \xi + 1 - \xi e^{-z}\right) + 1, \tag{3.13b}$$

where J is the standard symplectic structure matrix: $J = \left[\begin{smallmatrix} 0 & 1 \\ -1 & 0 \end{smallmatrix}\right]$. The equilibrium point $(y, z) = (0, 0)$ corresponds to $H(y, z) = 0$, and is surrounded by a family of periodic orbits, parametrised by $H(y, z) \in]0, 1[$.

Proof. The linear stability analysis of (3.11) in the equilibrium point $(y, z) = (0, 0)$ gives the following Jacobian matrix

$$Df_0(0, 0; \alpha) = \begin{bmatrix} 0 & 1 \\ -\xi & \alpha - \xi \end{bmatrix}.$$

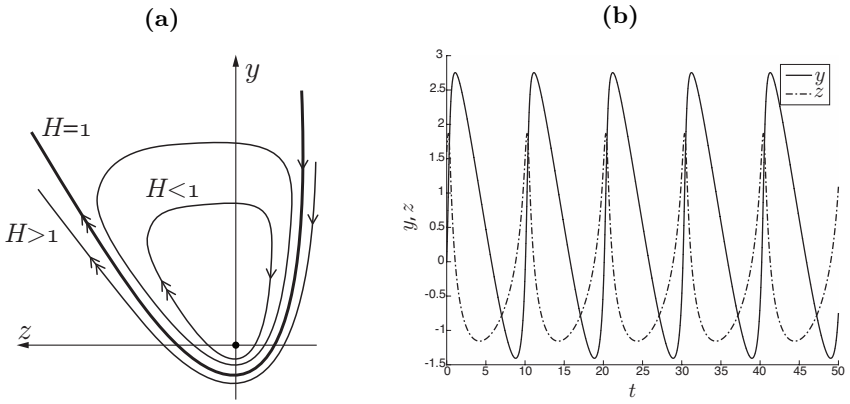

Figure 3.4: Behaviour of the reduced problem (3.12) for $\alpha = \xi$. In (a): phase space. The axis orientation is chosen in order to be consistent with the remaining figures of the chapter. In (b): simulation of (3.12) for $H = 0.4,\ \xi = 0.5$.

This matrix has determinant $\xi > 0$, and the trace is zero for $\alpha = \xi$. Hence a Hopf bifurcation occurs for $\alpha = \xi$. The direct substitution of (3.13) into (3.12) shows that (3.11) is Hamiltonian for $\alpha = \xi$. Therefore the Hopf bifurcation is degenerate. The intersection of the y-axis with the orbits $H(y, z) = h$ corresponds to the real roots of the Lambert equation

$$-\mathrm{e}^{-\xi y}(\xi y + 1) + 1 = h, \quad h \geq 0. \tag{3.14}$$

Equation (3.14) has a real root for any $h > 0$ in the region $y < 0$, while a second real root in the region $y > 0$ exists only for $h \in (0, 1)$ [CGH+96]. Thus, $(y, z) = (0, 0)$ is surrounded by periodic orbits for $H(y, z) \in]0, 1[$. □

The Hopf bifurcation of (3.11) for $\alpha = \xi$ is a known result [Rui83, PWD08, EBL08]. The function $H(y, z)$ has been used as a Lyapunov function in [GRRT84] without realising the Hamiltonian structure of (3.11).
From Proposition 3.1 we obtain a family of periodic orbits, all contained within $\alpha = \xi$. The phase space of (3.12) is illustrated in Figure 3.4(a) for positive values of $H(y, z)$. The intersection of the Hamiltonian trajectories with the y-axis is transversal for all $h > 0$, since the following condition holds:

$$\frac{\partial H}{\partial y}(y, 0) = \xi^2 y\, \mathrm{e}^{-\xi y} \neq 0, \quad \forall y \neq 0. \tag{3.15}$$

The trajectory identified with $H(y, z) = 1$ (that is in bold in Figure 3.4(a)) plays a special role since it separates the bounded orbits for $H \in (0, 1)$ from the unbounded ones for $H \geq 1$. Our analysis supports the results of Gu *et*

al [GRRT84] and contrasts [RR99] where it is claimed that (3.12) has no unbounded solutions.

Remark 3.2 *From* (3.15) *it follows that the function* $H(y,0)$ *defines a diffeomorphism between the points on the positive* y*-axis and the corresponding values* $h \in (0,1)$.

Figure 3.4(b) highlights that the reduced problem (3.12) has an intrinsic slow-fastness. Indeed the phase space of (3.12) is swept with different speeds depending on the region considered. This feature is represented in Figure 3.4(a), with the double arrow representing fast motion. In particular when $z > 0$ the trajectories are swept faster than for $z < 0$. This is due to the exponential term in (3.11). The fast sweep for $z > 0$ corresponds to the steep increase in the y coordinate of Figure 3.4(b). This fast dynamics for $z > 0$ resembles the slip that happens during an earthquake rupture, while the slow motion for $z < 0$ matches the healing phase, recall Figure 3.1. From this observation we tend to disagree with the terminology used in the literature, that calls the reduced problem the quasi-static slip phase [Rui83].
In order to describe the unbounded trajectories with $H(y,z) \geq 1$ for $y, z \to \infty$ and to extend the analysis to the case $\alpha \neq \xi$, we introduce a compactification of the reduced problem (3.11) and then we rewrite (3.11) on the Poincaré sphere.

3.5 Compactification of the reduced problem

We introduce the Poincaré northern hemisphere

$$\mathcal{S}^{2,+} := \{(Y,Z,W) \in \mathbb{R}^3 \big| \quad Y^2 + Z^2 + W^2 = 1, \quad W \geq 0\}.$$

The vector field on $\mathcal{S}^{2,+}$ is obtained as follows. First we write (3.11) as a vector field on the plane $W = 1$, using Y for y and Z for z. Then we project this vector field onto $\mathcal{S}^{2,+}$ by using central projection from the origin. We refer to [Chi06, §1.8] for further details. The plane $W = 1$ is now interpreted as the directional chart k_2

$$k_2 := \mathcal{S}^{2,+} \cap \{W > 0\}, \quad y_2 = \frac{Y}{W}, \; z_2 = \frac{Z}{W},$$

and the dynamics on chart k_2 follows directly from (3.11) by variable substitution

$$\begin{aligned} \dot{y}_2 &= \mathrm{e}^{z_2} - 1, \\ \dot{z}_2 &= \xi + \mathrm{e}^{z_2}\left(\alpha z_2 - \xi y_2 - \xi\right). \end{aligned} \tag{3.16}$$

By this construction, the (y_2, z_2)-plane is identified with the critical manifold C_0. The points at infinity in k_2 correspond to the condition $W = 0$, that is the

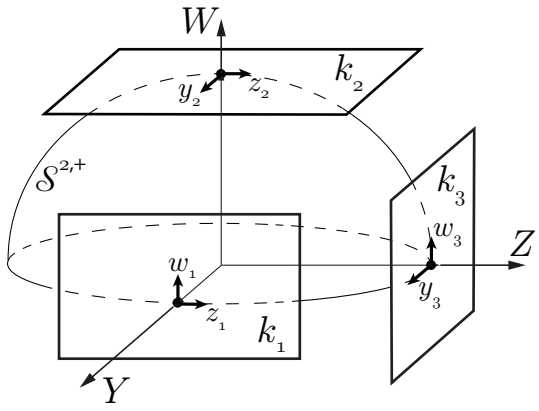

Figure 3.5: Poincaré sphere $\mathcal{S}^{2,+}$ and the directional charts $k_{1,2,3}$.

equator of $\mathcal{S}^{2,+}$. In reference to C_0, we shall therefore denote $W = 0$ by $C_{0,\infty}$ in the following. To study the dynamics on $C_{0,\infty}$ we introduce the two additional directional charts

$$k_3 := \mathcal{S}^{2,+} \cap \{Z > 0\}, \quad y_3 = \frac{Y}{Z}, w_3 = \frac{W}{Z},$$
$$k_1 := \mathcal{S}^{2,+} \cap \{Y > 0\}, \quad z_1 = \frac{Z}{Y}, w_1 = \frac{W}{Y}.$$

We follow the standard convention of Krupa and Szmolyan [KS01a] and use the subscript $i = 1, 2, 3$ to denote a quantity in chart k_i. We denote with k_{ij} the transformation from chart k_i to chart k_j for $i, j = 1, 2, 3$. We have the following change of coordinates

$$k_{23}: \quad w_3 = z_2^{-1}, \quad y_3 = y_2 z_2^{-1}, \tag{3.17a}$$
$$k_{21}: \quad w_1 = y_2^{-1}, \quad z_1 = z_2 y_2^{-1}, \tag{3.17b}$$
$$k_{31}: \quad w_1 = w_3 y_3^{-1}, \quad z_1 = y_3^{-1}, \tag{3.17c}$$

that are defined for $z_2 > 0$, $y_2 > 0$ and $y_3 > 0$ respectively. The inverse transformations $k_{ji} = k_{ij}^{-1}$ are defined similarly. Figure 3.5 shows a graphical representation of the sphere and of the directional charts.

Proposition 3.3 *There exists a time transformation that is smooth for $W > 0$ and that desingularizes the dynamics within $W = 0$, so that the reduced problem (3.11) has four equilibrium points $Q^{1,3,6,7}$ on $C_{0,\infty}$ where:*

- *Q^1 is an improper stable node with a single eigenvector tangent to $C_{0,\infty}$.*

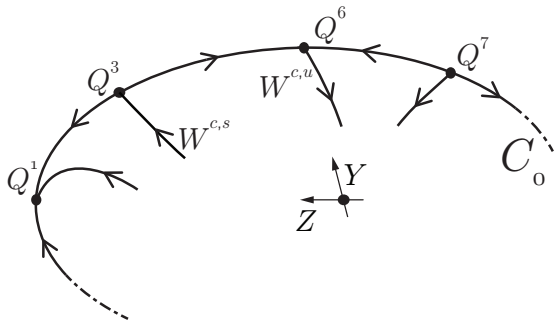

Figure 3.6: Equilibrium points on the compactified critical manifold C_0.

- *Q^3 has one unstable direction that is tangent to $C_{0,\infty}$ and a unique centre-stable manifold $W^{c,s}$.*
- *Q^6 has one stable direction that is tangent to $C_{0,\infty}$ and a unique centre-unstable manifold $W^{c,u}$.*
- *Q^7 is a proper unstable node.*

The stability properties of the equilibrium points are independent of α, in particular both $W^{c,s}$ and $W^{c,u}$ are smooth in α.

Figure 3.6 gives a topological representation of the statements of Proposition 3.3. The point Q^6 is actually a "0/0" singularity of the equations. We therefore obtain the picture in Figure 3.6 by blowing down two repeated blow-ups, and the details are available in subsection 3.5.2. We remark that we use superscripts as enumeration of the points $Q^m, m = 1, 3, 6, 7$ to avoid confusion with the subscripts that we have used to define the charts $k_i, i = 1, 2, 3$. The enumeration choice of the superscripts will become clear in section 3.7, where we will introduce the remaining points $Q^{2,4,5}$ in (3.45). In Proposition 3.4 we relate the structure at infinity of (3.11) to the dynamics on C_0 with respect to the parameter α.

Proposition 3.4 *Fix $c > 0$ sufficiently small and consider the parameter interval*

$$\alpha \in [\xi - c, \xi + c]. \tag{3.18}$$

Then Figure 3.7 describes the phase space of (3.11) with respect to α. In particular:

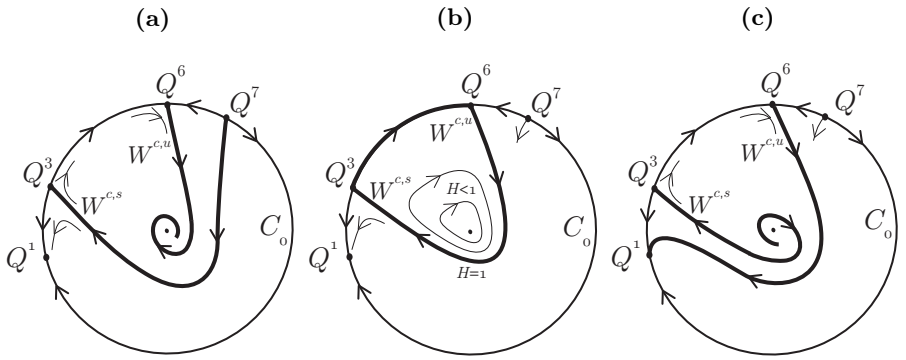

Figure 3.7: Bifurcation diagram of (3.11) with respect to the parameter α. Orbits spiral inwards for $\alpha < \xi$ (a) or outwards for $\alpha > \xi$ (c). In (b): $\alpha = \xi$.

- *When $\alpha < \xi$ the set $W^{c,s}$ separates the basin of attraction of $(y, z) = (0, 0)$ from the solutions that are forward asymptotic to Q^1.*
- *When $\alpha = \xi$ Proposition 3.1 holds. The set $H = 1$ corresponds to $W^{c,s} \cap W^{c,u}$.*
- *When $\alpha > \xi$ the set $W^{c,u}$ separates the solutions that are backwards asymptotic to the origin to the ones that are backwards asymptotic to Q^7.*

Therefore no limit cycles appear in the reduced problem for $\varepsilon = 0$ and $\alpha \neq \xi$.

Remark 3.5 *The local stability analysis of $(y, z) = (0, 0)$ can be directly obtained using $H(y, z)$ as a Lyapunov function. This is done by [GRRT84].*

In the rest of the section we prove the previous two propositions. In subsections 3.5.1 and 3.5.2 we perform an analysis of (3.11) in the two charts k_3 and k_1 respectively, to show Proposition 3.3. We prove Proposition 3.4 in subsection 3.5.3.

3.5.1 Chart k_3

We insert (3.17a) into the reduced problem (3.16) and obtain

$$\begin{aligned} \dot{w}_3 &= -w_3(\alpha - \xi y_3) + \xi w_3^2(1 - \mathrm{e}^{-\frac{1}{w_3}}), \\ \dot{y}_3 &= -y_3(\alpha - \xi y_3) + w_3(1 + \xi y_3)(1 - \mathrm{e}^{-\frac{1}{w_3}}), \end{aligned} \tag{3.19}$$

where we have divided the right-hand side by $\exp(1/w_3)$ to desingularize $w_3 = 0$.

Remark 3.6 *The division by* $\exp(1/w_3)$ *in* (3.19) *is formally performed by introducing the new time* t_3 *such that*

$$\mathrm{d}t_3 = \exp(1/w_3)\mathrm{d}t. \tag{3.20}$$

A similar desingularisation procedure is also used in the blow-up method.

System (3.19) has two equilibrium points

$$Q^1 := \quad (w_3, y_3) = (0, 0), \tag{3.21a}$$

$$Q^3 := \quad (w_3, y_3) = \left(0, \frac{\alpha}{\xi}\right). \tag{3.21b}$$

The point Q^1 is a stable improper node with the double eigenvalue $-\alpha$ and a single eigenvector $(0, 1)^T$. The point Q^3 has one unstable direction $(0, 1)^T$ due to the positive eigenvalue α and a centre direction $(-\alpha/(1 + \alpha), 1)^T$ due to a zero eigenvalue. Notice that for $\alpha = \xi$ then $Q^3 = (0, 1)$.

Lemma 3.7 *There exists a unique centre-stable manifold* $W^{c,s}$ *of the point* Q^3 *for* $w_3 \geq 0$. *This manifold is smooth in* α. *For* $\alpha = \xi$ *the set* $H = 1$ *coincides with* $W^{c,s}$.

Proof. A simple calculation shows that the centre manifold is given by

$$W^{c,s}: \quad y_3 = \frac{\alpha}{\xi} - \frac{1 + \alpha}{\alpha} w_3 + \mathrm{O}(\mathrm{e}^{-1/w_3}).$$

Inserting this into (3.19) gives the following reduced problem

$$\dot{w}_3 = -\frac{\xi}{\alpha} w_3^2 (1 + \mathrm{O}(\mathrm{e}^{-1/w_3})).$$

As a consequence, Q^3 has a saddle-like behaviour for $w_3 \geq 0$. The centre-stable manifold $W^{c,s}$ is unique and stable on this half plane for all α, and it is also smooth in α. For $\alpha = \xi$ we rewrite the Hamiltonian (3.13b) in chart k_3, and insert the condition $H = 1$ to obtain the implicit equation

$$\xi(y_3 - 1) + w_3(\xi + 1) - \xi w_3 \, \mathrm{e}^{-\frac{1}{w_3}} = 0. \tag{3.22}$$

In this equation $w_3 \to 0^+$ gives $y_3 \to 1$. Therefore $H = 1$ belongs to $W^{c,s}$ and the dynamics within it is $\dot{w}_3 = -w_3^2(1 + \mathrm{O}(\mathrm{e}^{-1/w_3}))$. □

Remark 3.8 *With respect to t_3 the points within $W^{c,s}$ decay algebraically to Q^3, while the decay towards the stable node Q^1 is exponential. Using (3.20) it follows that all these points reach $w_3 = 0$ in finite time with respect to the original slow time t. This is a formal proof of the finite time blow-up of solutions of (3.11) for $\alpha > \xi$, that was also observed by Gu et al [GRRT84] and by Pomeau and Berre [PB11].*

3.5.2 Chart k_1

We insert (3.17b) into the reduced problem (3.16) to obtain the dynamics in chart k_1

$$\begin{aligned} \dot{w} &= w^2(1 - \mathrm{e}^{\frac{z}{w}}), \\ \dot{z} &= w(\xi + z)(1 - \mathrm{e}^{\frac{z}{w}}) + \mathrm{e}^{\frac{z}{w}}(\alpha z - \xi), \end{aligned} \tag{3.23}$$

where we have dropped the subscript for the sake of readability. We observe that the exponential term in (3.23) is not well defined in the origin. For this reason we introduce the blow-up transformation

$$w = \bar{r}\bar{\omega}, \qquad z = \bar{r}\bar{\zeta}, \tag{3.24}$$

where $(\bar{\omega}, \bar{\zeta}) \in S^1 = \{(\bar{\omega}, \bar{\zeta}) : \bar{\omega}^2 + \bar{\zeta}^2 = 1\}$ and $\bar{r} \geq 0$. We consider the charts

$$\kappa_1 : \quad \bar{\zeta} = 1, \quad w = r_1\omega_1, \quad z = r_1, \tag{3.25a}$$

$$\kappa_2 : \quad \bar{\omega} = 1, \quad w = r_2, \quad z = r_2\zeta_2, \tag{3.25b}$$

$$\kappa_3 : \quad \bar{\zeta} = -1, \quad w = r_3\omega_3, \quad z = -r_3. \tag{3.25c}$$

Next we perform an analysis of the blown-up vector field and the main results are summarised in Figure 3.8.

Chart κ_1 We insert (3.25a) into (3.23) and divide the right-hand side by $\exp(1/\omega_1)/r_1$ to get the desingularized dynamics in chart κ_1

$$\begin{aligned} \dot{\omega}_1 &= \omega_1(\xi - \alpha r_1) + r_1\omega_1^2\xi\left(1 - \mathrm{e}^{-\frac{1}{\omega_1}}\right), \\ \dot{r}_1 &= -r_1(\xi - \alpha r_1) - r_1^2\omega_1(\xi + r_1)\left(1 - \mathrm{e}^{-\frac{1}{\omega_1}}\right). \end{aligned} \tag{3.26}$$

System (3.26) has one equilibrium point in $(\omega_1, r_1) = (0, \xi/\alpha)$ that corresponds to the point Q^3 (3.21b). Furthermore (3.26) has a second equilibrium point in $O_1 := (\omega_1, r_1) = (0, 0)$ with eigenvalues ξ, $-\xi$ and corresponding eigenvectors $(1, 0)^T$ and $(0, 1)^T$. Both the eigendirections of O_1 are invariant and we denote by γ_1 the heteroclinic connection between Q^3 and O_1 along the r_1-axis.
The initial condition $p_{1,\text{in}}$ on $W^{c,s}$ with $\omega_1 = \delta > 0$ is connected through the stable and the unstable manifolds of O_1 to the point $p_{1,\text{out}} := (\omega_1, r_1) = (\delta^{-1}, 0)$ as shown in Figure 3.8(a).

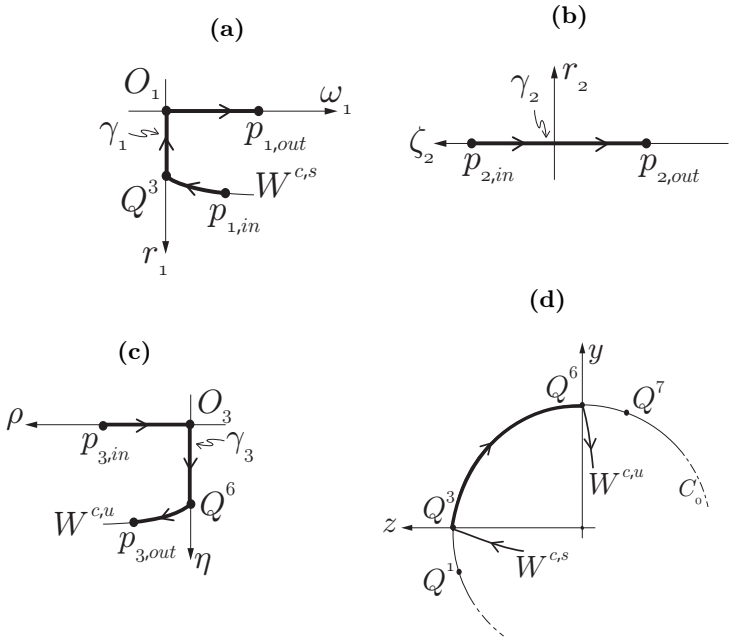

Figure 3.8: Blow-up of (3.23) in chart k_1. (a), (b) and (c) represent the charts κ_1, κ_2 and κ_3 respectively. In (d): behaviour at infinity after the blow-down.

Chart κ_2 We insert (3.25b) into (3.23) and divide the right-hand side by $\exp(\zeta_2)/r_2$ to obtain the desingularized vector field. In this chart there are no equilibrium points, yet the line $r_2 = 0$ is invariant and ζ_2 decreases monotonically along it. The orbit entering from chart κ_1 has the initial condition $p_{2,\text{in}} := \kappa_{12}(p_{1,\text{out}}) = (\zeta_2, r_2) = (\delta, 0)$ that lies on the invariant line $r_2 = 0$. Thus, from $p_{2,\text{in}}$ we continue to the point $p_{2,\text{out}} := (\zeta_2, r_2) = (-\delta^{-1}, 0)$, as shown in Figure 3.8(b).

Chart κ_3 We introduce (3.25c) into (3.23) and divide by w_3 to obtain the desingularized dynamics in chart κ_3

$$\dot{\omega}_3 = \omega_3\xi - \frac{\mathrm{e}^{-1/\omega_3}}{r_3}(\alpha r_3 + \xi + \xi r_3\omega_3),$$
$$\dot{r}_3 = -r_3(\xi - r_3) + \frac{\mathrm{e}^{-1/\omega_3}}{\omega_3}(\xi - r_3^2\omega_3 + r_3(\alpha + \xi\omega_3)).$$

This system has a proper unstable node

$$Q^7 := \quad (\omega_3, r_3) = (0, \xi),$$

with double eigenvalue ξ and eigenvectors $(1,0)^T$ and $(0,1)^T$. For $w_3 = r_3 = 0$ the quantity $\mathrm{e}^{-1/\omega_3}/r_3$ is not well defined. We deal with this singularity by first multiplying the right-hand side of the vector field by $r_3\omega_3$

$$\begin{aligned}\dot{\omega}_3 &= r_3\omega_3^2\xi - \omega_3\,\mathrm{e}^{-1/\omega_3}(\alpha r_3 + \xi + \xi r_3\omega_3),\\ \dot{r}_3 &= -r_3^2\omega_3(\xi - r_3) + r_3\,\mathrm{e}^{-1/\omega_3}(\xi - r_3^2\omega_3 + r_3(\alpha + \xi\omega_3)).\end{aligned} \tag{3.27}$$

Next, we introduce the blow-up transformation

$$\omega_3 = \rho, \qquad r_3 = \frac{\mathrm{e}^{-1/\rho}}{\rho}\eta. \tag{3.28}$$

We substitute (3.28) into (3.27) and we divide by $\exp(-1/\rho)/\rho$ to obtain the desingularized vector field

$$\begin{aligned}\dot{\rho} &= \xi\rho^2(\eta - 1) - \rho\eta\,\mathrm{e}^{-1/\rho}(\rho\xi + \alpha),\\ \dot{\eta} &= -\eta\xi(\eta - 1) + \eta^2\frac{\mathrm{e}^{-1/\rho}}{\rho}(\eta\rho + \rho\xi + \alpha) - \eta^3\,\mathrm{e}^{-2/\rho}.\end{aligned} \tag{3.29}$$

Remark 3.9 *The blow-up map* (3.28) *is non-standard, since it is not written as an algebraic expression in* ρ*. To the authors' knowledge there is no former literature treating blow-ups of the form* (3.28) *and in particular the approach of [Kri17] does not treat this type of blow-ups.*

System (3.29) has two equilibrium points. The point $O_3 := (\rho, \eta) = (0,0)$ has one unstable direction $(0,1)^T$ associated with the eigenvalue ξ and one centre direction $(1,0)^T$ associated with the zero eigenvalue. The second equilibrium point

$$Q^6 := \quad (\rho, \eta) = (0,1),$$

has one stable direction $(0,1)^T$ associated with the eigenvalue $-\xi$ and one centre direction $(1,0)^T$ associated with the zero eigenvalue. The axis $\rho = 0$ is invariant, thus there exists an heteroclinic connection along the η-axis between the points O_3 and Q^6, that we denote by γ_3. See Figure 3.8(c).

Lemma 3.10 *There exists a unique centre-unstable manifold* $W^{c,u}$ *of the point* Q^6 *for* $\rho \geq 0$*, that is smooth in* α *and that contains solutions that decay algebraically to* Q^6 *backwards in time. For* $\alpha = \xi$ *the set* $H = 1$ *coincides with* $W^{c,u}$*.*

Proof. The centre direction of Q^6 is $\eta = 1$. This means that the centre manifold of Q^6 is of the form $\eta = 1 + \mathrm{O}(\rho^2)$. However, since $\eta = 1$ is invariant for (3.29) when ignoring the exponentially small terms, there are no algebraic

ρ^n-terms in the expansion of the centre manifold. Therefore the centre manifold turns out to be

$$W^{c,u}: \quad \eta = 1 + \frac{\mathrm{e}^{-1/\rho}}{\rho}\left(\frac{\alpha}{\xi} + \frac{1+\xi}{\xi}\rho + \mathrm{O}(\rho^2)\right),$$

which inserted in the ρ-equation (3.29) gives

$$\dot{\rho} = \rho^2\,\mathrm{e}^{-1/\rho}(1 + \mathrm{O}(\rho)).$$

Hence the equilibrium is a saddle-like for $\rho \geq 0$ and the centre manifold is unique and unstable on this half plane for all α. It is also smooth in α.
For $\alpha = \xi$ we rewrite the Hamiltonian (3.13b) in the (ρ, η) coordinates and then insert the condition $H = 1$ to obtain the implicit equation

$$\frac{1}{\eta} - 1 + \mathrm{e}^{-\frac{1}{\rho}}\left(\frac{1}{\rho} + 1 + \frac{1}{\xi}\right) = 0, \tag{3.30}$$

where we have multiplied the left-hand side by $\mathrm{e}^{-1/\rho}$ and divided it by ξ. Here $\rho \to 0^+$ gives $\eta \to 1$ so that $H = 1$ belongs to the centre manifold of Q^6. □

The orbit entering from chart κ_2 in the point $p_{3,\mathrm{in}} := \kappa_{23}(p_{2,\mathrm{out}}) = (\rho, \eta) = (\delta, 0)$ is connected through the stable and the unstable manifolds of O_3 to the point $p_{3,\mathrm{out}}$ on $W^{c,u}$ with $\omega_3 = \delta$ as shown in Figure 3.8(c).

Remark 3.11 *We observe that the singularity at the origin of chart k_1 (3.23), upon blow-ups (3.24) and (3.28), has turned into three hyperbolic equilibrium points O_1, O_3 and Q^6. After the blow-down we obtain the singular structure depicted in Figure 3.8(d).*

3.5.3 The reduced problem on $\mathcal{S}^{2,+}$

The previous analysis has described the phase space of (3.11) near infinity. In the following, we analyse the interaction of the unbounded solutions of the reduced problem (3.11) with the equilibrium points $Q^{1,3,6,7}$ for variations of the parameter α. We follow the Melnikov-type approach of Chow *et al* [CLW94], to describe how the closed orbits of the Hamiltonian system (3.12) break up near $\alpha = \xi$.
When $\alpha = \xi$, any bounded trajectory of (3.12) with $H = h,\ h \in (0, 1)$, intersects the y-axis in two points D, d that correspond to the two real roots of the Lambert equation (3.14). We denote by D the root with $y > 0$ while we denote by d the one with $y < 0$, see Figure 3.9(a).
For $\alpha - \xi$ small, we compute the forward and backward orbits $\gamma^+(t)$ and $\gamma^-(t)$

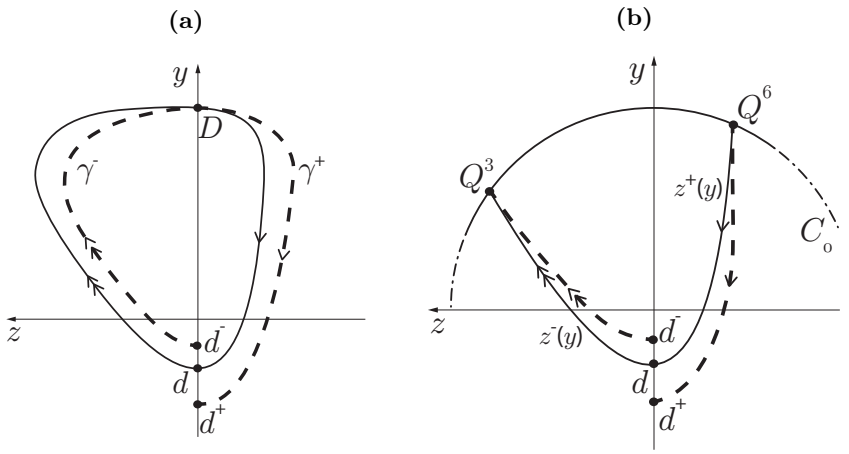

Figure 3.9: Perturbation of the Hamiltonian solutions for $\alpha - \xi$ small. In (a): closed orbit with $0 < H < 1$. In (b): heteroclinic connection for $H = 1$.

respectively emanating from D. The transversality condition (3.15) assures that $\gamma^+(t)$ and $\gamma^-(t)$ cross the y-axis for the first time in the points d^+ and d^- respectively. Hence we define the distance function

$$\begin{aligned}\Delta(\alpha) &= H(d^+) - H(d^-),\\ &= \int_0^{T^+} \dot{H}(\gamma^+(t))\,\mathrm{d}t + \int_{T^-}^0 \dot{H}(\gamma^-(t))\,\mathrm{d}t,\\ &= \int_0^{T^+} \nabla H(h)\cdot f_0(y,z;\alpha)\,\mathrm{d}t + \int_{T^-}^0 \nabla H(h)\cdot f_0(y,z;\alpha)\,\mathrm{d}t,\end{aligned} \tag{3.31}$$

where $T^\pm = T^\pm(\alpha) \gtrless 0$ is the flow-time between D and d^+ and between D and d^- respectively. We Taylor expand (3.31) around $\alpha = \xi$

$$\Delta(\alpha) = (\alpha - \xi)\Delta_\alpha(h) + \mathrm{O}((\alpha-\xi)^2), \tag{3.32}$$

with the quantity $\Delta_\alpha(h)$ defined as

$$\begin{aligned}\Delta_\alpha(h) &= \int_{T_h^-}^{T_h^+} \nabla H(h)\cdot \frac{\partial f_0}{\partial \alpha}(y,z;\xi)\,\mathrm{d}t\\ &= \int_{T_h^-,}^{T_h^+} \xi\,\mathrm{e}^{-\xi y}\, z(\mathrm{e}^z - 1)\,\mathrm{d}t.\end{aligned} \tag{3.33}$$

In (3.33) we have denoted with $(y,z)(t)$ the solution of (3.12) for $H = h$ and $\alpha = \xi$. The times $T_h^\pm = T_h^\pm(\xi)$ are the forward and backward times from D to

d. The integrand of (3.33) is always positive for $z \neq 0$ and therefore $\Delta_\alpha(h)$ is positive for any $h \in (0,1)$. We conclude from (3.32) that the forward flow $\gamma^+(t)$ spirals outwards for $\alpha > \xi$ while it spirals inwards for $\alpha < \xi$, in agreement with Figure 3.7.
We now extend the analysis above to the case of $H = 1$. In this case the points d^+ and d^- are the intersections of $W^{c,u}$ and $W^{c,s}$ with the y-axis respectively, see Figure 3.9(b). From the previous analysis, we know that $W^{c,s}$ and $W^{c,u}$ depend smoothly on α.

Lemma 3.12 *For $\alpha = \xi$ there is a unique heteroclinic connection between Q^3 and Q^6 on C_0. This connection is through the manifolds $W^{c,s}$ and $W^{c,u}$ and it corresponds to the set $H = 1$ in (3.13b). This set can be written as the union of two graphs $z = z^{\pm}(y)$ (see Figure 3.9(b)) with $y \geq -1/\xi$ so that $z^-(y)$ ($z^+(y)$ resp.) approaches Q^3 (Q^6) as $z^- = \mathrm{O}(y)$ ($z^+ = \mathrm{O}(\ln(y))$) for $y \to \infty$.*

Proof. We rewrite the trajectory $H = 1$ as the graphs $z = z^{\pm}(y)$ for $y \geq -1/\xi$. The behaviour in forward time follows by considering the point $p_{1,\mathrm{in}}$ in condition (3.22) and blowing it down to the original variables (y, z). Similarly for the behaviour in backwards time by considering $p_{3,\mathrm{out}}$ in condition (3.30), see Figure 3.8. □

Figure 3.7(b) follows from Lemma 3.12. When $\alpha = \xi$ the manifolds $W^{c,s}$ and $W^{c,u}$ cross the y-axis in the point $d := (y, z) = (-1/\xi, 0)$. We define the distance function $\Delta(\alpha)$ as in (3.31), we Taylor expand it around $\alpha = \xi$ as in (3.32) and we define $\Delta_\alpha(1)$ as in (3.33). Since the integrand of (3.33) is positive for $H = 1$ we just need to show that the improper integral (3.33) exists. From the reduced problem (3.11) we observe that $\dot{y} = \mathrm{e}^z - 1$, thus we rewrite (3.33) with respect to y as

$$\Delta_\alpha(1) = \int_{-1/\xi}^{+\infty} \xi\, \mathrm{e}^{-\xi y}\, z^-(y)\, \mathrm{d}y - \int_{-1/\xi}^{+\infty} \xi\, \mathrm{e}^{-\xi y}\, z^+(y)\, \mathrm{d}y. \tag{3.34}$$

Recall from Lemma 3.12 that $z^-(y)$ is asymptotically linear in y for $y \to \infty$, while $z^+(y)$ decreases logarithmically with respect to y. The expression (3.34) therefore exists because of the exponential decay of the term $\exp(-\xi y)$ and furthermore it is positive. We remark that $\Delta_\alpha(h)$ in (3.33) converges to $\Delta_\alpha(1)$ for $h \to 1$, since the orbit segment on $C_{0,\infty}$ does not give any contribution to (3.34).

Now we finish the proof of Proposition 3.4 by considering α as in (3.18). When $\alpha < \xi$ the set $W^{c,u}$ contracts to the origin, because $\Delta(\alpha) < 0$ in (3.32). Furthermore the set $W^{c,s}$ is backwards asymptotic to Q^7 and acts as a separator between the basin of attraction of the origin and the basin of attraction of Q^1. A

similar argument covers the case $\alpha > \xi$. This concludes the proof of Proposition 3.4 and justifies Figures 3.7(a) and 3.7(c). Therefore no periodic orbit exists on C_0 for $\alpha > \xi$ and $\varepsilon = 0$.

3.6 Analysis of the perturbed problem for $\varepsilon > 0$

Consider the original problem (3.1) and $0 < \mu < 1$ small but fixed. Then the compact manifold

$$S_0 = \{(x, y, z) \in C_0 | \quad 0 \leq H(y, z) \leq 1 - \mu\}, \tag{3.35}$$

is normally hyperbolic for $\varepsilon = 0$. Therefore Fenichel's theory guarantees that for ε sufficiently small there exists a locally invariant manifold S_ε that is $\mathrm{O}(\varepsilon)$-close to S_0 and is diffeomorphic to it. Moreover the flow on S_ε converges to the flow of the reduced problem (3.11) for $\varepsilon \to 0$. A computation shows that S_ε at first order is

$$z = -(x + \xi y) + \varepsilon\xi\, \mathrm{e}^{-2(x+\xi y)} \left(\alpha(x + \xi y) + \xi(y + 1) - \xi\, \mathrm{e}^{x+\xi y}\right) + \mathrm{O}(\varepsilon^2),$$

hence we have the following vector field $f_\varepsilon(y, z; \alpha, \varepsilon)$ on S_ε

$$f_\varepsilon(y, z; \alpha, \varepsilon) := \begin{cases} \dot{y} &= \mathrm{e}^z - 1 - \varepsilon\xi\chi\, \mathrm{e}^{2z} + \mathrm{O}(\varepsilon^2), \\ \dot{z} &= \chi - \varepsilon\xi\chi\, \mathrm{e}^{2z}(\alpha z - \xi y + \alpha - \xi + 1) + \mathrm{O}(\varepsilon^2), \end{cases} \tag{3.36}$$

with $\chi(y, z) = \alpha z\, \mathrm{e}^z - \xi y\, \mathrm{e}^z - \xi\, \mathrm{e}^z + \xi$.

Proposition 3.13 *Consider the compact manifold S_0 defined in (3.35). Then S_0 perturbs to a locally invariant slow manifold S_ε for $0 < \varepsilon \ll 1$. On S_ε the origin of (3.36) undergoes a supercritical Hopf bifurcation for*

$$\alpha = \alpha_H := \xi - \varepsilon\xi^2 + \mathrm{O}(\varepsilon^2),$$

with a negative first Lyapunov coefficient

$$a = -\frac{1}{8}\varepsilon\xi^3(1 + \xi) + \mathrm{O}(\varepsilon^2) < 0. \tag{3.37}$$

Therefore for $\alpha \in (\alpha_H, \alpha_H + c\varepsilon)$ with c sufficiently small, there exists a family of locally unique attracting limit cycles with amplitude of order $\mathrm{O}\left(\sqrt{-(\alpha - \alpha_H)/a}\right)$.

The proof of Proposition 3.13 follows from straightforward computations. We remark that since (3.37) is proportional to ε, it follows that the results of Proposition 3.13 are valid only for a very small interval of α around α_H. We use the analysis of subsection 3.5.3 to extend the small limit cycles of Proposition 3.13 into larger ones.

Proposition 3.14 *Consider the slow manifold S_ε of Proposition 3.13. On S_ε there exists a family of closed periodic orbits for*

$$\alpha = \alpha_M(h) := \xi - \varepsilon \frac{\Delta_\varepsilon(h)}{\Delta_\alpha(h)} + \mathrm{O}(\varepsilon^2), \tag{3.38}$$

where $h \in [c_1(\mu), 1 - c_2(\mu)]$ with $(c_1, c_2)(\mu)$ small. The quantity $\Delta_\varepsilon(h)$ is defined as

$$\Delta_\varepsilon(h) = \int_{T_h^-}^{T_h^+} \nabla H(h) \cdot \frac{\partial f_\varepsilon}{\partial \varepsilon}(y, z; \xi, 0)\, \mathrm{d}t, \tag{3.39}$$

while $\Delta_\alpha(h) > 0$ was defined in (3.33).

Proof. By Fenichel's theorem we know that the flow on S_ε converges to the flow of the reduced problem (3.11) for $\varepsilon \to 0$. Therefore we can define the distance function $\Delta(\alpha, \varepsilon)$ similarly to (3.31) whose Taylor expansion around $\alpha = \xi$ and $\varepsilon = 0$ is

$$\Delta(\alpha, \varepsilon) = (\alpha - \xi)\Delta_\alpha(h) + \varepsilon \Delta_\varepsilon(h) + \mathrm{O}((\alpha - \xi + \varepsilon)^2), \tag{3.40}$$

with $\Delta_\alpha(h)$ and $\Delta_\varepsilon(h)$ defined in (3.33) and (3.39) respectively. The integrand of $\Delta_\alpha(h)$ is strictly positive for all $h \in (0, 1)$, therefore we can apply the Implicit Function Theorem to (3.40) for $\Delta(\alpha, \varepsilon) = 0$ and obtain the result (3.38). □

In Figure 3.10 we show a numerical computation of the leading order coefficient in (3.38) for an interval of energies $H = h \in (0, 0.6]$. No saddle-node bifurcations occur in this interval and hence the periodic orbits are all asymptotically stable. We expect a similar behaviour for larger values of h but we did not manage to compute this due to the intrinsic slow-fastness of the reduced problem. It might be possible to study the term $-\Delta_\varepsilon(h)/\Delta_\alpha(h)$ analytically by using the results of Lemma 3.12, but the expressions are lengthy and we did not find an easy way. The analysis above can only explain the limit cycles that appear for $\alpha - \xi = \mathrm{O}(\varepsilon)$, and it does not justify the limit cycles of Figure 3.1 that appear for larger values of $\alpha - \xi$. For this reason, we proceed to study the full problem (3.1) at infinity, introducing its compactification through the Poincaré sphere.

3.7 Statement of the main result

In this section we find a connection at infinity between the points Q^1 and Q^6 (recall Proposition 3.3) that will establish a return mechanism to C_0 of the unbounded solutions of (3.5) when $\varepsilon = 0$ and $\alpha > \xi$. This mechanism will be

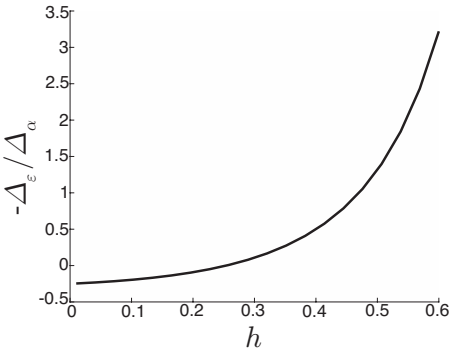

Figure 3.10: Plot of the leading order coefficient in (3.38) for $\xi = 0.5$ and $h \in (0, 0.6]$.

the foundation for the existence of limit cycles when $0 < \varepsilon \ll 1$ and $\alpha - \xi \geq c > 0$. Similar to section 3.5, we introduce a four-dimensional Poincaré sphere $\mathcal{S}^{3,+}$

$$\mathcal{S}^{3,+} := \left\{ (X, Y, Z, W) \in \mathbb{R}^4 \middle| \quad X^2 + Y^2 + Z^2 + W^2 = 1, \quad W \geq 0 \right\}.$$

The fast problem (3.5) is interpreted as a directional chart K_2 on $\mathcal{S}^{3,+}$ defined for $W = 1$

$$K_2 := \mathcal{S}^{3,+} \cap \{W > 0\}, \quad x_2 = \frac{X}{W}, y_2 = \frac{Y}{W}, z_2 = \frac{Z}{W}, \tag{3.41}$$

therefore the vector field in chart K_2 is obtained by introducing the subscript in (3.5)

$$\begin{aligned} x_2' &= -\varepsilon \, \mathrm{e}^{z_2} (x_2 + (1 + \alpha) z_2), \\ y_2' &= \varepsilon \, (\mathrm{e}^{z_2} - 1), \\ z_2' &= -\mathrm{e}^{-z_2} \left(y_2 + \frac{x_2 + z_2}{\xi} \right). \end{aligned} \tag{3.42}$$

The points at infinity in K_2 correspond to $W = 0$ which is a sphere S^2. We introduce the two directional charts

$$K_3 := \mathcal{S}^{3,+} \cap \{Z > 0\}, \quad x_3 = \frac{X}{Z}, y_3 = \frac{Y}{Z}, w_3 = \frac{W}{Z}, \tag{3.43a}$$

$$K_1 := \mathcal{S}^{3,+} \cap \{Y > 0\}, \quad x_1 = \frac{X}{Y}, z_1 = \frac{Z}{Y}, w_1 = \frac{W}{Y}. \tag{3.43b}$$

We have the following transformations between the charts

$$K_{23}: \quad w_3 = z_2^{-1}, \quad x_3 = x_2 z_2^{-1}, \quad y_3 = y_2 z_2^{-1}, \tag{3.44a}$$

$$K_{21}: \quad w_1 = y_2^{-1}, \quad x_1 = x_2 y_2^{-1}, \quad z_1 = z_2 y_2^{-1}, \tag{3.44b}$$

$$K_{31}: \quad w_1 = w_3 y_3^{-1}, \; x_1 = x_3 y_3^{-1}, \quad z_1 = y_3^{-1}, \tag{3.44c}$$

that are defined for $z_2 > 0$, $y_2 > 0$ and $y_3 > 0$ respectively. The inverse transformations are defined similarly. The three points $Q^1, Q^3 \in K_3$ and $Q^6 \in K_1$

$$\begin{aligned} Q^1 &:= \quad (x_3, y_3, w_3) = (-1, 0, 0), \\ Q^3 &:= \quad (x_3, y_3, w_3) = \left(-1-\alpha, \frac{\alpha}{\xi}, 0\right), \\ Q^6 &:= \quad (x_1, z_1, w_1) = (-\xi, 0, 0), \end{aligned}$$

introduced in Proposition 3.3, and the three points $Q^2, Q^4 \in K_3$ and $Q^5 \in K_1$

$$Q^2 := \quad (x_3, y_3, w_3) = (-1-\alpha, 0, 0), \tag{3.45a}$$

$$Q^4 := \quad (x_3, y_3, w_3) = \left(-1-\alpha, \frac{2\alpha}{\xi}, 0\right), \tag{3.45b}$$

$$Q^5 := \quad (x_1, z_1, w_1) = \left(-\frac{\xi}{2\alpha}(1+\alpha), \frac{\xi}{2\alpha}(1-\alpha), 0\right), \tag{3.45c}$$

are going to play a role in the following, together with the lines

$$L_0 := \quad \{(x_3, y_3, w_3) | \quad x_3 + 1 + \alpha = 0,\ w_3 = 0\}, \tag{3.46a}$$

$$C_{0,\infty} := \quad \{(x_3, y_3, w_3) | \quad x_3 + \xi y_3 + 1 = 0,\ w_3 = 0\}. \tag{3.46b}$$

Notice that the line L_0 corresponds to the intersection of the family of nullclines (3.10) with infinity through K_{23}, and that $Q^{2,4} \in L_0$, while $Q^5 \in C_{0,\infty}$. We construct the following *singular cycle*.

Definition 3.15 Let Γ_0 be the singular cycle consisting of the points $Q^{1,2,4,5,6}$ and of the union of the following sets

- $\gamma^{1,2}$ connecting Q^1 with Q^2. In chart K_3 the segment $\gamma^{1,2}$ is:

$$\gamma^{1,2} := \{(x_3, y_3, w_3) \in K_3 | \quad x_3 \in (-1-\alpha, -1), y_3 = 0, w_3 = 0\}. \tag{3.47}$$

- $\gamma^{2,4}$ connecting Q^2 with Q^4 along L_0. In chart K_3 the segment $\gamma^{2,4}$ is:

$$\gamma^{2,4} := \left\{(x_3, y_3, w_3) \in K_3 | \quad x_3 = -1-\alpha, y_3 \in \left(0, \frac{2\alpha}{\xi}\right), w_3 = 0\right\}. \tag{3.48}$$

- $\gamma^{4,5}$ connecting Q^4 with Q^5. This segment is a fast fibre of (3.7) and in chart K_1 the segment $\gamma^{4,5}$ is:

$$\gamma^{4,5} := \left\{(x_1, z_1, w_1) \in K_1 |\ x_1 = -\frac{\xi(1+\alpha)}{2\alpha}, z_1 \in \left(\frac{\xi(1-\alpha)}{2\alpha}, \frac{\xi}{2\alpha}\right), w_1 = 0\right\}. \tag{3.49}$$

- $\gamma^{5,6}$ connecting Q^5 with Q^6 on $C_{0,\infty}$. In chart K_1 the segment $\gamma^{5,6}$ is:

$$\gamma^{5,6} := \left\{ (x_1, z_1, w_1) \in K_1 |\ x_1 = -\xi - z_1, z_1 \in \left(0, \frac{\xi(1-\alpha)}{2\alpha}\right), w_1 = 0 \right\}. \tag{3.50}$$

- $W^{c,u}$ connecting Q^6 with Q^1 on the critical manifold C_0.

In section 3.8 we identify Γ_0 using the blow-up method repeatedly on system (3.42). Figure 3.11 shows Γ_0 and its different segments: 3.11(a) displays the complete cycle while 3.11(b) and 3.11(c) illustrate the portions of Γ_0 that are visible in the charts K_3 and K_1 respectively. Γ_0 plays an important role in our main result, since we conjecture it to be the candidate *singular cycle*.

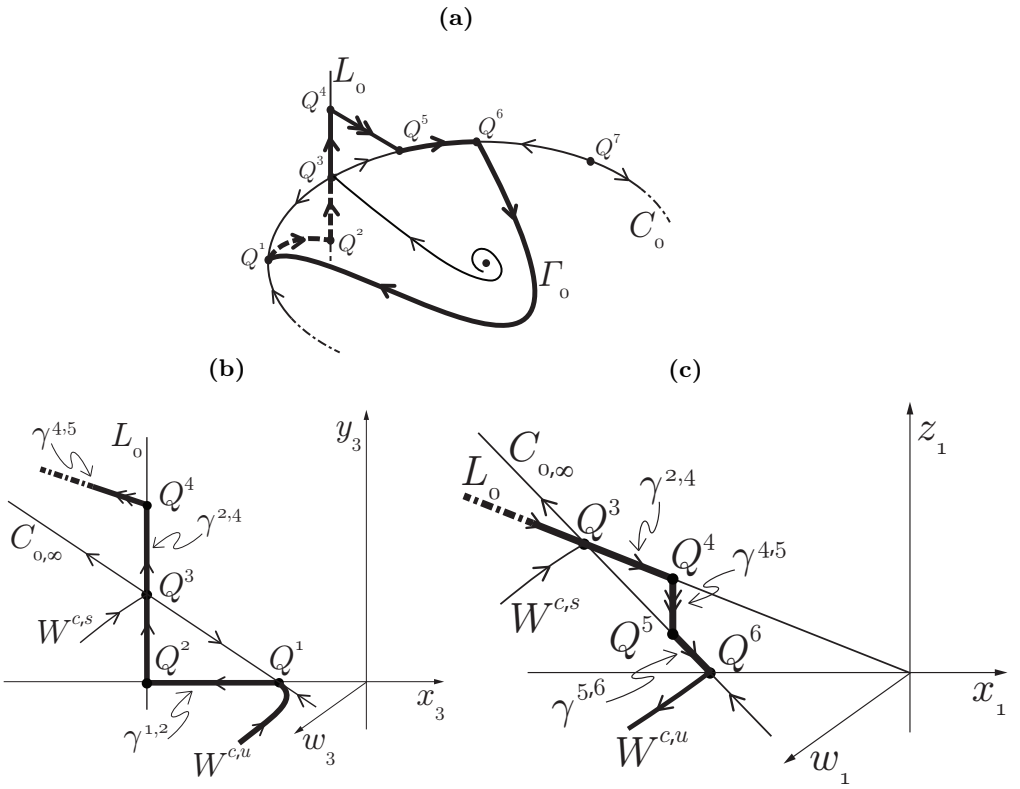

Figure 3.11: In (a): illustration of Γ_0. In (b): chart K_3, where we see the segments $\gamma^{1,2}, \gamma^{2,4}$ and partially $\gamma^{4,5}$. In (c): chart K_1, where we see $\gamma^{4,5}, \gamma^{5,6}$ and partially $\gamma^{2,4}$. In this cartoon we have assumed $\xi < \alpha < 1$ so that $\gamma^{4,5}$ lands on C_0 to the *left* of Q^6.

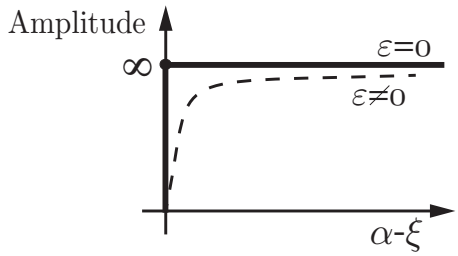

Figure 3.12: Conjectured bifurcation diagram of the limit cycles for $\varepsilon \ll 1$.

Conjecture 3.16 *Fix $\alpha > \xi$. Then for $0 < \varepsilon \ll 1$ there exists an attracting limit cycle Γ_ε that converges to the* singular cycle Γ_0 *for $\varepsilon \to 0$.*

Remark 3.17 *Here we collect the results of sections 3.6 and 3.7. When $\varepsilon = 0$ and $\alpha = \xi$ then there exists a family of periodic solutions on $\mathcal{S}^{3,+}$, corresponding to the Hamiltonian orbits with $H \in (0, 1)$. For $\alpha > \xi$ only the cycle Γ_0 persists. When $0 < \varepsilon \ll 1$ and $\alpha - \xi = \mathrm{O}(\varepsilon)$, there exists a limit cycle resembling the bounded Hamiltonian orbits. For larger values of $\alpha - \xi$, we conjecture that the limit cycle tends to Γ_0. Notice that Γ_0 is different from the limit of the Hamiltonian cycles $H = 1$ as $\alpha \to \xi$. Therefore further work is needed to prove the existence of the family of limit cycles in the intermediate regime $\mathrm{O}(\varepsilon) < \alpha - \xi < \mathrm{O}(1)$. The introduction in (3.42) of the trivial equation $\beta' = 0$, where $\beta = \alpha - \xi$, and a subsequent blow-up in β may be helpful. Figure 3.12 shows the conjectured bifurcation diagram of the periodic orbits.*

Figure 3.13 shows some numerical simulations supporting Conjecture 3.16: figure 3.13(a) illustrates the limit cycles Γ_ε for three different values of $\varepsilon \in \{10^{-8}, 10^{-4}, 10^{-2}\}$ with $\alpha = 0.9$ and $\xi = 0.5$, while figures 3.13(b) and 3.13(c) show the portions of Γ_ε that appear in the charts K_3 and K_1 respectively. The amplitudes of the orbits increase for decreasing values of the parameter ε, and both the plane C_0 and the line L_0 play an important role. Close to the origin the dynamics evolves on C_0, while sufficiently far from the origin L_0 becomes relevant. Indeed, in figure 3.13(b) we see that the solutions contract to L_0 following $\gamma^{1,2}$ and then they evolve by following $\gamma^{2,4}$. When the trajectories are close to Q^4, they follow $\gamma^{4,5}$ and contract again towards C_0 along a direction that tends to the fast fibre for $\varepsilon \to 0$, as we can see in figure 3.13(c).

A rigorous proof of Conjecture 3.16 requires an analysis both for $\varepsilon = 0$ and $0 < \varepsilon \ll 1$. In sections 3.8 and 3.9, we outline a procedure to prove the conjecture and we leave the full details of the proof to a future manuscript.

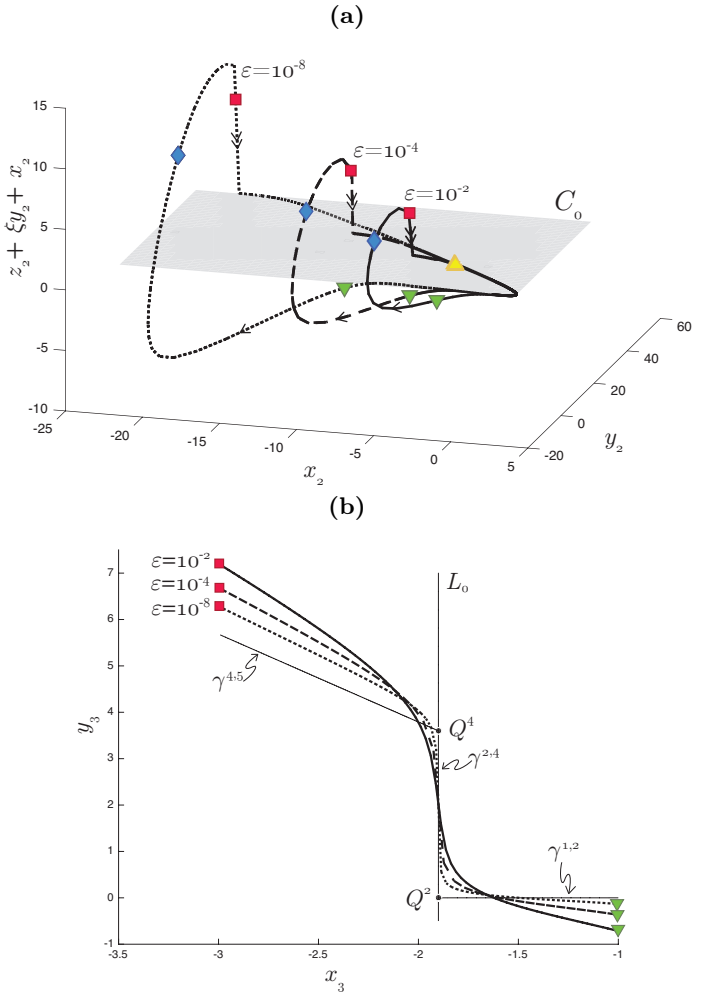

Figure 3.13: In (a): numerical simulation of (3.1) for $\varepsilon \in \{10^{-8}, 10^{-4}, 10^{-2}\}$, $\alpha = 0.9$ and $\xi = 0.5$. In (b): portion of Γ_ε visible in chart K_3, i.e. between the green lower triangle and the red square. In (c): portion of Γ_ε visible in K_1, i.e. between the blue diamond and the yellow upper triangle. We remark that the portion between the blue triangle and the red square is visible both in K_3 and K_1 since the two charts overlap for $y_3 > 0$ or $z_1 > 0$.

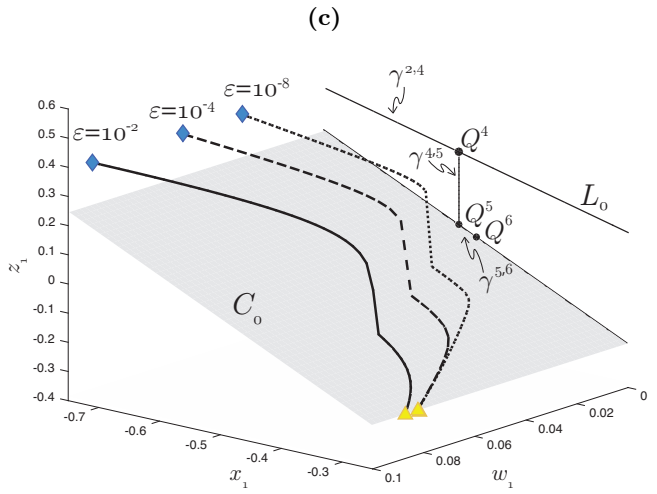

3.8 Identification of the segments of Γ_0 at infinity

This section lays out the foundations of a rigorous proof of Conjecture 3.16, by identifying the segments of Γ_0 (3.47)–(3.50) through a series of blow-ups. The analysis will mostly focus on the dynamics of chart K_3, where we identify the segments $\gamma^{1,2}, \gamma^{2,4}$ and $\gamma^{4,5}$ respectively. In chart K_1 we identify the segment $\gamma^{5,6}$. The results of this section are an expansion of the ones in section 8 of [BBK17b].

3.8.1 Identification of $\gamma^{1,2}$

Chart K_3 The point Q^1 is visible in chart K_3, where it has coordinates $(x_3, y_3, w_3) = (-1, 0, 0)$. We obtain the vector field in chart K_3 by inserting condition (3.44a) into the fast problem (3.42). This vector field is desingularized at $w_3 = 0$ by division of e^{1/w_3}

$$\begin{aligned} w_3' &= w_3\, \mathrm{e}^{-\frac{2}{w_3}}\, \frac{\tilde{x}}{\xi}, \\ \tilde{x}' &= -\varepsilon(\tilde{x} - \xi y_3 + \alpha) + \frac{\tilde{x}}{\xi}\, \mathrm{e}^{-\frac{2}{w_3}}(\tilde{x} - 1) + \varepsilon\xi w_3(1 - \mathrm{e}^{-\frac{1}{w_3}}), \\ y_3' &= \varepsilon w_3(1 - \mathrm{e}^{-\frac{1}{w_3}}) + y_3 \frac{\tilde{x}}{\xi}\, \mathrm{e}^{-\frac{2}{w_3}}, \\ \varepsilon' &= 0. \end{aligned} \tag{3.51}$$

System (3.51) is a four-dimensional vector field defined on $\mathbb{R}^4$ where we treat the parameter ε as a variable. Furthermore, we have introduced the new coordinate

$$\tilde{x} = x_3 + \xi y_3 + 1, \tag{3.52}$$

so that Q^1 is centred in the origin of chart K_3 and $\tilde{x} = 0$ implies that the solution lies on C_0.

Remark 3.18 *In this section we will identify the segments of Γ_0 in terms of $\tilde{x}$ instead of $x_{1,3}$ in order to simplify the exposition. To compare the results with the ones of Definition 3.15, one needs to use the coordinate transformation (3.52).*

The set $w_3 = \varepsilon = 0$ consists of non-hyperbolic equilibrium points of (3.51) and the two lines $C_{0,\infty}$ and L_0 (3.46) are contained within this set. Since we consider a regime of w_3 sufficiently small, we approximate $1 - \mathrm{e}^{-1/w_3} \simeq 1$ in the y_3-equation of (3.51) to simplify the computations. Qualitatively, this has no effects on the results.
We blow-up (3.51) around Q^1, in order to extend the hyperbolicity of C_0 up to infinity. To do so, we need to get rid of the exponential terms. We deal with it by introducing a new variable q

$$q = \mathrm{e}^{-\frac{2}{w_3}}, \tag{3.53}$$

so that the extended system contains only algebraic terms in its variables [Kri17]. Indeed by differentiating (3.53) with respect to time we obtain

$$\begin{aligned} q' &= 2w_3^{-2} w_3' \, \mathrm{e}^{-\frac{2}{w_3}}, \\ &= 2w_3^{-1} q^2 \frac{\tilde{x}}{\xi}, \end{aligned} \tag{3.54}$$

where we have used (3.51) and (3.53). By inserting (3.54) into (3.51), we obtain the five-dimensional vector field

$$\begin{aligned} w_3' &= w_3^2 q \frac{\tilde{x}}{\xi}, \\ \tilde{x}' &= -\varepsilon w_3(\tilde{x} - \xi y_3 + \alpha) + w_3 q \frac{\tilde{x}}{\xi}(\tilde{x} - 1) + \varepsilon \xi w_3^2, \\ y_3' &= \varepsilon w_3^2 + y_3 w_3 q \frac{\tilde{x}}{\xi}, \\ q' &= 2q^2 \frac{\tilde{x}}{\xi}, \\ \varepsilon' &= 0, \end{aligned} \tag{3.55}$$

where we have multiplied the right-hand side by w_3. The evolution of q in (3.55) is slaved by w_3 through (3.53). However, this dependence is not explicit and we will refer to it only when needed. We refer to [Kri17] for further details on this approach.
System (3.55) has a 3-dimensional space of non-hyperbolic equilibrium points for $\varepsilon = q = 0$, since each point has a quintuple zero eigenvalue. To overcome the degeneracy we introduce the blow-up map

$$q = \bar{r}\bar{q}, \quad \varepsilon = \bar{r}\bar{\epsilon}, \tag{3.56}$$

with $(\bar{q}, \bar{\epsilon}) \in S^1$ and $\bar{r} \geq 0$ while the variables $(w_3, \tilde{x}, y_3) \in \mathbb{R}^3$ in (3.55) are kept unchanged. We remark that the quantity ε in (3.56) is a constant, hence the blown-up space is foliated by invariant submanifolds. We study the two local charts

$$\mathcal{K}_1 : \bar{q} = 1, \quad q = r_1, \quad \varepsilon = r_1\epsilon_1, \tag{3.57a}$$
$$\mathcal{K}_2 : \bar{\epsilon} = 1, \quad q = r_2 q_2, \quad \varepsilon = r_2. \tag{3.57b}$$

Notice that $q_2 = \mathrm{O}(1)$ in chart $\mathcal{K}_2$ corresponds to $w = \mathrm{O}(\ln^{-1}\varepsilon^{-1})$ or $z_2 = \mathrm{O}(\ln\varepsilon^{-1})$ through (3.53). This is the relevant regime for the naïve identification of L_0 as in (3.9).
We enter chart K_3 in a point sufficiently close to Q^1, that is identified by $P_{K_3,\mathrm{in}} : (w_3, \tilde{x}, y_3, q, \varepsilon) = (\delta, 0, \delta, \exp(-2\delta^{-1}), 0)$, with $\delta > 0$ and small.

Chart $\mathcal{K}_1$ System (3.55) rewritten in chart $\mathcal{K}_1$ is

$$\begin{aligned}
w' &= w^2\frac{\tilde{x}}{\xi},\\
\tilde{x}' &= -\epsilon w(\tilde{x} - \xi y + \alpha) + w\frac{\tilde{x}}{\xi}(\tilde{x} - 1) + \xi\epsilon w^2,\\
y' &= \epsilon w^2 + yw\frac{\tilde{x}}{\xi},\\
\epsilon' &= -2\epsilon\frac{\tilde{x}}{\xi},\\
r' &= 2r\frac{\tilde{x}}{\xi},
\end{aligned} \tag{3.58}$$

where we have dropped the subscript and divided out the common factor r. $P_{K_3,\mathrm{in}}$ is transformed to $P_{\mathcal{K}_1,\mathrm{in}} : (w, \tilde{x}, y, \epsilon, r) = (\delta, 0, \delta, 0, \exp(-2\delta^{-1}))$ by (3.57a). This origin of (3.58) is still degenerate with all zero eigenvalues. To overcome the degeneracy, we introduce the following blow-up of $C_{0,\infty}$

$$w = \bar{r}\bar{w}, \quad \tilde{x} = \bar{r}\bar{\tilde{x}}, \quad \epsilon = \bar{r}\bar{\epsilon}, \tag{3.59}$$

with $(\bar{w}, \bar{\tilde{x}}, \bar{\epsilon}) \in S^2$ and $\bar{r} \geq 0$ small, while the variables $(y, r) \in \mathbb{R} \times \mathbb{R}^+$ are kept unchanged. We focus on the three local charts

$$\mathtt{K}_1 : \bar{w} = 1, \quad w = r_1, \quad \tilde{x} = r_1 \tilde{x}_1, \quad \epsilon = r_1 \epsilon_1, \tag{3.60a}$$

$$\mathtt{K}_2 : \bar{\epsilon} = 1, \quad w = r_2 w_2, \quad \tilde{x} = r_2 \tilde{x}_2, \quad \epsilon = r_2, \tag{3.60b}$$

$$\mathtt{K}_3 : \bar{\tilde{x}} = 1, \quad w = r_3 w_3, \quad \tilde{x} = r_3, \quad \epsilon = r_3 \epsilon_3, \tag{3.60c}$$

where the change of coordinates $\mathtt{K}_{12}$ from chart $\mathtt{K}_1$ to chart $\mathtt{K}_2$, and $\mathtt{K}_{31}$ from chart $\mathtt{K}_3$ to chart $\mathtt{K}_1$ are defined by

$$r_2 = r_1 \epsilon_1, \quad w_2 = \epsilon_1^{-1}, \quad \tilde{x}_2 = \tilde{x}_1 \epsilon_1^{-1}, \tag{3.61a}$$

$$r_1 = r_3 w_3, \quad \tilde{x}_1 = w_3^{-1}, \quad \epsilon_1 = \epsilon_3 w_3^{-1}, \tag{3.61b}$$

for $\epsilon_1 > 0$ and $w_3 > 0$ respectively. Charts $\mathtt{K}_1$ and $\mathtt{K}_2$ are useful for the identification of $\gamma^{1,2}$, while we will use chart $\mathtt{K}_3$ in subsection 3.8.3 for the identification of $\gamma^{4,5}$.

Chart $\mathtt{K}_1$ We insert (3.60a) into (3.58) and divide the vector field by the common divisor r_1 to obtain the desingularized dynamics:

$$\begin{aligned}
r_1' &= r_1^2 \frac{\tilde{x}_1}{\xi}, \\
\tilde{x}_1' &= -\frac{\tilde{x}_1}{\xi} - \epsilon_1(\alpha + r_1 \tilde{x}_1 - \xi(r_1 + y)), \\
y' &= y r_1 \frac{\tilde{x}_1}{\xi} + \epsilon_1 r_1^2, \\
\epsilon_1' &= -\epsilon_1 \frac{\tilde{x}_1}{\xi}(2 + r_1), \\
r' &= 2r \frac{\tilde{x}_1}{\xi}.
\end{aligned} \tag{3.62}$$

The $\tilde{x}_1$-direction has gained hyperbolicity. We therefore obtain the following:

Lemma 3.19 *Let $\epsilon_1 < \delta$ with $\delta > 0$ fixed. Then in (3.62) there exists an attracting 4-dimensional centre manifold:*

$$\tilde{x}_1 = \epsilon_1 \left(-\alpha \xi + \xi^2 (r_1 + y) + \mathrm{O}(\epsilon_1) \right). \tag{3.63}$$

For the level sets $\varepsilon = const.$ and $q = \mathrm{e}^{-2/w_3}$, the centre manifold (3.63) is the extension of the slow-manifold S_ε introduced in Proposition 3.13 into chart $\mathtt{K}_1$.

As a consequence of Lemma 3.19 we have extended the hyperbolicity of C_0 up to $C_{0,\infty}$ for $\epsilon_1 = 0$. The dynamics within (3.63) is obtained by substituting

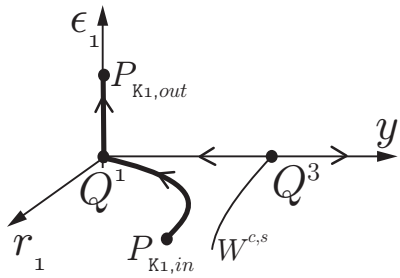

Figure 3.14: Dynamics within (3.63) projected along (r_1, y, ϵ_1).

(3.63) into (3.62) and by dividing the resulting vector field by ϵ_1:

$$\begin{aligned} r_1' &= r_1^2\left(-\alpha + \xi(r_1 + y) + \mathrm{O}(\epsilon_1)\right), \\ y' &= r_1^2 + y r_1\left(-\alpha + \xi(r_1 + y) + \mathrm{O}(\epsilon_1)\right), \\ \epsilon_1' &= -\epsilon_1(2 + r_1)\left(-\alpha + \xi(r_1 + y) + \mathrm{O}(\epsilon_1)\right), \\ r' &= 2r\left(-\alpha + \xi(r_1 + y) + \mathrm{O}(\epsilon_1)\right). \end{aligned} \tag{3.64}$$

System (3.64) has three invariant sets for $r_1 = 0, \epsilon_1 = 0$ and $r = 0$. In chart $\mathtt{K}_1$, the point $P_{\mathcal{K}_1,\mathrm{in}}$ has coordinates $P_{\mathtt{K}_1,\mathrm{in}} : (r_1, \tilde{x}_1, y, \epsilon_1, r) = (\delta, 0, \delta, 0, \exp(-2\delta^{-1}))$, and it lies on the invariant set $\epsilon_1 = 0$. The forward dynamics of $P_{\mathtt{K}_1,\mathrm{in}}$ contracts towards the invariant set $r = 0$, and since the other coordinates do not depend on r, we neglect this direction from now on. The remaining non-trivial dynamics is

$$\begin{aligned} r_1' &= r_1\left(-\alpha + \xi(r_1 + y) + \mathrm{O}(\epsilon_1)\right), \\ y' &= r_1 + y\left(-\alpha + \xi(r_1 + y) + \mathrm{O}(\epsilon_1)\right), \end{aligned} \tag{3.65}$$

where we have rescaled the right-hand side by dividing out the common factor r_1. System (3.65) has two equilibrium points $(r_1, y) = (0, 0)$ and $(r_1, y) = (0, \alpha/\xi)$.

Remark 3.20 *The two equilibrium points $(r_1, y) = (0, 0)$ and $(r_1, y) = (0, \alpha/\xi)$ of system (3.65) are the blown-up transformation of Q^1 and Q^3 respectively and their linear stability properties coincide with the ones stated in Proposition 3.3, see Figure 3.14.*

By construction, the point $P_{\mathtt{K}_1,\mathrm{in}}$ lies in the basin of attraction of Q^1, and therefore it contracts towards it. The plane $r_1 = 0$ is foliated with vertical invariant lines that expand exponentially along the ϵ_1-direction, as shown in Figure 3.14. We set $P_{\mathtt{K}_1,\mathrm{out}} := (r_1, \tilde{x}_1, y, \epsilon_1) = (0, -\delta(\alpha\xi + \mathrm{O}(\delta)), 0, \delta)$, with δ sufficiently small so that the point belongs to (3.63). We continue $P_{\mathtt{K}_1,\mathrm{out}}$ by using chart $\mathtt{K}_2$.

Chart $\mathtt{K}_2$ The dynamics on $\mathtt{K}_2$ is obtained by substituting (3.60b) into (3.58) and by dividing the right-hand side by the common divisor r_2

$$\begin{aligned} r_2' &= -2r_2\frac{\tilde{x}_2}{\xi},\\ w_2' &= w_2\frac{\tilde{x}_2}{\xi}(2+r_2w_2),\\ \tilde{x}_2' &= 2\frac{\tilde{x}_2^2}{\xi} - w_2(\alpha+r_2\tilde{x}_2) + w_2\frac{\tilde{x}_2}{\xi}(r_2\tilde{x}_2-1) + w_2\xi(r_2w_2+y),\\ y' &= r_2^2w_2^2 + yr_2w_2\frac{\tilde{x}_2}{\xi}. \end{aligned} \tag{3.66}$$

This systems has an equilibrium point in the origin with four zero eigenvalues. We introduce in (3.66) the blow-up transformation

$$w_2 = \rho^2, \quad \tilde{x}_2 = -\rho x, \tag{3.67}$$

and divide by the common divisor ρ, so that we obtain the desingularized vector field

$$\begin{aligned} r_2' &= 2r_2\frac{x}{\xi},\\ \rho' &= -\frac{\rho x}{2\xi}(2+r_2\rho^2),\\ x' &= \alpha - \frac{x^2}{\xi} - r_2\rho x - \frac{\rho x}{\xi}(r_2\rho x+1) - \xi(r_2\rho^2+y) + r_2\frac{x^2\rho^2}{2\xi},\\ y' &= r_2^2\rho^3 - yr_2\rho^2\frac{x}{\xi}. \end{aligned} \tag{3.68}$$

Lemma 3.21 *The point $P_{\mathtt{K}_1,out}$ is transformed in chart $\mathtt{K}_2$ into the point*

$$P_{\mathtt{K}_2,in} = \mathtt{K}_{12}(P_{\mathtt{K}_1,out}) := \quad (r_2,\rho,x,y) = (0,\delta^{-1/2},\alpha\xi\delta^{1/2}+\mathrm{O}(\delta^{1/2}),0).$$

The solution with initial condition in $P_{\mathtt{K}_2,in}$ converges towards the stable node

$$P_2 := \quad (r_2,\rho,x,y) = (0,0,\sqrt{\alpha\xi},0), \tag{3.69}$$

along the invariant plane $r_2 = 0$, see Figure 3.15.

Proof. We obtain $P_{\mathtt{K}_2,\mathrm{in}}$ by applying the transformation (3.61a) on point $P_{\mathtt{K}_1,\mathrm{out}}$ and then the blow-up (3.67). System (3.68) is invariant on the set $r_2 = 0$, and we rewrite the dynamics within this set as parameter independent. We do this, by introducing the new variables (ρ_1, x_1, t_1) such that $\rho = \sqrt{\alpha\xi}\rho_1, x = \sqrt{\alpha\xi}x_1, t_2 = \sqrt{\alpha/\xi}t_1$, where t_2 is the time in equation (3.68). Hence for $r_2 = 0$, we get the non-trivial dynamics

$$\begin{aligned} \dot{\rho}_1 &= -\rho_1 x_1,\\ \dot{x}_1 &= 1 - x_1^2 - \rho_1 x_1, \end{aligned} \tag{3.70}$$

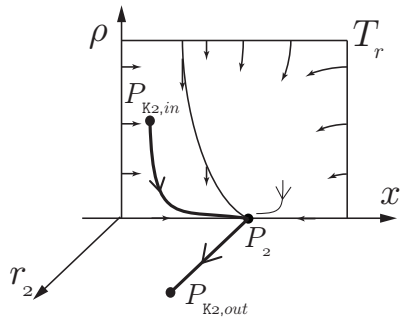

Figure 3.15: Trapping region.

with the dot meaning the derivative with respect to t_1. System (3.70) has one equilibrium point in $(\rho, x) = (0, 1)$, that is a stable node. The region $\rho_1 \geq 0, x_1 \geq 0$ is invariant for system (3.70) and we construct the trapping region

$$T_r := \{x_1 \geq 0\} \cap \{\rho_1 \geq 0\} \cap \{x_1 \leq 2\} \cap \{\rho_1 \leq \delta^{-1}\},$$

such that the stable node is the only equilibrium point within it. At the boundaries of T_r the vector field points everywhere inside the region itself, see Figure 3.15. Moreover, a direct analysis of the nullclines excludes the presence of limit cycles in T_r. We conclude that the solution departing from $P_{\mathrm{K}_2,\mathrm{in}}$ must be forward asymptotic to $(\rho, x) = (0, 1)$, that in the original coordinates corresponds to P_2 (3.69). □

We continue the analysis of (3.66) by following the unstable manifold of the equilibrium point P_2 on the invariant plane $w_2 = 0$. After a rescaling by the common factor $\tilde{x}_2$, we find that r_2 expands exponentially so that we fix the exit point $P_{\mathrm{K}_2,\mathrm{out}} : (r_2, w_2, \tilde{x}_2, y, r) = (\delta, 0, 0, 0, 0)$. We blow-down $P_{\mathrm{K}_2,\mathrm{out}}$ to chart $\mathcal{K}_1$ and map it to chart $\mathcal{K}_2$ so that we get $P_{\mathcal{K}_2,\mathrm{in}} : (w, \tilde{x}, y, r, q) = (0, 0, 0, 0, \delta^{-1})$.

Chart $\mathcal{K}_2$ The dynamics in chart $\mathcal{K}_2$ is given by

$$\begin{aligned}
r' &= 0,\\
q' &= 2q^2\frac{\tilde{x}}{\xi},\\
w' &= w^2 q\frac{\tilde{x}}{\xi},\\
\tilde{x}' &= -w(\tilde{x} - \xi y + \alpha) + wq\frac{\tilde{x}}{\xi}(\tilde{x} - 1) + \xi w^2,\\
y' &= w^2 + ywq\frac{\tilde{x}}{\xi},
\end{aligned} \tag{3.71}$$

where we have dropped the subscript and rescaled the right-hand side by r. We notice that chart $\mathcal{K}_2$ is foliated by sets $r = \varepsilon = const.$ and the point $P_{\mathcal{K}_2,\text{in}}$ lies on the invariant set $r = 0$. We reduce the following analysis to the four variables (w, x, y, q) since they are independent of r. For $w = q = 0$ we have that system (3.71) is a plane of non-hyperbolic equilibrium points. To overcome the loss of hyperbolicity we introduce the following blow-up map after having dropped the subscript:

$$w = \bar{r}\bar{w}, \quad q = \bar{r}\bar{q},$$

where $(\bar{w}, \bar{q}) \in S^1$ and $\bar{r} \geq 0$. We restrict our analysis to the two charts:

$$\hat{\mathtt{K}}_1 : \quad w = r_1, \qquad q = r_1 q_1, \tag{3.72a}$$

$$\hat{\mathtt{K}}_2 : \quad w = r_2 w_2, \qquad q = r_2, \tag{3.72b}$$

starting from $\hat{\mathtt{K}}_2$, since $q > 0$ in $P_{\mathcal{K}_2,\text{in}}$.

Chart $\hat{\mathtt{K}}_2$ We insert (3.72b) into (3.71) and divide by the common factor r_2 to obtain the vector field in chart $\hat{\mathtt{K}}_2$

$$\begin{aligned} r_2' &= 2r_2\frac{\tilde{x}}{\xi}, \\ w_2' &= w_2\frac{\tilde{x}}{\xi}(r_2 w_2 - 2), \\ \tilde{x}' &= -w_2(\tilde{x} - \xi y + \alpha) + r_2 w_2\frac{\tilde{x}}{\xi}(\tilde{x} - 1) + \xi r_2 w_2^2, \\ y' &= r_2 w_2^2 + y r_2 w_2\frac{\tilde{x}}{\xi}. \end{aligned} \tag{3.73}$$

In this chart, $P_{\mathcal{K}_2,\text{in}}$ is transformed into $P_{\hat{\mathtt{K}}_2,\text{in}} : (r_2, w_2, \tilde{x}, y) = (\delta^{-1}, 0, 0, 0)$ and it lies on a set of non-hyperbolic equilibria. We drop the subscript and introduce the further blow-up map

$$r = \bar{r}\bar{s}, \quad w = \bar{r}^2\bar{w}, \quad \tilde{x} = -\bar{r}\bar{\tilde{x}},$$

with $(\bar{s}, \bar{w}, \bar{\tilde{x}}) \in S^2$ and $\bar{r} \geq 0$, so that all the coordinates but y are blown-up at this stage. We focus on the two directional charts

$$\tilde{\mathtt{K}}_1 : r = r_1, \quad w = r_1^2 w_1, \quad \tilde{x} = -r_1\tilde{x}_1, \tag{3.74a}$$

$$\tilde{\mathtt{K}}_2 : r = r_2 s_2, \quad w = r_2^2 w_2, \quad \tilde{x} = -r_2. \tag{3.74b}$$

Chart $\tilde{\mathrm{K}}_1$ We insert (3.74a) into (3.73) and divide by the common factor r_1 to obtain the dynamics in chart $\tilde{\mathrm{K}}_1$

$$\begin{aligned} r_1' &= -2r_1\frac{\tilde{x}_1}{\xi},\\ w_1' &= w_1\frac{\tilde{x}_1}{\xi}(-r_1^3w_1+6),\\ \tilde{x}_1' &= w_1(-r_1\tilde{x}_1-\xi y+\alpha)+r_1^2w_1\frac{\tilde{x}_1}{\xi}(-r_1\tilde{x}_1-1)+2\frac{\tilde{x}_1^2}{\xi}-\xi r_1^3w_1^2,\\ y' &= r_1^4w_1^2-yr_1^3w_1\frac{\tilde{x}_1}{\xi}. \end{aligned} \tag{3.75}$$

The point $P_{\tilde{\mathrm{K}}_2,\mathrm{in}}$ is mapped to $P_{\tilde{\mathrm{K}}_1,\mathrm{in}}:(r_1,w_1,\tilde{x}_1,y)=(\delta^{-1},0,0,0)$ and it lies on the invariant set $w_1=0$. On such set the dynamics reduces to

$$\begin{aligned} r_1' &= -2r_1\frac{\tilde{x}_1}{\xi},\\ \tilde{x}_1' &= 2\frac{\tilde{x}_1^2}{\xi},\\ y' &= 0. \end{aligned} \tag{3.76}$$

In (3.76) there is a plane of equilibria for $\tilde{x}_1=0$, that is attracting for $\tilde{x}_1<0$ and repelling for $\tilde{x}_1>0$. We divide the right-hand side of (3.76) by $\tilde{x}_1$ to study the evolution of r_1 within this plane and we find that r_1 decreases exponentially. Therefore, the solution departing from $P_{\tilde{\mathrm{K}}_1,\mathrm{in}}$ contracts towards $r_1=0$ and expands along $\tilde{x}_1$, as shown in Figure 3.16(a). We set $P_{\tilde{\mathrm{K}}_1,\mathrm{out}}:(r_1,w_1,\tilde{x}_1,y)=(0,0,\delta,0)$ and move to chart $\tilde{\mathrm{K}}_2$, where $P_{\tilde{\mathrm{K}}_1,\mathrm{out}}$ is mapped to the point $P_{\tilde{\mathrm{K}}_2,\mathrm{in}}:(s_2,w_2,r_2,y)=(\delta^{-1},0,0,0)$.

Chart $\tilde{\mathrm{K}}_2$ We substitute (3.74b) in (3.73) and divide the right-hand side by the common factor r_2 to obtain the vector field in chart $\tilde{\mathrm{K}}_2$

$$\begin{aligned} r_2' &= r_2w_2\left(\alpha-r_2-\xi y-r_2^2\frac{s_2}{\xi}(r_2+1)-\xi r_2^3s_2w_2\right),\\ w_2' &= w_2\left(\frac{2}{\xi}-r_2^3s_2w_2\frac{1}{\xi}+2w_2(r_2+\xi y-\alpha)+2r_2^2w_2\frac{s_2}{\xi}(r_2+1)+2\xi r_2^3s_2w_2^2\right),\\ s_2' &= s_2\left(-\frac{2}{\xi}+w_2(r_2+\xi y-\alpha)+r_2^2w_2\frac{s_2}{\xi}(r_2+1)+\xi r_2^3s_2w_2^2\right),\\ y' &= r_2^3w_2s_2\left(r_2w_2-\frac{y}{\xi}\right). \end{aligned} \tag{3.77}$$

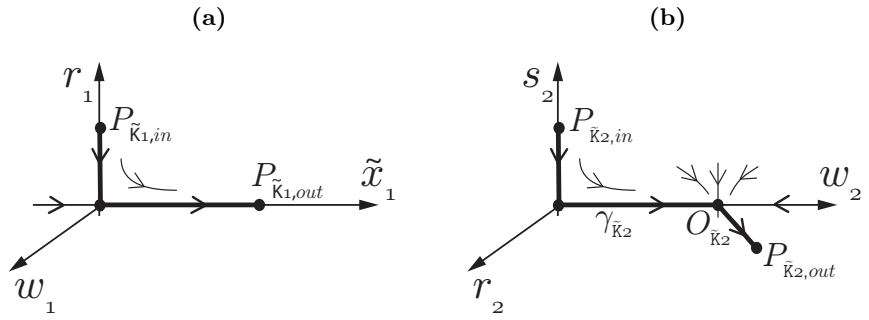

Figure 3.16: (a): singular dynamics in chart $\tilde{\mathrm{K}}_1$ projected in the $(r_1, \tilde{x}_1, w_1)$-coordinates. (b): singular dynamics in chart $\tilde{\mathrm{K}}_2$ projected in the (s_2, w_2, r_2)-coordinates.

Lemma 3.22 *There exists a singular trajectory $\gamma_{\tilde{K}_2}$, connecting $P_{\tilde{K}_2,in}$ to the point*

$$O_{\tilde{K}_2} := (r_2, w_2, s_2, y) = (0, (\alpha\xi)^{-1}, 0, 0), \tag{3.78}$$

as shown in Figure 3.16(b).

Proof. The set $r_2 = 0$ corresponds to the blow-up of the point Q^1, and $P_{\tilde{K}_2,\mathrm{in}}$ lies on this set. When $r_2 = 0$, (3.77) reduces to

$$\begin{aligned} w_2' &= 2w_2\left(\frac{1}{\xi} - w_2\alpha\right), \\ s_2' &= -s_2\left(\frac{2}{\xi} + w_2\alpha\right), \\ y' &= 0. \end{aligned}$$

This system has two equilibria: $(w_2, s_2) = (0, 0)$ is a saddle with eigenvalues $2/\xi, -2/\xi$ and eigenvectors $(1,0)^T, (0,1)^T$ respectively, and $O_{\tilde{K}_2} : (w_2, s_2) = ((\alpha\xi)^{-1}, 0)$ is a proper stable node with eigenvalues $-2/\xi, -3/\xi$ and eigenvectors $(1,0)^T, (0,1)^T$ respectively. Hence there exists a singular trajectory $\gamma_{\tilde{K}_2}$ departing from $P_{\tilde{K}_2,\mathrm{in}}$, that contracts to the saddle, and then to the stable node, by following the unstable manifold of the saddle. □

Along the invariant plane $s_2 = 0$, (3.77) reduces to

$$\begin{aligned} r_2' &= r_2 w_2(\alpha - r_2), \\ w_2' &= \frac{2w_2}{\xi}\left(1 - w_2\xi(\alpha - r_2)\right), \end{aligned}$$

and $O_{\tilde{\mathrm{K}}_2} : (r_2, w_2) = (0, (\alpha\xi)^{-1})$ is a saddle with eigenvalues $1/\xi, -2/\xi$ and corresponding eigenvectors $(3\alpha^2\xi/2, 1)^T, (0, 1)^T$ respectively. We define $P_{\tilde{\mathrm{K}}_2,\mathrm{out}} := (r_2, w_2, s_2, y) = (\delta, 2\delta(3\alpha^2\xi)^{-1}, 0, 0)$ a point along the unstable manifold of $O_{\tilde{\mathrm{K}}_2}$.

We blow-down $P_{\tilde{\mathrm{K}}_2,\mathrm{out}}$ to chart $\hat{\mathrm{K}}_2$ we map it to chart $\hat{\mathrm{K}}_1$ so that we get $P_{\hat{\mathrm{K}}_1,\mathrm{in}} := (r_1, q_1, \tilde{x}, y) = (0, 3\alpha^2\xi/(2\delta^3), -\delta, 0)$.

Chart $\hat{\mathrm{K}}_1$ We substitute (3.74a) in (3.73) and divide the right-hand side by the common factor r_1 to obtain the vector field in chart $\tilde{\mathrm{K}}_1$

$$\begin{aligned} r_1' &= r_1^2 q_1 \frac{\tilde{x}}{\xi}, \\ q_1' &= q_1^2 \frac{\tilde{x}}{\xi}(2 - r_1), \\ \tilde{x}' &= -\tilde{x} + \xi y - \alpha + r_1 q_1 \frac{\tilde{x}}{\xi}(\tilde{x} - 1) - \xi r_1, \\ y' &= r_1 + y r_1 q_1 \frac{\tilde{x}}{\xi}. \end{aligned} \tag{3.79}$$

In the following important lemma we identify the line L_0 and the segment $\gamma^{1,2}$.

Lemma 3.23 *In chart $\hat{\mathrm{K}}_1$ there exists an attracting 3-dimensional centre manifold*

$$\tilde{x} = -\alpha + \xi y - \xi r_1 + \mathrm{O}(y + r_1 + q_1)^2, \tag{3.80}$$

whose intersection with the plane $r_1 = q_1 = 0$ corresponds to the line L_0. The trajectory $\gamma^{1,2}$ defined in (3.47) connects the point $O_{\tilde{\mathrm{K}}_2}$ (3.78) to

$$P_{\hat{\mathrm{K}}_1,cm} := (r_1, q_1, \tilde{x}, y) = (0, 3\alpha^2\xi/(2\delta^3), -\alpha, 0), \tag{3.81}$$

along a stable fibre, where $O_{\tilde{\mathrm{K}}_2}$ lies on the blow-up of Q^1 and $P_{\hat{\mathrm{K}}_1,cm}$ lies on the blow-up of Q^2.

Proof. System (3.79) has a line of equilibria for $r_1 = q_1 = 0, \tilde{x} = \xi y - \alpha, y \in \mathbb{R}$. This line corresponds to L_0 through the coordinate changes (3.57b) and (3.74a). The linearized dynamics around L_0 is hyperbolic only in the x-direction and furthermore is stable. Therefore the centre manifold (3.80) appears for r_1, q_1 sufficiently small. The point $P_{\hat{\mathrm{K}}_1,\mathrm{in}}$ has a solution backwards asymptotic to $O_{\tilde{\mathrm{K}}_2}$ and forward asymptotic to $P_{\hat{\mathrm{K}}_1,\mathrm{cm}} \in L_0$ through a stable fibre, where $P_{\hat{\mathrm{K}}_1,\mathrm{cm}}$ lies on the blow-up of Q^2. We denote this connection by $\gamma^{1,2}$. □

3.8.2 Identification of $\gamma^{2,4}$

We insert (3.80) into (3.79) to obtain the dynamics within the centre manifold

$$\begin{aligned} r_1' &= r_1^2 \frac{q_1}{\xi}\left(-\alpha + \xi y - \xi r_1 + \mathrm{O}(y + r_1 + q_1)^2\right), \\ q_1' &= q_1^2 \frac{2 - r_1}{\xi}\left(-\alpha + \xi y - \xi r_1 + \mathrm{O}(y + r_1 + q_1)^2\right), \\ y' &= r_1 + y r_1 \frac{q_1}{\xi}\left(-\alpha + \xi y - \xi r_1 + \mathrm{O}(y + r_1 + q_1)^2\right), \end{aligned}$$

and $q_1 = r_1 = 0, y \in \mathbb{R}$ identifies a line of non-hyperbolic equilibrium points, that corresponds to L_0. We gain hyperbolicity of L_0 by introducing the blow-up transformation

$$r_1 = \rho\sigma, \quad q_1 = \rho, \tag{3.82}$$

where $\rho \geq 0, \sigma \geq 0$. In chart (3.82) the point Q^2 (3.45a) is blown-up to the σ-axis $\{y = \rho = 0, \sigma \geq 0\}$. Similarly, Q^4 (3.45b) corresponds to the line $\{y = 2\alpha/\xi, \rho = 0, \sigma \geq 0\}$. We divide the vector field of chart (3.82) by the common divisor ρ and obtain

$$\begin{aligned} \sigma' &= 2\sigma\left(\rho\sigma - 1\right)\left(-\frac{\alpha}{\xi} + y - \rho\sigma + \mathrm{O}(y + \sigma + \rho)^2\right), \\ y' &= \sigma + y\rho\sigma\left(-\frac{\alpha}{\xi} + y - \rho\sigma + \mathrm{O}(y + \sigma + \rho)^2\right), \\ \rho' &= \rho(2 - \rho\sigma)\left(-\frac{\alpha}{\xi} + y - \rho\sigma + \mathrm{O}(y + \sigma + \rho)^2\right). \end{aligned} \tag{3.83}$$

The point $P_{\hat{\mathrm{K}}_1,\mathrm{cm}}$ (3.81) is mapped into the point $P_{\mathrm{in}} : (\sigma, y, \rho) = (0, 0, 3\alpha^2\xi/(2\delta^3))$, and this lies in the invariant plane $\sigma = 0$.

Lemma 3.24 (3.83) *has two invariant planes for* $\rho = 0$ *and* $\sigma = 0$. *Their intersection* $\rho = \sigma = 0$ *is a line of equilibrium points. We have:*

- *On the plane* $\sigma = 0$ *the solution contracts towards the equilibrium at the origin along the strong stable manifold:*

$$W^s(0,0,0) := \left\{(\sigma, y, \rho) \in \mathbb{R}^2 \times \mathbb{R}^+ | \quad \sigma = 0, y = 0, \rho \geq 0\right\}. \tag{3.84}$$

- *There exists an heteroclinic connection*

$$\gamma^{2,4} = \left\{(\sigma, y, \rho) \in \mathbb{R}^2 \times \mathbb{R}^+ | \sigma = 2\frac{\alpha}{\xi}y - y^2, y \in \left(0, 2\frac{\alpha}{\xi}\right), \rho = 0\right\}, \tag{3.85}$$

joining $(\sigma, y, \rho) = (0, 0, 0)$ *backwards in time with* $(\sigma, y, \rho) = (0, 2\alpha/\xi, 0)$ *forward in time.*

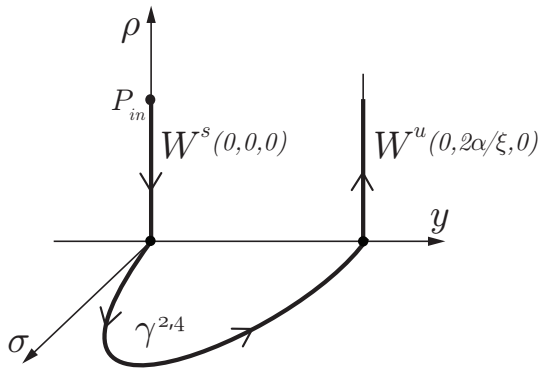

Figure 3.17: Dynamics in chart $\hat{K}_1$. The plane $\rho = 0$ corresponds to the blown-up line L_0.

- *The point* $(\sigma, y, \rho) = (0, 2\alpha/\xi, 0)$ *has a strong unstable manifold*

$$W^u(0, 2\alpha/\xi, 0) = \left\{(\sigma, y, \rho) \in \mathbb{R}^2 \times \mathbb{R}^+ |\ \sigma = 0, y = 2\alpha/\xi, \rho \geq 0\right\}. \quad (3.86)$$

The results of Lemma 3.24 are summarised in Figure 3.17.

Remark 3.25 *Upon blowing down, the expression in* (3.85) *gives* $\gamma^{2,4}$ *in* (3.48). *We use the same symbol in* (3.85) *and* (3.48) *for simplicity.*

Proof. On the invariant plane $\sigma = 0$ we have

$$\begin{aligned} \dot{y} &= 0, \\ \dot{\rho} &= 2\rho\left(y - \frac{\alpha}{\xi}\right)(1 + \mathrm{O}(\rho)). \end{aligned} \quad (3.87)$$

This plane is foliated with invariant lines in the y-direction. The solution of (3.87) with $y = 0$ is (3.84) and contracts towards the invariant plane $\rho = 0$. Hence this trajectory acts as a strong stable manifold. We substitute $\rho = 0$ in (3.83) and, after dividing by σ, we obtain the explicit solution (3.85) given the initial condition in the origin. This solution is forward asymptotic to $(\sigma, y, \rho) = (0, 2\alpha/\xi, 0)$. The strong unstable manifold (3.86), is the solution of (3.87) with $y = 2\alpha/\xi$. □

3.8.3 Identification of $\gamma^{4,5}$

The invariance of the unstable manifold $W^u(0, 2\alpha/\xi, 0)$ persists in the blown-down chart $\hat{\mathtt{K}}_1$. We continue the analysis on chart $\hat{\mathtt{K}}_2$ (3.72b), so that we can describe the behaviour of the dynamics for large values of q_1. We desingularize the vector field by dividing by the common divisor r_2, and we find that there are two invariant planes for $r_2 = 0$ and $w_2 = 0$. $W^u(0, 2\alpha/\xi, 0)$ enters chart $\hat{\mathtt{K}}_2$ on the plane $r_2 = 0$ and contracts towards the origin. We continue this trajectory by following the unstable manifold of the origin on the plane $w_2 = 0$. Here we exit the chart $\hat{\mathtt{K}}_2$ with r_2 large. Consequently we blow-down the orbit to chart $\mathcal{K}_2$, where we enter with $w = 0$ and q large, and we find that the orbit evolves on an invariant line with q increasing. Eventually the chart $\mathcal{K}_2$ is no longer suited to describe the trajectory. We use (3.57) to move back to chart $\mathcal{K}_1$ and, in this chart, the trajectory γ_1^2 becomes

$$\mathcal{K}_{21}(\gamma_1^2) := \left\{ (r, w, \tilde{x}, y, \epsilon) \in \mathbb{R}^{2,+} \times \mathbb{R}^3 | w = r = 0, \tilde{x} = \alpha, y = \frac{2\alpha}{\xi}, \epsilon \geq 0 \right\}. \tag{3.88}$$

Recall from (3.53) and (3.57a) that r is slaved by w, since $r = \mathrm{e}^{-2/w}$, therefore (3.58) has a redundant equation in r that we can drop since the dynamics of $(w, \tilde{x}, y, \epsilon)$ is independent of r.
In chart $\mathcal{K}_1$ (3.58), the set $w = \tilde{x} = 0$ is filled of non-hyperbolic equilibrium points. We blow-up this set by using the map (3.59), and subsequently we enter chart $\mathtt{K}_3$.

Chart $\mathtt{K}_3$ We substitute (3.60c) into (3.58) and divide by the common factor r_3 to obtain the dynamics in chart $\mathtt{K}_3$

$$\begin{aligned}
r_3' &= r_3 w_3 \left(-\epsilon_3 (r_3 - \xi y + \alpha) + \frac{r_3 - 1}{\xi} + \xi r_3 \epsilon_3 w_3 \right), \\
w_3' &= \frac{w_3^2}{\xi} \left(1 + \xi \epsilon_3 (r_3 - \xi y + \alpha) - \xi^2 r_3 \epsilon_3 w_3 \right), \\
y' &= r_3 w_3 \left(r_3 \epsilon_3 w_3 + \frac{y}{\xi} \right), \\
\epsilon_3' &= -\frac{2\epsilon_3}{\xi} + \epsilon_3 w_3 \left(\epsilon_3 (r_3 - \xi y + \alpha) + \frac{1 - r_3}{\xi} - \xi r_3 \epsilon_3 w_3 \right), \\
r' &= \frac{2r}{\xi}.
\end{aligned} \tag{3.89}$$

The ϵ_3-direction has gained hyperbolicity. The variable r in (3.89) is slaved by $r_3 w_3$ because $r = \mathrm{e}^{-2/r_3 w_3}$ by (3.53), (3.57a) and (3.60c). We drop r from now on, since the remaining dynamics on $(r_3, w_3, y, \epsilon_3)$ is independent of it.

Lemma 3.26 *The set*

$$\mathcal{C}_{\mathrm{K}_3} := \left\{(r_3, w_3, y, \epsilon_3) \in \mathbb{R}^4 \mid \quad r_3 \in [0, 2\alpha], w_3 \in [0, \delta], y \in [0, 4\alpha/\xi], \epsilon_3 = 0\right\},$$

with $\delta > 0$ sufficiently small, is an attracting centre manifold having a foliation of smooth stable fibres along which ϵ_3 contracts like $\mathrm{e}^{-2t/\xi}$ in forward time.

Proof. $w_3 = \epsilon_3 = 0$ is a line of equilibria for (3.89). The linearization about any point along this line gives $-2/\xi$ as the only non-zero eigenvalue, with the ϵ_3-direction the corresponding eigenvector. We therefore obtain the centre manifold by standard theory. □

It follows that the singular trajectory (3.88) contracts to the point $P_{\mathrm{K}_3} := (r_3, w_3, y, \epsilon_3) = (\alpha, 0, 2\alpha/\xi, 0)$ under the attraction of the centre manifold $\mathcal{C}_{\mathrm{K}_3}$. The dynamics within the centre manifold is obtained by setting $\epsilon_3 = 0$ in (3.89). This gives a new layer problem

$$\begin{aligned} r_3' &= r_3 w_3 \frac{r_3 - 1}{\xi}, \\ w_3' &= \frac{w_3^2}{\xi}, \\ y' &= r_3 w_3 \frac{y}{\xi}, \end{aligned} \tag{3.90}$$

that is reminiscent of the original layer problem of (3.55) for $\varepsilon = 0$ through the blow-ups (3.57a) and (3.60c). The set $w_3 = 0$ is a set of equilibria for (3.90). We obtain a slow flow within $w_3 = 0$ by dividing the right-hand side of (3.90) by the common factor w_3 so that we obtain

$$\begin{aligned} r_3' &= \frac{r_3}{\xi}(r_3 - 1), \\ w_3' &= \frac{w_3}{\xi}, \\ y' &= y\frac{r_3}{\xi}. \end{aligned} \tag{3.91}$$

In (3.91), the evolution of the variables (r_3, y) does not depend upon w_3. Furthermore, both r_3 and w_3 are now hyperbolic directions.

Lemma 3.27 *Assume $\xi < \alpha < 1$. On the invariant set $w_3 = 0$, the solution of (3.91) departing from P_{K_3} contracts towards the point Q^5 (3.45c) by following the "fast fibre"*

$$\gamma^{4,5}: \quad y(t) = \frac{2\alpha}{\xi(1-\alpha)}(1 - r_3(t)), \tag{3.92}$$

for $r_3(t) \to 0$, where (3.92) is the explicit expression of $\gamma^{4,5}$.

PROOF. In (3.91) the solution departing from $P_{\mathtt{K}_3}$ contracts towards $r_3 = 0$ when $\xi < \alpha < 1$. Furthermore, we observe that

$$\frac{\mathrm{d}r_3}{r_3 - 1} = \frac{\mathrm{d}y}{y}.$$

By integrating this equation with initial condition in $P_{\mathtt{K}_3}$ and $\xi < \alpha < 1$, we obtain the solution (3.92). Thus, when $r_3 \to 0$, by (3.92) we have $y_3 \to 2\alpha/(\xi(1-\alpha))$, that is the point $Q^5 \in C_{0,\infty}$. □

REMARK 3.28 *The results in chart* $\mathtt{K}_3$ *are obtained within the assumption* $\xi < \alpha < 1$. *The reason for this is that the point* Q^5 (3.45c) *has coordinates* $(\tilde{x}_3, y_3, w_3) = (0, 2\alpha/(\xi(1-\alpha)), 0)$ *in chart* K_3, *so that it is visible in chart* K_3 *(and in its blow-ups) only when* $\xi < \alpha < 1$.
However, Conjecture 3.16 only requires $\xi < \alpha$. *To identify* $\gamma^{4,5}$ *for* $\alpha \geq 1$, *one needs to consider the dynamics in chart* K_1, *so that* Q^5 *is again visible.*
However, in chart K_1 *the analysis is complicated by the presence of terms of the type* e^{z_1/w_1} *in the vector field. Such terms require complicated blow-ups in order to desingularize the point* $z_1 = w_1 = 0$, *similar to what done in subsection 3.5.2 and for this reason, in this exposition we only focus on the case* $\xi < \alpha < 1$, *even though we believe the result also to be valid for* $\alpha \geq 1$.

REMARK 3.29 *Consider* $0 < \varepsilon \ll 1$. *Recall from* (3.53), (3.57a) *and* (3.60c) *that* $\varepsilon = \mathrm{e}^{-2/r_3 w_3}\, r_3 \epsilon_3$. *Since we enter chart* $\mathtt{K}_3$ *with* $r_3 = \alpha$ *and* $\epsilon_3 = \delta$ *small, we have consequently that* $w_3 = \mathrm{O}(\ln^{-1}(\varepsilon^{-1})) \ll 1$ *and* $w = r_3 w_3 = \mathrm{O}(\ln^{-1}(\varepsilon^{-1}))$.
In (3.91) *we notice that the rate of contraction of* r_3 *coincides with the rate of expansion of* w_3. *Since chart* $\mathtt{K}_3$ *is defined by* $w = r_3 w_3$ (3.60c), *it follows that while* r_3 *decreases from* α *to* $\mathrm{O}(\ln^{-1}(\varepsilon^{-1}))$, w_3 *increases with the same rate up to* $\mathrm{O}(1)$, *so that the product* $w = r_3 w_3 = \mathrm{O}(\ln^{-1}(\varepsilon^{-1}))$ *remains of the same order. Furthermore, since* $r = \mathrm{e}^{-2/r_3 w_3}$, *we realise that* $r = \mathrm{O}(\varepsilon^k)$ *with* $0 < k < 1$, *when we exit a neighbourhood of the saddle in* (3.91), *see the following section.*

3.8.4 Identification of $\gamma^{5,6}$

On the invariant set $r_3 = 0$, the w_3-direction is unstable. We follow the solution from the point $P_{\mathtt{K}_3,out} := (r_3, w_3, y, \epsilon_3) = (0, \delta, 2\alpha/(\xi(1-\alpha)), 0)$ into chart $\mathtt{K}_1$ by using the transformation (3.61b). Here, we enter in a point $P_{\mathtt{K}_1,in} := (r_1, \tilde{x}_1, y, \epsilon_1) = (0, \delta^{-1}, 2\alpha/(\xi(1-\alpha)), 0)$ where we have again dropped the r-coordinate since this is slaved by r_1. Because of Lemma 3.19, the solution departing from $P_{\mathtt{K}_1,in}$ contracts towards the centre manifold (3.63), where we have re-gained hyperbolicity of C_0 at $C_{0,\infty}$ for $\epsilon_1 = 0$. We continue the analysis

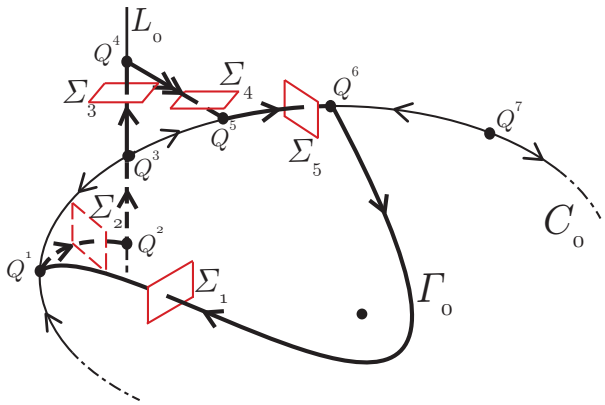

Figure 3.18: Sections $\Sigma_i, i = 1, \ldots, 5$.

by considering the reduced problem in chart k_1 (3.23), that is

$$w_1' = -w_1^2(e^{z_1/w_1} - 1),$$
$$z_1' = e^{z_1/w_1}(\alpha z_1 - \xi) - w_1(\xi + z_1)(e^{z_1/w_1} - 1).$$

By repeating the analysis of section 3.5, we can identify the singular trajectory $\gamma^{5,6}$ that connects Q^5 to the point Q^6. From the point Q^6 the solution is connected to the point Q^1 through the manifold $W^{c,u}$. This closes the singular cycle Γ_0.

3.9 Construction of the Poincaré map and outline of the proof

In order to prove Conjecture 3.16, we wish to construct a Poincaré map that has an attracting fixed point. To construct such map, we introduce five local sections $\Sigma_i,\ i = 1 \ldots 5$, as illustrated in Figure 3.18, such that

Σ_1 is transversal to the unstable manifold $W^{c,u}$ and close to Q^1;
Σ_2 is transversal to the segment $\gamma^{1,2}$ and close to Q^2;
Σ_3 is transversal to the segment $\gamma^{2,4}$ and close to Q^4;
Σ_4 is transversal to the segment $\gamma^{4,5}$ and close to Q^5;
Σ_5 is transversal to the segment $\gamma^{5,6}$ and close to Q^6.

We compose the Poincaré map of five local transitions maps $\Pi_i,\ i = 1 \ldots 5$

$$\Pi := \Pi_5 \circ \Pi_4 \circ \Pi_3 \circ \Pi_2 \circ \Pi_1,$$

where each local map is defined in a suitable neighbourhood of the singular cycle Γ_0, and describes respectively

$\Pi_1 : \Sigma_1 \to \Sigma_2$, passage by the improper stable node Q^1;
$\Pi_2 : \Sigma_2 \to \Sigma_3$, contraction to the line L_0 and evolution along it;
$\Pi_3 : \Sigma_3 \to \Sigma_4$, identification of the fast fibre near Q^4 ;
$\Pi_4 : \Sigma_4 \to \Sigma_5$, contraction towards the attracting slow manifold;
$\Pi_5 : \Sigma_5 \to \Sigma_1$, passage by the point Q^6 and evolution on the slow manifold.

Proposition 3.4 and the use of the blow-up method in section 3.8 have allowed us to identify the singular orbit Γ_0 and its dynamical properties using local hyperbolic methods. Thanks to this analysis, in the blown-up charts K_3 and K_1 we can track a full neighbourhood $N \subset \Sigma_1$ of $\Sigma_1 \cap W^{c,u}$ along the local transition maps $\Pi_i,\ i = 1, \dots, 5$. In this way, we can obtain the desired return map $\Pi : N \to N$ for ε sufficiently small. Furthermore, for $\varepsilon = 0$ the forward flow of N contracts to the point Q^1, providing the desired contraction of Π and establishing, by the Contraction Mapping Theorem, the existence of the limit cycle Γ_ε satisfying $\Gamma_\varepsilon \to \Gamma_0$ for $\varepsilon \to 0$.

Remark 3.30 *We decide not to call Conjecture 3.16 a theorem because there are some difficulties that we have not fully entangled in the previous section. Our blow-up approach has allowed us to gain hyperbolicity of C_0 near Q^5, but we have not extended this result up to Q^6. Here terms like e^{z_1/w_1} appear, and we would have to combine the approach of section 3.5 with the introduction of a suitable variable q so that we can obtain an extended vector field containing only algebraic terms [Kri17].*

We establish the contraction to the point Q^1 for $\varepsilon = 0$ by studying the local transition map Π_1. We outline the construction of such map in subsection 3.9.1, and we leave the analysis of the remaining four local maps $\Pi_i,\ i = 2, \dots, 5$ to another manuscript.

3.9.1 Analysis of Π_1, passage by the improper node Q^1

We construct the map Π_1 as the combination of the local transition maps

$$\Pi_1 := \pi_5 \circ \pi_4 \circ \pi_3 \circ \pi_2 \circ \pi_1,$$

where $\pi_i,\ i = 1, \dots, 5$ are defined in Table 3.1.

The contraction to the point Q^1 for $\varepsilon = 0$ is described by the local map π_1, that we explicitly describe in the following. We leave the detailed description of the remaining four local maps $\pi_i,\ i = 2, \dots, 5$ to another manuscript.

Table 3.1: Local maps $\pi_i,\ i = 1, \dots, 5$

map	chart	from ... to	equation
π_1	$\mathtt{K}_1$	$\Sigma_1 \to \Sigma_{\mathtt{K}_1,\mathrm{out}}$	(3.62)
π_2	$\mathtt{K}_2$	$\Sigma_{\mathtt{K}_2,\mathrm{in}} \to \Sigma_{\mathtt{K}_2,\mathrm{out}}$	(3.66)
π_3	$\tilde{\mathtt{K}}_1$	$\Sigma_{\tilde{\mathtt{K}}_1,\mathrm{in}} \to \Sigma_{\tilde{\mathtt{K}}_1,\mathrm{out}}$	(3.75)
π_4	$\tilde{\mathtt{K}}_2$	$\Sigma_{\tilde{\mathtt{K}}_2,\mathrm{in}} \to \Sigma_{\tilde{\mathtt{K}}_2,\mathrm{out}}$	(3.77)
π_5	$\hat{\mathtt{K}}_1$	$\Sigma_{\hat{\mathtt{K}}_1,\mathrm{in}} \to \Sigma_2$	(3.79)

Map π_1 We analyse the map π_1 in chart $\mathtt{K}_1$. Here we define Σ_1 and $\Sigma_{\mathtt{K}_1,\mathrm{out}}$ as

$$\Sigma_1 := \left\{ r_1 = \delta, |y| \le \beta_1, \epsilon_1 \in \left[0, \varepsilon_0 \frac{\mathrm{e}^{2/\delta}}{\delta}\right], r = \mathrm{e}^{-2/r_1}, |\tilde{x}_1| \le \beta_2 \right\},$$
$$\Sigma_{\mathtt{K}_1,\mathrm{out}} := \{ r_1 \in [0, \beta_3], |y| \le \beta_4, \epsilon_1 = \delta, r = \mathrm{e}^{-2/r_1}, |\tilde{x}_1| \le \beta_5 \},$$

with $\beta_i > 0,\ i = 1, \dots, 5$ and ε_0 positive and sufficiently small such that $0 < \varepsilon \le \varepsilon_0$. In the assumption that β_1, δ are sufficiently small, system (3.64) is equivalent to

$$\begin{aligned} r_1' &= -r_1^2, \\ y' &= -y r_1 + \frac{r_1^2}{G(r_1, y, \epsilon_1)}, \\ \epsilon_1' &= \epsilon_1 (2 + r_1), \\ r' &= -2r, \end{aligned} \tag{3.93}$$

where we have divided the right-hand side by the factor $G(r_1, y, \epsilon_1) := \alpha - \xi(r_1 + y) + \mathrm{O}(\epsilon_1)$, that does not vanish in a small neighbourhood of the origin.

Lemma 3.31 *For system (3.93), the transition map*

$$\pi_1 : \Sigma_1 \to \Sigma_{\mathtt{K}_1,out}, \quad (\delta, y_{in}, \epsilon_{1,in}, \mathrm{e}^{-2/\delta}, \tilde{x}_{1,in}) \mapsto (r_{1,out}, y_{out}, \delta, \mathrm{e}^{-2/r_{1,out}}, \tilde{x}_{1,out}),$$

is well defined for δ, β_i sufficiently small, and satisfies

$$\tilde{x}_{1,out} = \delta \left(-\alpha\xi + \xi^2 (r_{1,out} + y_{out}) + \mathrm{O}(\delta) \right) + \mathrm{O}(\mathrm{e}^{-c/\epsilon_{1,in}}),$$

using (3.63), and

$$\frac{y_{in}}{1 + \delta T} + \frac{\delta}{2\alpha} \frac{\ln(1 + \delta T)}{1 + \delta T} \le y_{out} \le \frac{y_{in}}{1 + \delta T} + \frac{2\delta}{\alpha} \frac{\ln(1 + \delta T)}{1 + \delta T}, \tag{3.94}$$

where T is the solution of the Lambert equation

$$\delta = \epsilon_{1,in}\, \mathrm{e}^{2T} (1 + \delta T). \tag{3.95}$$

The phase space of (3.93) *is foliated by the invariant manifolds*

$$\begin{aligned} r_1(t)\epsilon_1(t)r(t) &= \delta\epsilon_{1,in}\,\mathrm{e}^{-2/\delta} = const., \\ r(t) &= \mathrm{e}^{-2/r_1(t)}\,. \end{aligned} \tag{3.96}$$

On such manifolds, $r_1(t)$ *decays algebraically,* $\epsilon_1(t)$ *expands exponentially and* $y(t)$ *decays at most algebraically.*

Proof. Using the stable foliation of (3.63), we reduce to the centre manifold (3.63). The explicit solution of (3.93) with initial condition in $\Sigma_1 : (r_1, y, \epsilon_1, r)(0) = (\delta, y_{in}, \epsilon_{1,in}, \mathrm{e}^{-2/\delta})$ is

$$\begin{aligned} r_1(t) &= \frac{\delta}{1+\delta t}, \\ \epsilon_1(t) &= \epsilon_{in}\,\mathrm{e}^{2t}(1+\delta t), \\ r(t) &= \mathrm{e}^{-2(1+\delta t)/\delta}\,. \end{aligned} \tag{3.97}$$

In (3.97) we have not computed the solution for $y(t)$, since this is more complicated and we give bounds for it below. The expression (3.95), for the transition time from Σ_1 to $\Sigma_{\mathrm{K}_1,out}$, is computed from the solution for $\epsilon_1(t)$ in (3.97). Suppose that the solution of (3.93) for y is of the form

$$y(t) = \frac{z(t)}{1+\delta t}, \tag{3.98}$$

where $z(0) = y_{in}$. Then we get the following equation for z

$$z' = \frac{\delta^2}{1+\delta t}\frac{1}{G(r_1, y, \epsilon_1)}. \tag{3.99}$$

For δ, β_i sufficiently small, we can bound $G(r_1, y, \epsilon_1)$ as $\alpha/2 \le G \le 2\alpha$ so that (3.99) is bounded by

$$\frac{1}{2\alpha}\frac{\delta^2}{1+\delta t} \le z' \le \frac{2}{\alpha}\frac{\delta^2}{1+\delta t}.$$

By integrating this equation for $t \in [0, T]$ we obtain

$$\frac{\delta}{2\alpha}\ln(1+\delta T) \le z(T) - y_{in} \le \frac{2\delta}{\alpha}\ln(1+\delta T).$$

(3.94) follows by inserting this solution in (3.98) where $y(T) = y_{out}$.
We now show (3.96). Recall from (3.53), (3.57a) and (3.60a) that $q = r$ $(= \mathrm{e}^{-2/w_3})$ and that $\varepsilon = r_1\epsilon_1 r$ $(= const.)$. In (3.97) we recover that $r(t)$ is slaved by $r_1(t)$, as we can rewrite $r(t) = \mathrm{e}^{-2/r_1(t)}$. From (3.97), it follows that for $0 < \varepsilon \ll 1$, the phase plane of (3.93) is foliated by invariant manifolds with $r_1(t)\epsilon_1(t)\,\mathrm{e}^{-2/r_1(t)} = \delta\epsilon_{1,in}\,\mathrm{e}^{-2/\delta} = const.$ □

We now explicit condition (3.94) in terms of ε. The transition time T can be written in terms of ε as

$$e^{2T}(1+\delta T) = e^{-2/\delta}\,\delta^2\varepsilon^{-1},$$

where we have used (3.95) and (3.96). The time T that satisfies this equation is

$$T = \frac{1}{2}W(2\delta\varepsilon^{-1}) - \frac{1}{\delta},$$

where W is the so-called LambertW function [CGH+96]. For $\varepsilon \to 0$, the transition time T is asymptotic to

$$T \to \frac{1}{2}\left((\ln(2\delta\varepsilon^{-1}) - \ln(\ln(2\delta\varepsilon^{-1})) + o(1)\right) - \frac{1}{\delta}. \tag{3.100}$$

By substituting (3.100) in (3.94), we get the following first order estimate

$$\frac{\delta}{2\alpha}\frac{\ln(\ln(\varepsilon^{-1}))}{\ln(\varepsilon^{-1})}(1+o(1)) \leq y_{out} \leq \frac{2\delta}{\alpha}\frac{\ln(\ln(\varepsilon^{-1}))}{\ln(\varepsilon^{-1})}(1+o(1)),$$

that can be furthermore bounded as

$$\frac{\delta}{4\alpha}\frac{\ln(\ln(\varepsilon^{-1}))}{\ln(\varepsilon^{-1})} \leq y_{out} \leq \frac{4\delta}{\alpha}\frac{\ln(\ln(\varepsilon^{-1}))}{\ln(\varepsilon^{-1})}.$$

This provides the desired contraction to the point Q^1 for $0 < \varepsilon \ll 1$.

3.10 Summary of results

We have considered the one-dimensional spring-block model that describes the earthquake faulting phenomenon. We have used geometric singular perturbation theory and the blow-up method to provide a detailed description of the periodicity of the earthquake episodes, in particular we have untangled the increase in amplitude of the cycles for $\varepsilon \to 0$ and their relaxation oscillation structure. We have shown that the limit cycles arise from a degenerate Hopf bifurcation. The degeneracy is due to an underlying Hamiltonian structure that leads to large amplitude oscillations. Using the Poincaré compactification together with the blow-up method, we have described how these limit cycles behave near infinity in the limit of $\varepsilon \to 0$. A full detailed proof of Conjecture 3.16 will be the subject of a separate manuscript.

We have observed that the terminology of quasi-static slip motion to define the reduced problem (3.11) is misleading. Indeed, the solutions of (3.11) have an intrinsic slow-fast structure resembling the stick-slip oscillations. Our analysis

also shows that the periodic solutions of (3.1) cannot be investigated by studying the so-called quasi-static slip phase and the stick-slip phase separately, as it is done in [Rui83, GRRT84], since the two phases are connected by the nonlinear terms of (3.1). We also suggest suitable coordinate sets and time rescales to deal with the stiffness of (3.1) during numerical simulations. We hope that a deeper understanding of the structure of the earthquake cycles may be of help to the temporal predictability of the earthquake episodes.
We have shown that some of the ideas of this chapter can be used to study the continuum formulation of the Burridge and Knopoff model with Ruina state law, in particular to analyse the travelling wave solutions. Moreover, we conjecture that these ideas can also be used to study of the one-dimensional spring-block model with Dieterich state law. We elaborate on this latter point in the following section.

3.11 Outline of future work

The results of this chapter have been obtained by using Ruina's state law. It is natural to ask whether we would get similar results by choosing other rate-and-state friction laws. Is the spring-block model of Figure 3.2 going to have periodic solutions with other state laws? Are these periodic solutions of relaxation oscillation type? Do the equations have the same structure at the singular limit? If so, can we separate the dynamics into the slow dynamics on the critical manifold and a dynamics at infinity where an object equivalent to the line L_0 appears?

So far, there is no general agreement about which mathematical law best describes the experimental observations of friction on rocks [Mar98b, RM13, WPM15]. It is generally agreed that friction should be state dependent, where the state is accountable for the memory effects that have been observed in laboratory data. However, there is no general agreement on how many state variables friction should have and on what is the physical meaning of each state variable [Rui83, Gu86]. The simplest rate-and-state formulations consider only one state variable ψ, and in this case the friction coefficient μ has the form [GRRT84, Nak01]

$$\mu(v,\psi) = \mu_0 + a\ln\left(\frac{v}{v_0}\right) + b\ln\left(\frac{v_0\psi}{L}\right), \tag{3.101}$$

where a and b are positive empirical constants depending on the material properties, L is the characteristic displacement needed to recover the contact between the two surfaces when slip occurs, and μ_0 is the steady state friction coefficient for a fault sliding at the velocity v_0. Recall that we have already introduced

these parameters for equations (3.2) and (3.4). The friction force is given by $F_\mu = \sigma\mu$, where σ is the stress normal to the friction interface and we assume it to be constant and unitary, i.e. $\sigma = 1$ [Nak01].

The friction coefficient μ depends logarithmically with respect to the velocity v and to the state ψ in (3.101). This dependence has been interpolated from data obtained by laboratory experiments on rocks. The physical interpretation of these dependences is that the static friction coefficient increases logarithmically with respect to the hold time, and that the sliding friction coefficient decreases with respect to the velocity [Mar98b], where this latter phenomenon is also known as velocity weakening.
The formulation (3.101) has some limitations. In order for (3.101) to be well-defined, the argument of the logarithm needs to be strictly positive, and this means that (3.101) can describe only unilateral sliding that is, the mass can only slide in the same direction of the the driving plate v_0. Furthermore, for (3.101) the *stick* condition $v = 0$ is not well defined. In chapter 4, we present the problem of a friction oscillator where v changes sign repeatedly, so that (3.101) cannot be used to study the problem.

Equation (3.101) needs to be coupled with a description of the state evolution for ψ. The most common ODEs for the state are the Dieterich law [Die72, Die79],

$$\dot{\psi} = 1 - \frac{v\psi}{L}, \tag{3.102}$$

the Ruina law [Rui83]

$$\dot{\psi} = -\frac{v\psi}{L} \ln\left(\frac{v\psi}{L}\right), \tag{3.103}$$

and the Perrin law [Mar98b]

$$\dot{\psi} = 1 - \left(\frac{v\psi}{2L}\right)^2.$$

We call a rate-and-state friction law the coupling of the equation for $\mu(v, \psi)$ together with the dynamics for the state ψ.

The Dieterich law is also known as the *ageing* law or the *slowness* law because the state ψ evolves even for truly stationary contact $v = 0$, that is $\dot{\psi} = 1$. The Ruina law, that we have used in equation (3.2) to study the one-dimensional spring-block model, is also known as the *slip* law, because the state ψ can only evolve for $v > 0$. However, we remind the reader that the friction coefficient μ is not defined for $v = 0$, therefore such difference cannot be used to tell which law best describes the real friction force.

Remark 3.32 *We show how to derive the state variable θ, that we have used previously in this chapter, from ψ and how we have obtained model (3.2).*
The ODEs describing the one-dimensional spring-block model of Figure 3.2 can be written generically as

$$\begin{aligned} \dot{u} &= v - v_0, \\ M\dot{v} &= -\kappa u - F_\mu, \end{aligned} \tag{3.104}$$

where we need to explicit F_μ depending on the friction law that we wish to use. We define [Nak01]

$$\theta := v\psi/L. \tag{3.105}$$

The differentiation of (3.105) with respect to time gives $\dot{\theta} = b\dot{\psi}/\psi$ and by using Ruina's law (3.103) for $\dot{\psi}$ we obtain, after some manipulation,

$$\dot{\theta} = -\frac{v}{L}\left(b\ln\left(\frac{v}{v_0}\right) + \theta\right),$$

that is the differential equation for θ that appears in (3.2).
Notice that in order to get rid of the parameter μ_0 of (3.101) in (3.2), we have introduced the rescaling $\tilde{u} = u + \mu_0/\kappa$ and then we have dropped the tilde.

More recently, Putelat *et al.* have presented a new formulation of the rate-and-state friction law, the so-called spinodal law [PDW07, PWD08]

$$\begin{aligned} \mu(v,\psi) &= a\sinh^{-1}\left(\frac{v}{2v_0}\,\mathrm{e}^{\frac{E(\psi)}{k_B T}}\right), \\ \dot{\psi} &= \frac{1-\psi}{t_0} - \frac{|v|\psi}{L}, \end{aligned} \tag{3.106}$$

where the function $E(\psi)$ of (3.106) is given by

$$E(\psi) = \frac{k_B T}{a}\left(\mu_0 + b\ln\left(c + \frac{\psi(L + v_0 t_0)}{L}\right)\right).$$

In (3.106), k_B and T denote the Boltzmann constant and the absolute temperature respectively, t_0 is the characteristic timescale of static ageing and c is a constant that usually has the value $c = 10^{-3}$ [PDW10, WPM15]. This law is called spinodal because at the *steady state* $\dot{\psi} = 0$ the function $\mu(v, \psi(v))$ has a "N" shape, where $\psi(v)$ is the graph of $\dot{\psi} = 0$.
The spinodal law (3.106) resolves the limitations of (3.101) for $v \leq 0$ since the $\sinh^{-1}$ function is well defined in $\mathbb{R}$. Furthermore, this law interpolates well the experimental results of Heslot *et al.* [HBP+94, PD15].

In the following subsection 3.11.1, we outline the analysis of the one-dimensional spring-block model when using the Dieterich state law. We are interested to see

how general the results that we have obtained in this chapter are, and whether, by doing a rigorous mathematical analysis of the problem, it would be possible to identify which law, between the Dieterich and the Ruina one, best describes the problem. In addition, it would be interesting to study the one-dimensional spring-block model subject to the spinodal law. We leave such analysis to a future manuscript.

3.11.1 The one-dimensional spring-block model with Dieterich state law

We consider the one-dimensional spring-block model (3.104) with Dieterich's state law (3.102), that is

$$\begin{aligned}\dot{\psi} &= 1 - \frac{v\psi}{L},\\ \dot{u} &= v - v_0,\\ M\dot{v} &= -\kappa u - \mu(v,\psi),\end{aligned}$$

where μ is given by (3.101). We introduce $\theta = v\psi/L$ as in (3.105) and drop μ_0 as motivated in Remark 3.32, so that after some manipulation we get

$$\begin{aligned}\dot{\theta} &= \frac{b}{L}\left(v_0\,\mathrm{e}^{-\theta/b} - v\right),\\ \dot{u} &= v - v_0,\\ M\dot{v} &= -\kappa u - \left(\theta + a\ln\left(\frac{v}{v_0}\right)\right).\end{aligned}$$

We introduce the rescaling $\theta = ax, v = Ly, v = v_0 w, \tilde{t} = (L/v_0)t$ as we did in section 3.2, so that we obtain the non-dimensional system

$$\begin{aligned}\dot{x} &= (\alpha+1)\left(\mathrm{e}^{-\frac{x}{\alpha+1}} - w\right),\\ \dot{y} &= w - 1,\\ \varepsilon\dot{w} &= -y - \frac{x + \ln w}{\xi},\end{aligned}$$

where $\xi = (\kappa L)/a, \alpha = (b-a)/a$ and $\varepsilon = Mv_0^2/(\kappa L^2)$ are the same parameters as introduced in section 3.2, and in particular $0 < \varepsilon \ll 1$. We introduce $z = \ln w$ so that we get

$$\begin{aligned}\dot{x} &= (\alpha+1)\left(\mathrm{e}^{-\frac{x}{\alpha+1}} - \mathrm{e}^{z}\right),\\ \dot{y} &= \mathrm{e}^{z} - 1,\\ \varepsilon\dot{z} &= -\,\mathrm{e}^{-z}\left(y + \frac{x+z}{\xi}\right).\end{aligned} \tag{3.107}$$

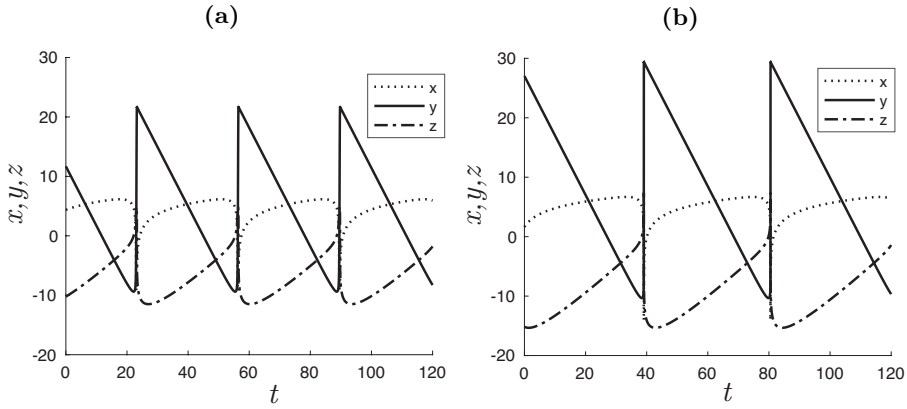

Figure 3.19: Numerical simulations of (3.107) for $\alpha = 0.9$ and $\xi = 0.5$. In (a): $\varepsilon = 10^{-2}$. In (b): $\varepsilon = 10^{-4}$.

Remark 3.33 *Recall that the ODEs describing the one-dimensional spring-block model with Ruina's state law are*

$$\begin{aligned} \dot{x} &= -\,\mathrm{e}^{z}\,(x + (1+\alpha)z)\,, \\ \dot{y} &= \mathrm{e}^{z} - 1, \\ \varepsilon\dot{z} &= -\,\mathrm{e}^{-z}\left(y + \frac{x+z}{\xi}\right). \end{aligned} \tag{3.108}$$

By comparing (3.107) *with* (3.108) *we see that the two systems differ only for the state equation* $\dot{x}$*, that is given by either Dieterich's or Ruina's formulation. For* $0 < \varepsilon \ll 1$ *both system are slow-fast, and at the singular limit* $\varepsilon = 0$ *they share the same critical manifold* C_0 *given by*

$$C_0 := \left\{(x, y, z) \in \mathbb{R}^3 \,\middle|\, \quad z = -x - \xi y\right\}. \tag{3.109}$$

This manifold, is normally hyperbolic and attracting for (3.107) *with the same linear stability properties* (3.8)*. This means that* C_0 *loses normal hyperbolicity exponentially fast for* $z \to +\infty$ *also for system* (3.107)*.*

In Figure 3.19 we can see that system (3.107) has periodic solutions that resemble relaxation oscillations, and that are very similar to the ones of Figure 3.1. We can also notice that for decreasing values of ε, both the amplitude and the period of the limit cycles increase.

The increase in amplitude of the periodic orbits for $\varepsilon \to 0$, and the fact that C_0 loses hyperbolicity exponentially fast at infinity, suggest that we could expect

some special dynamics at infinity for $\varepsilon = 0$, as in the previous case with Ruina's state law. Recall from section 3.3, that the line L_0 can be found naïvely as the x-nullcline of (3.108), that is $x + z(1+\alpha) = 0$, see (3.10). Given that the two problems (3.108) and (3.107) share the same structure, we would expect that the x-nullcline of (3.107) should also play a role for (3.107) when $z \gg \ln \varepsilon^{-1}$. The x-nullcline of (3.107) is given by $\mathrm{e}^{-\frac{x}{\alpha+1}} - \mathrm{e}^{z} = 0$. This latter condition implies $x + z(1+\alpha) = 0$, which is exactly the same expression as (3.10).

By introducing a four-dimensional Poincaré sphere for system (3.107), similarly to what we have done in section 3.7,

$$\mathcal{S}^{3,+} := \left\{ (X,Y,Z,W) \in \mathbb{R}^4 \middle| \quad X^2 + Y^2 + Z^2 + W^2 = 1, \quad W \geq 0 \right\},$$

we can rewrite the dynamics of (3.107) along the three charts K_1, K_2 and K_3 defined as in (3.43b), (3.41) and (3.43a) respectively. Figure 3.20 shows a numerical simulation of the limit cycles of (3.107) for $\varepsilon = \{10^{-2}, 10^{-4}, 10^{-6}\}$. These limit cycles sit on C_0 in a neighbourhood of the origin, as shown in Figure 3.20(a), and they contract towards the line L_0 when sufficiently far from the origin, see Figure 3.20(b). Surprisingly, Figures 3.20(b) and 3.20(c) indicate that the more ε decreases, the more the limit cycles contract towards the segments $\gamma^{1,2}, \gamma^{2,4}, \gamma^{4,5}$ and $\gamma^{5,6}$ that have been introduced in Definition 3.15. This suggests that the singular cycle Γ_0 of Definition 3.15 could play a role at the singular limit $\varepsilon = 0$ and $\alpha > \xi$ for system (3.107). At this stage though, we do not have arguments to conclude that this should be the case. However it looks reasonable that we could possibly formulate a conjecture similar to Conjecture 3.16 for $0 < \varepsilon \ll 1$ for system (3.107). In order to see whether this is the case, we first consider the reduced problem associated to (3.107) for $\varepsilon = 0$.

Remark 3.34 *We believe that the observations of Remark (3.33), together with the fact that L_0 and the singular cycle Γ_0 look to play a special role for solutions of (3.107), contribute to explain why it is difficult to tell which between the Dieterich and the Ruina law best represents the experimental results on friction. As we will see in the remaining part of the section, there are a few differences between the two formulations, but these are noticeable at unphysical regimes, i.e. for very large values of (x, y, z).*

Analysis of the reduced problem The reduced problem of (3.107) is obtained by setting $\varepsilon = 0$ in (3.107). This gives

$$f_0^D(x,y;\alpha) := \begin{cases} \dot{y} &= \mathrm{e}^{z} - 1, \\ \dot{z} &= \xi + \mathrm{e}^{z}(\alpha + 1 - \xi) - (1+\alpha)\,\mathrm{e}^{\frac{\xi y + z}{\alpha+1}} \end{cases} \tag{3.110}$$

where we have differentiated $z = -\xi y - x$ (3.109) with respect to time in order to rewrite (3.110) in terms of (y, z) so that it is consistent with (3.11). In this

section we use the superscript ^{D} to distinguish objects defined for the Dieterich problem (3.107) from the equivalent ones that we have defined for the Ruina problem (3.108).

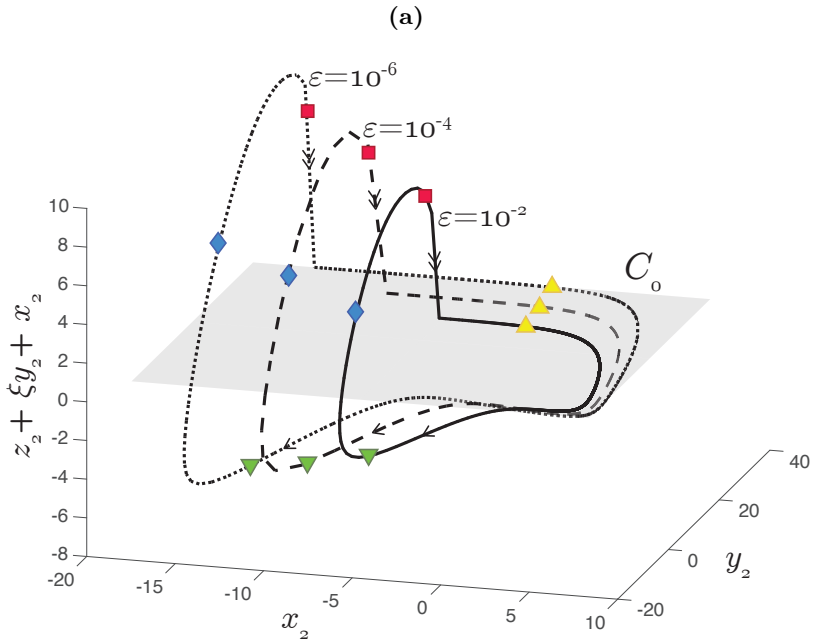

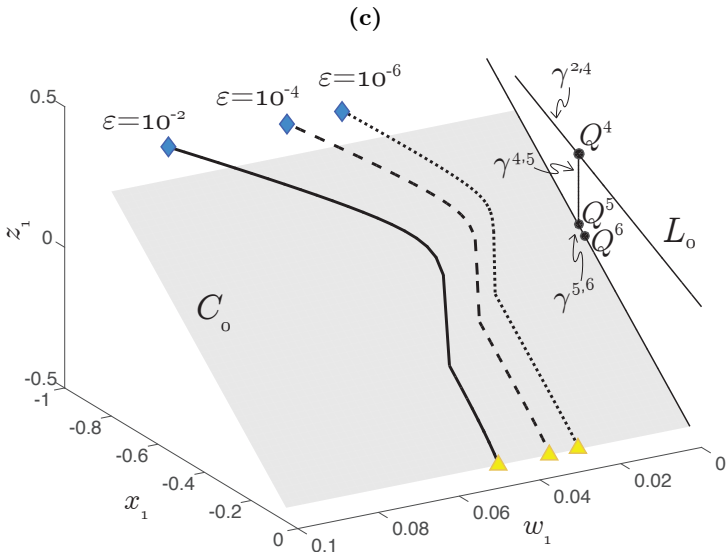

Figure 3.20: In (a): numerical simulation of the limit cycles of (3.1) for $\varepsilon \in \{10^{-6}, 10^{-4}, 10^{-2}\}$, $\alpha = 0.9$ and $\xi = 0.5$. In (b): portion of the periodic orbits visible in chart K_3, i.e. between the green lower triangle and the red square. In (c): portion of the periodic orbits visible in K_1, i.e. between the blue diamond and the yellow upper triangle. The portions between the blue triangle and the red square are visible both in K_3 and K_1 since the two charts overlap for $y_3 > 0$ or $z_1 > 0$.

Proposition 3.35 *The vector field (3.110) has an equilibrium point in $(y, z) = (0, 0)$, that undergoes a degenerate Hopf bifurcation for $\alpha = \xi$. In particular $f_0^D(y, z; \xi)$ is Hamiltonian, and it can be rewritten as*

$$f_0^D(y, z; \xi) = g^D(y, z) J \nabla H^D(y, z), \tag{3.111}$$

with

$$g^D(y, z) = \mathrm{e}^{\frac{\xi y + z}{1+\xi}}, \tag{3.112a}$$

$$H^D(y, z) = \frac{1+\xi}{\xi}\left(\mathrm{e}^{\frac{\xi(z-y)}{1+\xi}} + \xi y + \xi\,\mathrm{e}^{-\frac{\xi y + z}{1+\xi}} - 1 - \xi\right), \tag{3.112b}$$

where J is the standard symplectic structure matrix: $J = \left[\begin{smallmatrix} 0 & 1 \\ -1 & 0 \end{smallmatrix}\right]$. The equilibrium point $(y, z) = (0, 0)$ corresponds to $H^D(y, z) = 0$, and is surrounded by a family of periodic orbits, parametrised by $H^D(y, z) = h, h \geq 0$.

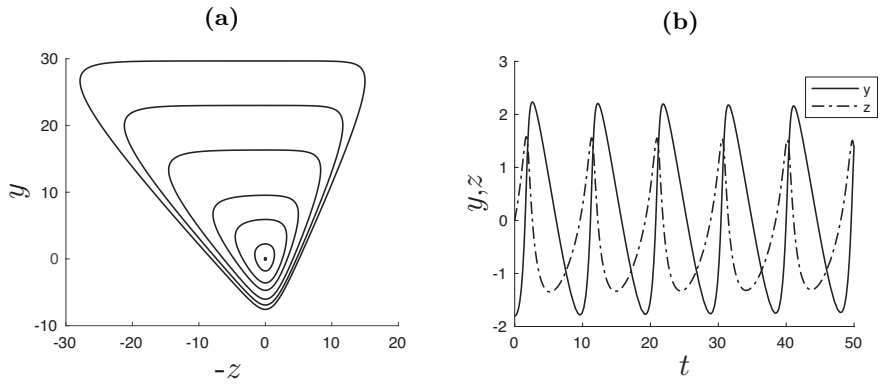

Figure 3.21: Numerical simulation of (3.111) for $\alpha = \xi = 0.5$. In (a): phase space for the level sets $H^D = [0.01; 1; 5; 10; 20; 30; 40]$ (3.112b). The axis orientation is chosen in order to facilitate the comparison with Figure 3.4(a). In (b): solution in forward time for $H^D = 1$.

Proof. The linear stability analysis of (3.110) in the equilibrium point $(y, z) = (0, 0)$ gives the following Jacobian matrix

$$Df_0^D(0, 0; \alpha) = \begin{bmatrix} 0 & 1 \\ -\xi & \alpha - \xi \end{bmatrix}.$$

This matrix has determinant $\xi > 0$, and the trace is zero for $\alpha = \xi$. Hence a Hopf bifurcation occurs for $\alpha = \xi$. The direct substitution of (3.112) into (3.111) shows that (3.110) is Hamiltonian for $\alpha = \xi$. Therefore the Hopf bifurcation is degenerate. □

From Proposition 3.35 we obtain a family of periodic orbits for $\alpha = \xi$. A numerical simulation of (3.111) is illustrated in Figure 3.21(a) for positive values of $H(y, z)$. These orbits have an intrinsic slow-fast structure, as shown in Figure 3.21(b), that is similar to the one that the orbits of the reduced problem (3.12) have, compare with Figure 3.4(b).

The intersection of the Hamiltonian trajectories with the y-axis is transversal for all $h > 0$, since the following condition holds:

$$\frac{\partial H^D}{\partial y}(y, 0) = (1 + \xi)\left(1 - \mathrm{e}^{-\frac{\xi y}{1+\xi}}\right) \neq 0, \quad \forall y \neq 0.$$

It follows that the function $H^D(y, 0)$ defines a diffeomorphism between the points on the positive y-axis and the corresponding values $h > 0$. The intersection of the y-axis with the orbits $H^D(y, z) = h$ corresponds to the real

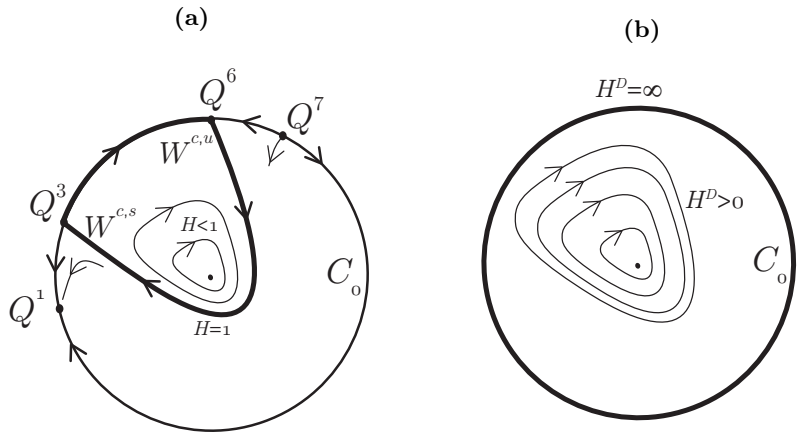

Figure 3.22: Comparison of the phase space of the reduced problem for $\alpha = \xi$ for the system with Ruina state law (a) and with the Dieterich state law (b). In bold the upper bound for the periodic orbits

roots of

$$e^{-\eta} + \eta - 1 = \frac{h\xi}{(1+\xi)^2}, \qquad \eta := \frac{\xi y}{1+\xi}. \tag{3.113}$$

Equation (3.113) has one root $h = 0$ and no roots exist for $h < 0$. For any $h > 0$, (3.113) has two roots, where one is for $y > 0$ and the other one is for $y < 0$. For $h \to +\infty$ the positive root behaves like $y = O(h)$, while the negative one behaves like $y = O(\ln(h^{-1}))$. It follows that the equilibrium point $(y, z) = (0, 0)$ is surrounded by periodic orbits for any $h > 0$. This makes a difference with the analogous expression for the Ruina case (3.14), where for $h \to 1$ the solution for $y < 0$ was bounded by $y \to -1/\xi$ from below, while in this case y is unbounded.

Here we have a first remarkable difference with the one-dimensional spring-block model with Ruina's state law. While in the case of (3.11) we had bounded orbits for $H \in]0, 1[$ and unbounded orbits for $H \geq 1$, the reduced problem (3.110) has bounded orbits for any $H^D = h$, where $h > 0$. Figure 3.22 compares the two phase spaces of (3.12) and (3.111), respectively.
It follows that there cannot by any saddle points on $C_{0,\infty}$ when $\alpha = \xi$ and hence, in this case the points Q^1, Q^3, Q^6 and Q^7 of Proposition 3.3 cannot play a special role for the reduced problem (3.110) for $\alpha = \xi$.

We use the Melnikov method of subsection 3.5.3 to study how the Hamiltonian system (3.111) breaks up near $\alpha = \xi$. In order to do so, we introduce a distance

function $\Delta^D(\alpha)$, equivalent to (3.31), so that

$$\begin{aligned}\Delta^D(\alpha) &= H^D(d^+) - H^D(d^-),\\ &= \int_0^{T^+} \dot{H}^D(\gamma^+(t))\,\mathrm{d}t + \int_{T^-}^0 \dot{H}^D(\gamma^-(t))\,\mathrm{d}t,\\ &= \int_0^{T^+} \nabla H^D(h)\cdot f_0^D(y,z;\alpha)\,\mathrm{d}t + \int_{T^-}^0 \nabla H^D(h)\cdot f_0^D(y,z;\alpha)\,\mathrm{d}t,\end{aligned} \tag{3.114}$$

where $D, d^{\pm}$ and $\gamma^{\pm}$ are defined in a similar fashion as in Figure 3.9(a). By Taylor expanding (3.114) around $\alpha = \xi$ we obtain

$$\Delta^D(\alpha) = (\alpha-\xi)\Delta_\alpha^D(h) + \mathrm{O}((\alpha-\xi)^2), \tag{3.115}$$

with the quantity $\Delta_\alpha^D(h)$ defined as

$$\begin{aligned}\Delta_\alpha^D(h) &= \int_{T_h^-}^{T_h^+} \nabla H^D(h)\cdot \frac{\partial f_0^D}{\partial\alpha}(y,z;\xi)\,\mathrm{d}t\\ &= \int_{T_h^-,}^{T_h^+} (\mathrm{e}^z - 1)\left(\mathrm{e}^{\frac{\xi(z-y)}{1+\xi}} + \frac{\xi y + z}{1+\xi} - 1\right)\mathrm{d}t.\end{aligned} \tag{3.116}$$

We cannot easily say whether (3.116) is always positive, but in Figure 3.23(a) we have computed (3.116) numerically for the case of $\xi = 0.5$ and $h \in]0,1]$. We can see that Δ_α^D is strictly positive for all $h \in]0,1]$. Furthermore, we have observed that by increasing the interval of h values, Δ_α^D continues increasing monotonically. Therefore, we conclude that for $\alpha - \xi \in [-c, c], c > 0$ small, no periodic orbit exists on the critical manifold C_0 for the reduced problem (3.110). Instead, for $\alpha > \xi$ orbits will spiral outwards, while they will spiral inwards for $\alpha < \xi$, so that the local phase space around the origin of (3.110) should look like the one of Figure 3.7.

Analysis of the perturbed problem for $\varepsilon > 0$ The compact manifold

$$S_0^D = \{(x,y,z) \in C_0 |\quad 0 \le H^D(y,z) \le \mu^{-1}\}, \tag{3.117}$$

is normally hyperbolic for $\varepsilon = 0$ and $0 < \mu < 1$ small but fixed. Fenichel's theorems guarantee that for ε sufficiently small there exists a locally invariant manifold S_ε^D that is $\mathrm{O}(\varepsilon)$-close to S_0^D and is diffeomorphic to it. Moreover the flow on S_ε^D converges to the flow of the reduced problem (3.110) for $\varepsilon \to 0$. A computation shows that S_ε^D at first order is given by the graph

$$z^D = -(x+\xi y) + \varepsilon\xi\,\mathrm{e}^{-\xi y - x}\left((1+\alpha)\,\mathrm{e}^{-\frac{x}{1+\alpha}} + (\xi - \alpha - 1)\,\mathrm{e}^{-\xi y - x} - \xi\right) + \mathrm{O}(\varepsilon^2),$$

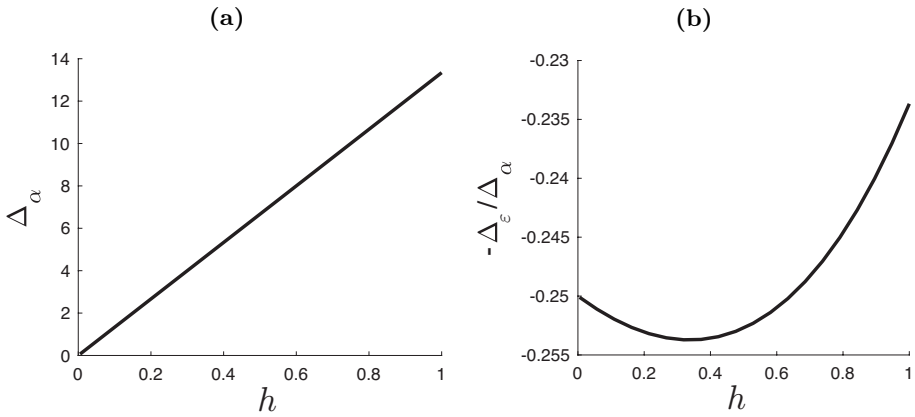

Figure 3.23: (a): Numerical computation of $\Delta_\alpha^D(h)$ for $\xi = 0.5$ and $h \in]0, 1]$. (b): Plot of the leading order coefficient in (3.120) for $\xi = 0.5$ and $h \in]0, 1]$.

so that we have the following vector field $f_\varepsilon^D(y, z; \alpha, \varepsilon)$ on S_ε^D

$$f_\varepsilon^D(y, z; \alpha, \varepsilon) := f_0^D(y, z; \alpha) - \varepsilon\xi\, \mathrm{e}^{2z}\, \phi(y, z) \begin{bmatrix} 1 \\ \alpha + 1 - \xi \end{bmatrix} + \mathrm{O}(\varepsilon^2), \tag{3.118}$$

with $\phi(y, z) := \xi + \mathrm{e}^z(\alpha + 1 - \xi) - (\alpha + 1)\, \mathrm{e}^{\frac{z+\xi y}{\alpha+1}}$.

Proposition 3.36 *Consider the compact manifold S_0^D defined in (3.117). Then S_0^D perturbs to a locally invariant slow manifold S_ε^D for $0 < \varepsilon \ll 1$. On S_ε^D the origin of (3.118) undergoes a subcritical Hopf bifurcation for*

$$\alpha = \alpha_H := \xi - \varepsilon\xi^2 + \mathrm{O}(\varepsilon^2),$$

with a positive first Lyapunov coefficient

$$a^D = \frac{1}{8}\varepsilon\xi^3 + \mathrm{O}(\varepsilon^2) > 0. \tag{3.119}$$

Therefore for $\alpha \in (\alpha_H, \alpha_H + c\varepsilon)$ with c sufficiently small, there exists a family of locally unique repelling limit cycles with amplitude of order $\mathrm{O}\left(\sqrt{-(\alpha - \alpha_H)/a^D}\right)$.

The proof of Proposition 3.36 follows from straightforward computations. Since (3.119) is proportional to ε, the results of Proposition 3.36 are valid only for a very small interval of α around α_H. We use the Melnikov analysis to extend the small limit cycles of Proposition 3.36 into larger ones.

Proposition 3.37 *Consider the slow manifold S_ε^D of Proposition 3.36. On S_ε^D there exists a family of closed periodic orbits for*

$$\alpha = \alpha_M(h) := \xi - \varepsilon \frac{\Delta_\varepsilon^D(h)}{\Delta_\alpha^D(h)} + \mathrm{O}(\varepsilon^2), \tag{3.120}$$

where $h \in [c_1(\mu), c_2(\mu)]$ with $(c_1, c_2)(\mu)$ sufficiently small. The quantity $\Delta_\varepsilon^D(h)$ is defined as

$$\Delta_\varepsilon^D(h) = \int_{T_h^-}^{T_h^+} \nabla H^D(h) \cdot \frac{\partial f_\varepsilon^D}{\partial \varepsilon}(y, z; \xi, 0)\, \mathrm{d}t, \tag{3.121}$$

while $\Delta_\alpha^D(h) > 0$ was defined in (3.116).

Proof. By Fenichel's theorem we know that the flow on S_ε^D converges to the flow of the reduced problem (3.110) for $\varepsilon \to 0$. Therefore, we can define the distance function $\Delta^D(\alpha, \varepsilon)$ similarly to (3.114), and whose Taylor expansion around $\alpha = \xi$ and $\varepsilon = 0$ is

$$\Delta^D(\alpha, \varepsilon) = (\alpha - \xi)\Delta_\alpha^D(h) + \varepsilon \Delta_\varepsilon^D(h) + \mathrm{O}((\alpha - \xi + \varepsilon)^2), \tag{3.122}$$

with $\Delta_\alpha^D(h)$ and $\Delta_\varepsilon^D(h)$ defined in (3.116) and (3.121) respectively. The integrand of $\Delta_\alpha^D(h)$ is strictly positive for all $h \in [c_1(\mu), c_2(\mu)]$, therefore we can apply the Implicit Function Theorem to (3.122) for $\Delta^D(\alpha, \varepsilon) = 0$ and obtain the result (3.120). □

In Figure 3.23(b) we show a numerical computation of the leading order coefficient in (3.120) for an interval of energies $H = h \in (0, 1]$. A saddle-node bifurcation occours for $h \simeq 0.4$. This implies that the family of unstable periodic orbits originating from the Hopf bifurcation is connected to a family of stable periodic orbits through the saddle-node bifurcation.
However, these stable periodic orbits appear on S_ε^D for $\alpha - \xi = \mathrm{O}(\varepsilon)$, so they do not correspond to the limit cycles of Figure 3.20(a) that appear for larger values of $\alpha - \xi$.

In order to explain the periodic orbits that we have seen in Figure 3.20 we would need to make a singular limit analysis in charts K_3 and K_1, similarly to what we have done in section 3.8. However, we expect this to be more difficult, due to the differences illustrated in Figure 3.22. We make the following considerations. Firstly, we conjecture that the singular trajectory Γ_0 of Definition 3.15 should play a role for $\alpha > \xi$, similarly to what expressed in Conjecture 3.16. This is supported from the numerical simulations of Figure 3.20 for $\alpha > \xi$ and $0 < \varepsilon \ll 1$. Thus for $\alpha > \xi$, we would expect the points Q^1, Q^5 and Q^6 to appear at $C_{0,\infty}$ and to be non-degenerate, even though our analysis on the reduced problem (3.110) has shown that there are no saddle points on $C_{0,\infty}$ for $\alpha = \xi$.

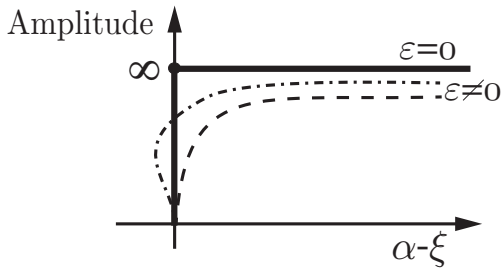

Figure 3.24: Conjectured bifurcation diagram of the limit cycles for $\varepsilon \ll 1$. The dashed line represents the model with Ruina law, while the dash-dotted line the one with Dieterich law.

Secondly, we suppose the periodic orbits of Figure 3.20 to belong to the family of periodic orbits that originates from the Hopf bifurcation for $\alpha = \xi$. Figure 3.24 gives a representation of our considerations.

So far, the analysis of the problem (3.107) is promising, in the sense that many results that we have obtained in this chapter are also shared by the model with the Dieterich state law. In the case that our conjectures are correct, the analysis of the spring-block model with Ruina's state law that we have done would become even more relevant. Indeed, in such case we would not only have unfolded the structure behind the periodic solutions in our model, but we would also have identified the mechanism for earthquake ruptures of two of the most well known state laws. In such case, it would be interesting to study the continuum formulation of the Burridge and Knopoff model with Dieterich state law, in order to see whether there are travelling wave solutions that are described by (3.107).
Of course, when we modify the function $\mu(v, \psi)$ and consider the spinodal law (3.106), more complications may occur, as we expect the critical manifold to change from (3.109), and the reduced problem will probably not be Hamiltonian. Furthermore, we expect the phase space of the one-dimensional spring-block model to change substantially when using the spinodal law, since this law introduces three equilibrium points [PDC17], while both the Dieterich and the Ruina law have only one equilibrium in $(x, y, z) = (0, 0, 0)$.

Chapter 4

Canards in stiction

We study the solutions of a friction oscillator subject to stiction. The vector field of this discontinuous model does not follow the Filippov convention, and the concept of Filippov solutions cannot be used. Furthermore, some Carathéodory solutions are unphysical. Therefore, we introduce the concept of stiction solutions: these are the Carathéodory solutions that are physically relevant, i.e., the ones that follow the stiction law. However, we find that some of the stiction solutions are forward nonunique in subregions of the slip onset. We call these solutions singular, in contrast to the regular stiction solutions that are forward unique. In order to further the understanding of the nonunique dynamics, we introduce a regularization of the model. This gives a singularly perturbed problem that captures the main features of the original discontinuous problem. We identify a repelling slow manifold that separates the forward slipping from the forward sticking solutions, leading to a high sensitivity to the initial conditions. On this slow manifold we find canard trajectories that have the physical interpretation of delaying the slip onset. We show that the regularized problem has a family of periodic orbits interacting with the canards. We observe that this family has a saddle stability and that it connects, in the rigid body limit, the two regular, slip-stick branches of the discontinuous problem, which were otherwise disconnected.

4.1 Introduction

Friction is a tangential reaction force that appears whenever two rough surfaces are in contact. This energy-dissipating force is desirable in car brakes [CCM+09], it occurs at the boundaries of the Earth's crustal plates during fault slip [Nak01, WPM15], and it causes the sound of string instruments [Aka02, FGHP98]. Friction may initiate undesirable noise, like the squeaking of the chalk on a blackboard or the squealing of train wheels in tight curves [HA00]. It may also induce chattering vibrations, as in machine tools [PW81] and in relay feedback systems [OA01].
The variety of the above-mentioned examples underlines the importance of understanding the friction force, although this is far from being accomplished. For instance, little is known on the shape of the friction law for small velocities, as it is difficult to verify it experimentally [PDW10, HOP96]. Yet, it is recognized that the maximal value of the friction force at *stick*, that is, at zero relative velocity, is higher than at *slip*, when the two surfaces are in relative motion [Rab51]. Several models of friction exist in the literature [OACdW+98, PRSV16, WSWK08, WPM15], and most of them are discontinuous at stick, like the stiction model. Stiction defines a maximum *static* friction force during stick and a lower *dynamic* friction force at slip. In subsets of the discontinuity, the stiction model has solutions that are forward nonunique. In these subsets, a numerical simulation requires a choice of forward integration, possibly discarding solutions.
In this chapter we aim to unveil, through a mathematical analysis, new features of the stiction law around the *slip onset*, i.e., when the surfaces start to slip. We show that, in certain circumstances, the slip onset is delayed with respect to the instant where the external forces have equalled the maximum static friction. This result, which in principle could be tested experimentally, has physical implications that may further the understanding of phenomena related to friction.
In this chapter we study the new features of the stiction law in a model of a friction oscillator subject to stiction [Sha86]. This is a discontinuous system, and one may attempt to study it by using the well-developed theory of Filippov (see [Fil88, DBBCK08]). However, it turns out that the model's vector field is not obtained from a linear convex combination of two adjacent equations, and for this reason we say that our model is non-Filippov. New concepts of solution of a discontinuous system are introduced, but they lack forward uniqueness in certain subregions of the slip onset. Here it is not possible to predict whether the oscillator will slip or stick in forward time. To deal with the nonuniqueness, a regularization is introduced [ST96, KH15a]: this gives a smooth, singularly perturbed problem that captures the main features of the original problem. Singular perturbation methods [Jon95] can be used to study the regularized system. The lack of uniqueness turns into a high sensitivity to the initial conditions, where a repelling slow manifold separates sticking from slipping solutions.

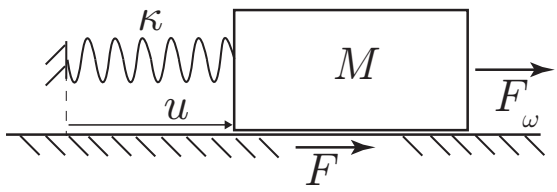

Figure 4.1: Model of a friction oscillator.

Along this manifold canard-like trajectories appear. These canard trajectories are the ones that delay the slip onset.
It is already known that the friction oscillator may exhibit chaotic [LC14, HOP98] and periodic behaviour [CS06, OA01, PS90]. This chapter shows, with a numerical computation, that there exists a family of slip-stick periodic orbits interacting with the canard solutions. This family connects, at the rigid body limit, the two branches of slip-stick orbits of the discontinuous problem. Furthermore, the orbits of this family are highly unstable, due to an "explosion" of the Floquet multipliers.
The chapter is structured as follows. Section 4.2 presents the model, and section 4.3 studies its geometrical structure. Section 4.4 introduces a concept of solution that makes sense for the discontinuous model, and section 4.5 introduces the regularization. Section 4.6 shows slip-stick periodic orbits interacting with the canard solutions. Finally, section 4.7 concludes the chapter and discusses the results. The results of this chapter are published in [BBK17a].

4.2 Model

A friction oscillator consists of a mass M that sits on a rough table, as shown in Figure 4.1, and that is subject to a periodic forcing $F_\omega(\bar{t}) := -A\sin(\omega\bar{t})$, with A and ω parameters and $\bar{t}$ time. The mass is connected to a spring of stiffness κ that at rest has zero length. Hence, the spring elongation u corresponds to the position of M. Besides, the motion of the mass on the rough table generates a frictional force F that aims to oppose this movement. The system of equations describing the friction oscillator is

$$\begin{aligned} \dot{u} &= v, \\ M\dot{v} &= -\kappa u + F_\omega(\bar{t}) + F. \end{aligned} \tag{4.1}$$

The friction force F is modelled as stiction. According to this law, F has different values depending on whether the slip velocity v is zero or not. During slip ($v \neq 0$), stiction is identical to the classical Coulomb law: the friction force is constant and acts in the opposite direction of the relative motion,

$$F = -N f_d \operatorname{sign} v \quad \text{when} \quad v \neq 0. \tag{4.2}$$

In equation (4.2) the parameter N is the normal force, f_d is the dimensionless dynamic friction coefficient, and the sign function is defined as

$$\operatorname{sign} \alpha := \begin{cases} 1 & \text{if } \alpha > 0, \\ -1 & \text{if } \alpha < 0. \end{cases}$$

Figure 4.2(a) illustrates the slipping law (4.2). For zero slip velocity ($v = 0$), it is necessary to consider whether this happens on a whole time interval or only instantaneously, i.e. whether $\dot{v}$ is also zero or not. The former case ($v = \dot{v} = 0$) defines the stick phase, and from (4.1) it follows that

$$F = w(\bar{t}, u) \quad \text{when} \quad v = 0 \quad \text{and} \quad |w| < N f_s, \tag{4.3}$$

where $w(\bar{t}, u) := \kappa u - F_\omega(\bar{t})$ is the sum of forces that induce the motion of M. The parameter f_s in (4.3) is the dimensionless static friction coefficient, and $f_s > f_d > 0$ [Rab51]. The idea is that the value of the static friction is exactly the one that counteracts the other forces acting on M, so that the mass will keep on sticking. However, the static friction (4.3) can only oppose the motion of M up to the maximum static friction $\pm N f_s$, and thus

$$F = N f_s \operatorname{sign} w \quad \text{when} \quad v = 0 \quad \text{and} \quad |w| > N f_s.$$

In this latter case the friction force is not sufficient to maintain $\dot{v} = 0$, and therefore the mass will slip in forward time. Figure 4.2(b) illustrates the friction law for $v = 0$. In compact form, stiction is written as

$$F(v, w) = \begin{cases} -N f_d \operatorname{sign} v & v \neq 0, \\ w & v = 0 \text{ and } |w| < N f_s, \\ N f_s \operatorname{sign} w & v = 0 \text{ and } |w| > N f_s. \end{cases}$$

The friction law is not defined for $v = 0$ and $|w| = N f_s$, where the external forces equal the maximum static friction during stick. Other modelling choices may fix a value of F in these points. These choices do not affect the results of the following analysis; see section 4.4. By rescaling

$$u = \frac{V}{\omega} x, \quad v = V y, \quad \bar{t} = \frac{t}{\omega},$$

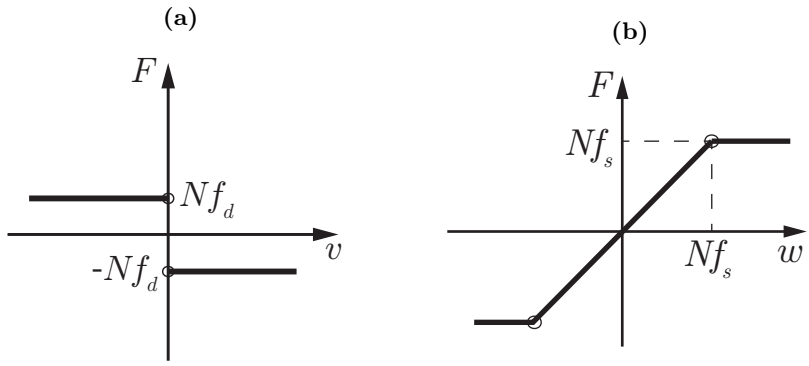

Figure 4.2: Stiction friction $F(v, w)$. (a): $v \neq 0$. (b): $v = 0$.

system (4.1) is rewritten in its dimensionless form

$$\begin{aligned} \dot{x} &= y, \\ \dot{y} &= -\xi(x,\theta) + \mu(y, \xi(x,\theta)), \\ \dot{\theta} &= 1, \end{aligned} \tag{4.4}$$

where $\theta \in \mathbb{T}^1$ is a new variable describing the phase of the periodic forcing, and that makes system (4.4) autonomous. In this new system the dot has the meaning of differentiation with respect to the time t, and $\gamma := \Omega/\omega$ is the ratio between the natural frequency of the spring $\Omega := \sqrt{\kappa/M}$ and the forcing frequency ω. Therefore, $\gamma \to \infty$ corresponds to the rigid body limit. Furthermore, in (4.4) we have introduced the function

$$\xi(x,\theta) := \frac{w}{A} = \gamma^2 x + \sin\theta.$$

Remark 4.1 *The function $\xi(x,\theta)$ is the sum of the rescaled external forces. In the following, we drop the function's arguments when they are unnecessary and simply refer to it as ξ. In some plots (like in Figure 4.3) we will replace x by $\xi(x,\theta)$ to get better pictures.*

In (4.4), the function μ describes the dimensionless stiction law:

$$\mu(y, \xi(x,\theta)) = \begin{cases} -\mu_d \operatorname{sign} y & y \neq 0, \\ \xi & y = 0 \text{ and } |\xi| < \mu_s, \\ \mu_s \operatorname{sign} \xi & y = 0 \text{ and } |\xi| > \mu_s, \end{cases} \tag{4.5}$$

where $\mu_{d,s} := Nf_{d,s}/A$. System (4.4) together with the friction function (4.5) is the model used in the rest of the analysis. In compact form it is written

as $\dot{z} = Z(z)$, where $z := (x, y, \theta) \in \mathbb{R}^2 \times \mathbb{T}^1$, and $\mathbb{T}^1 := \mathbb{R}/2\pi\mathbb{Z}$. The vector field $Z(z)$ is not defined on the two lines $\{y = 0, \xi = \pm\mu_s\}$. Section 4.3 studies the phase space of (4.4) using geometrical tools from piecewise-smooth theory [DBBCK08, Fil88].

4.3 Geometric analysis of the discontinuous system

This section analyses the friction oscillator (4.4) with stiction friction (4.5) in the context of piecewise-smooth dynamical systems. The notation is consistent with the one in [GHS10]. System (4.4) is smooth in the two regions

$$G^+ := \{(x, y, \theta) \in \mathbb{R}^2 \times \mathbb{T}^1 \mid y > 0\},$$
$$G^- := \{(x, y, \theta) \in \mathbb{R}^2 \times \mathbb{T}^1 \mid y < 0\}.$$

Let $Z^+(z)$ ($Z^-(z)$) be the vector field $Z(z)$ restricted to G^+ (G^-) and extended to the closure of G^+ (G^-). These two smooth vector fields have the explicit form

$$Z^\pm = \begin{cases} \dot{x} &= y, \\ \dot{y} &= -\xi(x, \theta) \mp \mu_d, \\ \dot{\theta} &= 1. \end{cases}$$

The set $\Sigma := \{(x, y, \theta) \in \mathbb{R}^2 \times \mathbb{T}^1 \mid y = 0\}$ is a surface of discontinuity of $Z(z)$, and it is called the *switching manifold*. The vector field $Z(z)$ is well defined in $\Sigma \setminus \{\xi = \pm\mu_s\}$, and its dynamics on the y-coordinate is

$$\dot{y} = -\xi(x, \theta) + \mu\,(0, \xi(x, \theta)) \begin{cases} > 0 & \text{for} \quad \xi < -\mu_s, \\ = 0 & \text{for} \quad |\xi| < \mu_s, \\ < 0 & \text{for} \quad \xi > \mu_s. \end{cases}$$

Therefore, it is natural to subdivide Σ into the three sets

$$\Sigma_c^+ := \{(x, y, \theta) \in \mathbb{R}^2 \times \mathbb{T}^1 \mid y = 0 \text{ and } \xi < -\mu_s\},$$
$$\Sigma_s := \{(x, y, \theta) \in \mathbb{R}^2 \times \mathbb{T}^1 \mid y = 0 \text{ and } -\mu_s < \xi < \mu_s\},$$
$$\Sigma_c^- := \{(x, y, \theta) \in \mathbb{R}^2 \times \mathbb{T}^1 \mid y = 0 \text{ and } \xi > \mu_s\}$$

that are shown in Figure 4.3(a). The set Σ_c^+ (Σ_c^-) is called the *crossing region pointing upwards* (*downwards*) because orbits here switch from G^- to G^+ (from G^+ to G^-). The strip Σ_s is called the *sticking region* because trajectories within it are not allowed to switch to $G^\pm$, and they correspond to solutions where the

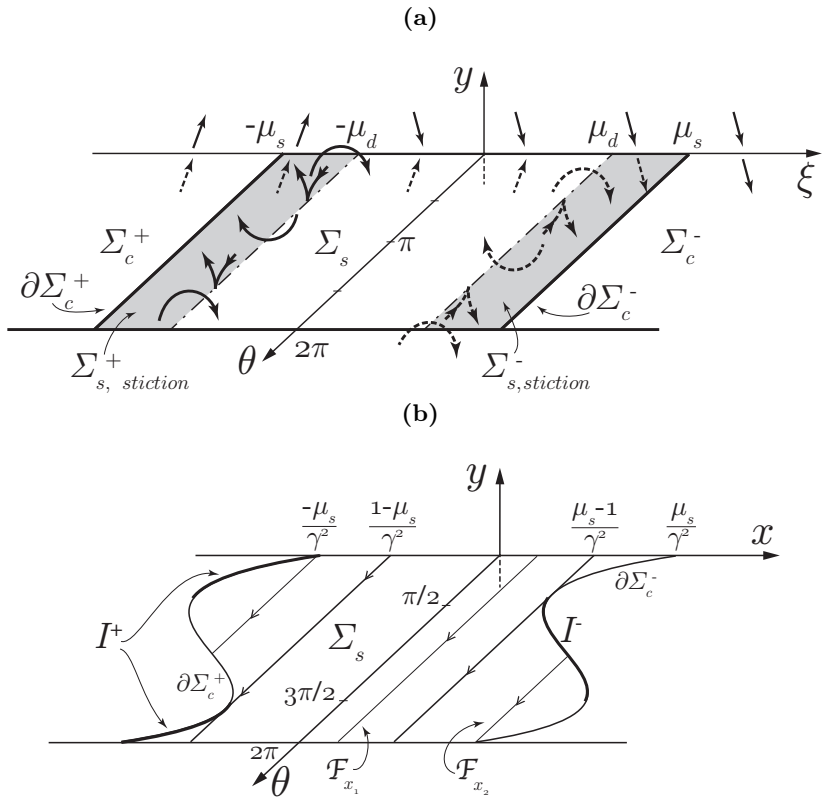

Figure 4.3: (a) Vector fields $Z^{\pm}$ and their tangencies at $\xi = \mp\mu_d$ in the $(\xi(x,\theta), y, \theta)$-space. Z^{-} is dashed because it is below Σ_s. The grey bands indicate where $Z^{\pm}$ suggest crossing, but instead the solution for $y = 0$ is sticking. (b) Phase space of Z_s in the (x, y, θ)-space with the tangencies at $\theta = \{\pi/2, 3\pi/2\}$. The leaf $\mathcal{F}_{x_1}$ is a full circle, while $\mathcal{F}_{x_2}$ is an arc of a circle. The intervals of nonuniqueness $I^{\pm}$ are introduced in Proposition 4.9.

mass sticks to the table. Let $Z_s(z)$ be the smooth vector field $Z(z)$ restricted to Σ_s and extended to the closure of Σ_s. This two-dimensional vector field has the explicit form $(\dot{x}, \dot{\theta}) = (0, 1)$, and thus Σ_s is foliated by invariant arcs of circles

$$\mathcal{F}_{x_0} := \{(x, y, \theta) \in \Sigma_s \mid x = x_0\} \tag{4.6}$$

since $\theta \in \mathbb{T}^1$. Figure 4.3(b) shows the foliation $\mathcal{F}_{x_0}$. The boundaries of Σ_s with $\Sigma_c^{\pm}$ define the two sets

$$\partial\Sigma_c^+ := \{(x, y, \theta) \in \mathbb{R}^2 \times \mathbb{T}^1 \mid y = 0 \text{ and } \xi = -\mu_s\},$$
$$\partial\Sigma_c^- := \{(x, y, \theta) \in \mathbb{R}^2 \times \mathbb{T}^1 \mid y = 0 \text{ and } \xi = \mu_s\}.$$

The vector field $Z(z)$ is not defined on $\partial\Sigma_c^{\pm}$, but the three vector fields $Z_s(z)$ and $Z^{\pm}(z)$ are. Indeed, $\partial\Sigma_c^{\pm}$ belong to the closure of both Σ_s and $G^{\pm}$. Hence, on $\partial\Sigma_c^{\pm}$, solutions may be forward nonunique. This will be discussed in section 4.4.

Propositions 4.3 and 4.5 below say where the vector fields $Z_s(z)$, $Z^{\pm}(z)$ are tangent to $\partial\Sigma_c^{\pm}$ and Σ, respectively. The results are shown in Figure 4.3. First, a definition introduces the concepts of visible and invisible tangency.

Definition 4.2 Let $\hat{\Sigma} := \{z \in \mathbb{R}^n \mid \chi(z) > 0\}$, where $\chi : \mathbb{R}^n \to \mathbb{R}$ is a smooth and regular function such that $\nabla\chi(z) \neq 0$ for every $z \in \mathbb{R}^n$. Furthermore, let $\hat{Z} : \hat{\Sigma} \to \mathbb{R}^n$ be a smooth vector field having a smooth extension to the boundary of $\hat{\Sigma}$, that is, for $\chi(z) = 0$. In addition, let $\mathcal{L}_{\hat{Z}}\chi(z) := \nabla\chi \cdot \hat{Z}(z)$ denote the Lie derivative of χ with respect to $\hat{Z}(z)$.

The vector field $\hat{Z}(z)$ is tangent to the set $\chi(z) = 0$ at $p \in \hat{\Sigma}$ if $\mathcal{L}_{\hat{Z}}\chi(p) = 0$. The tangency is called visible (invisible) if $\mathcal{L}^2_{\hat{Z}}\chi(p) > 0$ ($\mathcal{L}^2_{\hat{Z}}\chi(p) < 0$), where $\mathcal{L}^2_{\hat{Z}}\chi(p)$ is the second-order Lie derivative. The tangency is a cusp if $\mathcal{L}^2_{\hat{Z}}\chi(p) = 0$ but $\mathcal{L}^3_{\hat{Z}}\chi(p) \neq 0$.

In other words, the tangency is visible if the orbit $\dot{z} = \hat{Z}(z)$ starting at p stays in $\hat{\Sigma}$ for all sufficiently small $|t| > 0$, and it is invisible if it never does so [DBBCK08, pp. 93 and 237]. A quadratic tangency is also called a *fold* [Tei93].

Proposition 4.3 *$Z_s(z)$ is tangent to $\partial\Sigma_c^-$ ($\partial\Sigma_c^+$) in the isolated points $\theta \in \{\pi/2, 3\pi/2\}$. The tangency is visible (invisible) for $\theta = \pi/2$ and invisible (visible) for $\theta = 3\pi/2$.*

Proof. Define the function $\chi(x, \theta) = \mu_s - \xi(x, \theta)$ so that it is defined within Σ and its zeroes belong to $\partial\Sigma_c^-$. Then $\mathcal{L}_{Z_s}\chi(p) = 0$ in $\theta = \{\pi/2, 3\pi/2\}$. Moreover, $\mathcal{L}^2_{Z_s}\chi(p) = \sin\theta$. Hence, $\theta = \pi/2$ ($\theta = 3\pi/2$) is a visible (invisible) fold. Similar computations prove the result for $\partial\Sigma_c^+$. □

Corollary 4.4 *If $\mu_s > 1$, then the invariant leaves $\mathcal{F}_x$ of (4.6) with $|\gamma^2 x| < \mu_s - 1$ are periodic with period 2π. The remaining leaves of (4.6), having $|\gamma^2 x| \geq \mu_s - 1$, escape Σ_s in finite time. If $\mu_s < 1$, no periodic solutions exist on Σ_s.*

PROOF. The sticking trajectory $\gamma^2 x(t) = \mu_s - 1$ ($\gamma^2 x(t) = -\mu_s + 1$) is tangent to $\partial\Sigma_c^-$ ($\partial\Sigma_c^+$) because $\xi(x, \pi/2) = \mu_s$ ($\xi(x, 3\pi/2) = -\mu_s$). These two lines coincide for $\mu_s = 1$. When $\mu_s > 1$ the orbits $|\gamma^2 x(t)| < \mu_s - 1$ are included within the two tangent orbits. Hence, they never intersect the boundaries $\partial\Sigma_c^{\pm}$ and therefore are periodic with period 2π. Instead, the trajectories $\mu_s > |\gamma^2 x(t)| \geq \mu_s - 1$ exit Σ_s in finite time. □

The orbit $\mathcal{F}_{x_1} \subset \Sigma_s$ of Figure 4.3(b) is periodic, while $\mathcal{F}_{x_2}$ leaves Σ_s in finite time. The period $T = 2\pi$ corresponds to a period $\bar{T} = 2\pi/\omega$ in the original time $\bar{t}$, as is often mentioned in the literature [CS06, Sha86]. The condition $\mu_s > 1$ corresponds to $Nf_s > A$; that is, the maximum static friction force is larger than the amplitude of the forcing F_ω. This interpretation makes it an obvious condition for having sticking solutions.

PROPOSITION 4.5 *The vector field Z^- (Z^+) is tangent to Σ on the line $\xi = \mu_d$ ($\xi = -\mu_d$). The tangency is invisible (visible) for $\theta \in]\pi/2, 3\pi/2[$, and it is visible (invisible) for $\theta \in [0, \pi/2[$ and $\theta \in]3\pi/2, 2\pi[$, while it is a cusp on the isolated points $\theta = \{\pi/2, 3\pi/2\}$.*

PROOF. Define the function $\chi(x, y, \theta) = -y$ so that it is defined in G^- and it is zero in Σ. Then $\mathcal{L}_{Z^-}\chi(p) = \xi(x, \theta) - \mu_d = 0$ on the line $\xi = \mu_d$, $\theta \in \mathbb{T}^1$. Moreover, $\mathcal{L}^2_{Z^-}\chi(p) = \cos\theta$. This is negative for $\theta \in]\pi/2, 3\pi/2[$ and positive for $\theta \in [0, \pi/2[$ and $\theta \in]3\pi/2, 2\pi[$. The points $\theta = \pi/2$ and $\theta = 3\pi/2$ have $\mathcal{L}^2_{Z^-}\chi(p) = 0$, but $\mathcal{L}^3_{Z^-}\sigma(p) \neq 0$. Similar computations prove the result for $Z^+(z)$. □

The knowledge of the tangencies is sufficient to describe the local phase space of system (4.4) around the discontinuity Σ, as Figure 4.3 shows. Section 4.4 discusses how forward solutions of $Z(z)$, which are smooth within each set $G^{\pm}$ and Σ_s, connect at the boundaries of these regions. It is futile to study solutions in backwards time because when an orbit lands on Σ_s, the information of when it has landed is lost.

4.4 Forward solutions of the discontinuous system

Classical results on existence and uniqueness of solutions require Lipschitz continuous right-hand sides and therefore do not apply to discontinuous systems like (4.4). A class of discontinuous systems for which some results are known is

the one of Filippov type [Fil88, a) §4]. We call a Filippov type system a system where the linear convex combination of the vector fields $Z^{\pm}(z)$ is sufficient to describe the dynamics within the switching manifold Σ. Filippov's convex method is useful, especially when there is no vector field already defined on Σ. Let $Z_y^{\pm}(z)$ be the y component of $Z^{\pm}(z)$ in a point $z \in \Sigma$. Then Filippov's convex method defines the *crossing region* as the subset of Σ where $Z_y^+ \cdot Z_y^-(z) > 0$, while the *sliding region* $\Sigma_{s,\text{Filippov}}$ satisfies $Z_y^+ \cdot Z_y^-(z) < 0$ [Fil88, §4], [DBBCK08, p. 76]. The idea is that solutions inside the sliding region cannot exit Σ because $Z^{\pm}(z)$ do not allow it.

Remark 4.6 *System* (4.4) *together with the friction law* (4.5) *is not of Filippov type. Indeed, the sliding region of system* (4.4) *is*

$$\Sigma_{s,\text{Filippov}} := \{(x, y, \theta) \in \mathbb{R}^2 \times \mathbb{T}^1 \mid y = 0 \ \text{ and } \ -\mu_d < \xi < \mu_d\},$$

which is a strip within Σ_s *whenever* $\mu_d < \mu_s$. *In the two remaining bands*

$$\Sigma^-_{s,\text{stiction}} := \{(x, y, \theta) \in \mathbb{R}^2 \times \mathbb{T}^1 \mid y = 0 \ \text{ and } \ \xi \in]\mu_d, \mu_s[\},$$
$$\Sigma^+_{s,\text{stiction}} := \{(x, y, \theta) \in \mathbb{R}^2 \times \mathbb{T}^1 \mid y = 0 \ \text{ and } \ \xi \in]-\mu_s, -\mu_d[\},$$

which are coloured in grey in Figure 4.3(a), the vector field $Z_s(z)$ *does not belong to the convex closure of* $Z^{\pm}(z)$. *Here Filippov's method predicts orbits to switch from* G^+ *to* G^- *or vice versa, but the actual solution of model* (4.4) *lies within* Σ_s. *When* $\mu_d = \mu_s$, *the friction law* (4.5) *equals the classical Coulomb friction and* Σ_s *coincides with* $\Sigma_{s,\text{Filippov}}$. *This case has been studied in [GHS10, KP08, CSS07].*

The two grey bands $\Sigma^{\pm}_{s,\text{stiction}}$ are unstable to perturbations in y. Consider, for instance, a trajectory in $\Sigma^-_{s,\text{stiction}}$ that is pushed to G^- by an arbitrary small perturbation: this solution will evolve far from $\Sigma^-_{s,\text{stiction}}$ by following $Z^-(z)$. Another notion of forward solution of a discontinuous system is the *Carathéodory solution* [Cor08], [Fil88, §1]. This is an absolutely continuous function $z(t)$ that satisfies

$$z(t) = z(0) + \int_0^t Z(z(s))\, ds, \quad t \geq 0, \tag{4.7}$$

where the integral is in a Lebesgue sense. Hence, in order to have a Carathéodory solution, $Z(z)$ need only be defined almost everywhere.

Proposition 4.7 *For every* $z_0 = z(0) \in \mathbb{R}^2 \times \mathbb{T}^1$ *there exists a global forward Carathéodory solution of model* (4.4) *satisfying* (4.7) *for every* $t \geq 0$.

Proof. For every z_0 there exists at least one local classical solution of either $Z^{\pm}(z)$ or $Z_s(z)$. A forward solution of (4.7) is obtained by piecing together such

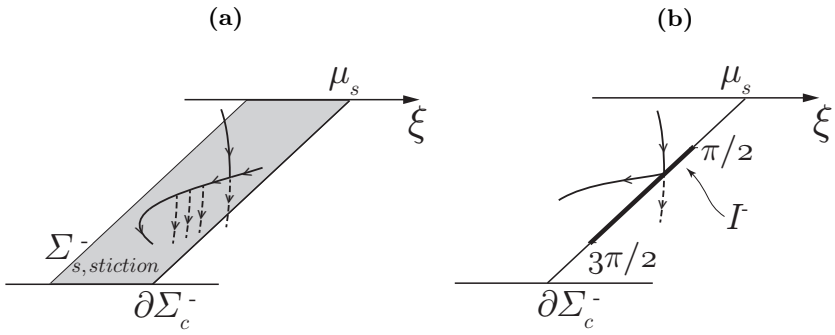

Figure 4.4: (a): A Carathéodory solution with a pathological nondeterminacy of the forward motion on the grey band. (b): Stiction solutions interacting with the line of forward nonuniqueness I^-.

local orbits on Σ. This can be done for every $t > 0$ since $Z^{\pm}(z)$ and $Z_s(z)$ are each linear in (x, y), excluding the possibility of blow-up in finite time. □

Not every forward Carathéodory solution has a physical meaning. Consider, for instance, a trajectory that under the forward flow (4.4) lands inside $\Sigma^-_{s,\text{stiction}}$, as shown in Figure 4.4(a). There are two ways to obtain a forward solution at this point: either leave Σ and follow the vector field $Z^-(z)$, or remain on Σ_s. Besides, the forward trajectory on Σ_s may switch to G^- at any point within $\Sigma^-_{s,\text{stiction}}$. The orbits switching to G^- appear to be mathematical artifacts, as they do not satisfy the condition $|\xi| > \mu_s$ of the stiction law (4.5). There is a need to have a concept of solution that discards all these pathologies. The following definition does so by using a "minimal" approach.

Definition 4.8 A stiction solution $t \mapsto z(t)$, with $t \geq 0$, is a Carathéodory solution that leaves Σ_s only at the boundaries $\partial\Sigma^{\pm}_c$.
A stiction solution is called *singular* if for some $t_1 \geq 0$ the point $z(t_1)$ belongs to one of the following sets:

$$I^+ := \{(x, y, \theta) \in \mathbb{R}^2 \times \mathbb{T}^1 \mid \xi = -\mu_s, y = 0, \theta \in [\pi/2, 3\pi/2]\ \},$$
$$I^- := \{(x, y, \theta) \in \mathbb{R}^2 \times \mathbb{T}^1 \mid \xi = \mu_s, \quad y = 0, \theta \in [0, \pi/2] \cup [3\pi/2, 2\pi[\ \}.$$

Otherwise, the stiction solution is called *regular*.

The sets $I^{\pm}$ belong to the boundary lines $\partial\Sigma^{\pm}_c$. Three vector fields are defined on $\partial\Sigma^{\pm}_c$: $Z_s(z)$ and $Z^{\pm}(z)$. In particular, on both $I^{\pm}$, the vector field $Z_s(z)$ points inside Σ_s, as follows from Proposition 4.3; compare with Figure 4.3(b). Proposition 4.9 describes the existence and uniqueness of stiction solutions for

model (4.4).

Proposition 4.9 *There exists a stiction solution $z(t)$ of problem (4.4) for any initial condition $z_0 = z(0) \in \mathbb{R}^2 \times \mathbb{T}^1$. Regular stiction solutions are forward unique, while singular stiction solutions are forward nonunique.*

Proof. Stiction solutions are Carathéodory solutions, and hence they exist. Consider a trajectory $z(t)$ that reaches I^- at a time t_1, as shown in Figure 4.4(b). Two different forward solutions satisfy (4.7): either leave Σ and follow the vector field $Z^-(z)$, or remain on Σ_s. Hence, the singular stiction solution is forward nonunique at I^-, and similarly at I^+. On the contrary, if $z(t) \notin I^\pm$ at any $t \geq 0$, then there is always only one way to piece together the vector fields at the boundaries $\partial\Sigma_c^\pm$, and therefore $z(t)$ is forward unique. □

The nonuniqueness of models with stiction friction has been mentioned in [BS95, OACdW+98], without any further explanation. It is not possible to predict whether, for singular stiction solutions, the mass will slip or stick in forward time. Hence, numerical simulations that use stiction friction have to make a choice at the points of nonuniqueness to compute the forward flow, often without noticing that a choice is made. This means that solutions may unawarely be discarded. Section 4.5 investigates the nonuniqueness by regularization.

4.5 Regularization

We consider the regularization of the vector field $Z(z)$ given by the 1-parameter family $Z_\varepsilon(z)$ of smooth vector fields

$$Z_\varepsilon(z) := \frac{1}{2}Z^+(z)(1 + \phi(\varepsilon^{-1}y)) + \frac{1}{2}Z^-(z)(1 - \phi(\varepsilon^{-1}y)), \tag{4.8}$$

for $0 < \varepsilon \ll 1$. The function $\phi(y)$ is an odd C^k-function ($1 \leq k \leq \infty$) that satisfies

$$\phi(y) = \begin{cases} 1, & y \geq 1, \\ \mu_s/\mu_d, & y = \delta, \end{cases} \quad \text{and} \quad \phi_y(y) \begin{cases} > 0, & 0 < y < \delta, \\ = 0, & y = \{\delta, 1\}, \\ < 0, & \delta < y < 1, \end{cases} \quad \phi_{yy}(\delta) < 0, \tag{4.9}$$

where $0 < \delta < 1$. This function is shown in Figure 4.5. The regularized problem $\dot{z} = Z_\varepsilon(z)$ has the advantages of being smooth, and of approximating the discontinuous problem (4.4) for $0 < \varepsilon \ll 1$. In particular, by the first

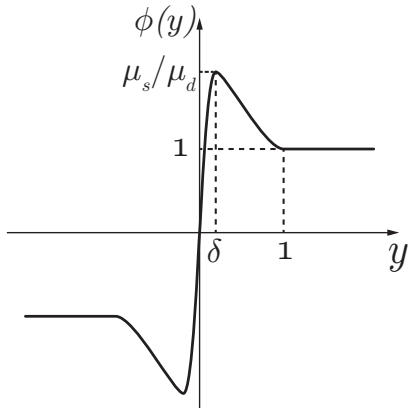

Figure 4.5: A regularization function $\phi(y)$.

property of (4.9), it follows that $Z_\varepsilon(z) = Z^\pm(z)$ for $y \gtrless \pm\varepsilon$, so that the two problems coincide outside of the *region of regularization* $y \in]-\varepsilon, \varepsilon[$.

Remark 4.10 *It is not necessary to have $\phi(y) \equiv 1$ when $y \geq 1$ in order for ϕ to be a regularization function of (4.8). For instance, a class of analytic functions such that $\phi(y) \to 1^\pm$ as $y \to \pm\infty$ could also be used, and the results of this chapter are not expected to change. However, the analysis of the regularized problem is more complicated for functions where $\phi(y) \to 1^\pm$ as $y \to \pm\infty$ because one needs to deal with the loss of compactness at infinity; see [Kri17].*

In noncompact form $\dot{z} = Z_\varepsilon(z)$ is the singularly perturbed problem

$$\begin{aligned} \dot{x} &= y, \\ \dot{y} &= -\xi(x,\theta) - \mu_d \phi(\varepsilon^{-1} y), \\ \dot{\theta} &= 1, \end{aligned} \tag{4.10}$$

with $\xi(x,\theta) = \gamma^2 x + \sin\theta$ the function introduced in section 4.2. When solutions of (4.10) enter the region of regularization, it is easier to follow them in the rescaled coordinate $\hat{y} = \varepsilon^{-1} y$ so that $y = \pm\varepsilon$ become $\hat{y} = \pm 1$. In the new scale, system (4.10) becomes the multiple timescale problem

$$\begin{aligned} \dot{x} &= \varepsilon \hat{y}, \\ \varepsilon \dot{\hat{y}} &= -\xi(x,\theta) - \mu_d \phi(\hat{y}), \\ \dot{\theta} &= 1, \end{aligned} \tag{4.11}$$

which is also known as the *slow problem* [Jon95]. By introducing the fast time $\tau := t/\varepsilon$, system (4.11) is equivalent to the *fast problem*

$$\begin{aligned} x' &= \varepsilon^2 \hat{y}, \\ \hat{y}' &= -\xi(x,\theta) - \mu_d \phi(\hat{y}), \\ \theta' &= \varepsilon, \end{aligned} \tag{4.12}$$

with the prime meaning the differentiation with respect to the fast time τ. The parameter ε measures both the perturbation from the discontinuous system, as in equation (4.8), and the separation of the timescales. The standard procedure for solving multiple timescale problems is to combine the solutions of the *layer problem*

$$\hat{y}' = -\xi(x,\theta) - \mu_d \phi(\hat{y}), \quad (x,\theta)(\tau_0) = (x_0, \theta_0) \tag{4.13}$$

with the ones of the *reduced problem*

$$\begin{aligned} \dot{x} &= 0, \\ 0 &= -\xi(x,\theta) - \mu_d \phi(\hat{y}), \\ \dot{\theta} &= 1, \end{aligned} \tag{4.14}$$

where (4.13) and (4.14) are the limit for $\varepsilon \to 0$ of the fast and slow problems (4.12) and (4.11). The set of equilibrium points of the layer problem (4.13) is called the *critical manifold*:

$$C_0 := \{(x, \hat{y}, \theta) \in \mathbb{R}^2 \times \mathbb{T}^1 \mid \quad \xi(x,\theta) + \mu_d \phi(\hat{y}) = 0\}, \tag{4.15}$$

and the solutions of the reduced problem (4.14) are constrained to it. The critical manifold is said to be *normally hyperbolic* in the points where

$$\left.\frac{\partial \hat{y}'}{\partial \hat{y}}\right|_{C_0} = -\mu_d \phi_y(\hat{y}^{C_0})$$

is nonzero and $\hat{y}^{C_0} = \phi^{-1}(-\xi(x,\theta)/\mu_d)$. It follows that C_0 is not normally hyperbolic on the two *fold lines*

$$f^{\pm} := \{(x, \hat{y}, \theta) \in \mathbb{R}^2 \times \mathbb{T}^1 \mid \xi = \mp\mu_s, \hat{y} = \pm\delta\}.$$

These lines separate C_0 into three normally hyperbolic subsets:

$$\begin{aligned} C_r^+ &:= \{(x, \hat{y}, \theta) \in C_0 \mid \delta < \hat{y} < 1\}, \\ C_a &:= \{(x, \hat{y}, \theta) \in C_0 \mid -\delta < \hat{y} < \delta\}, \\ C_r^- &:= \{(x, \hat{y}, \theta) \in C_0 \mid -1 < \hat{y} < -\delta\}, \end{aligned}$$

as shown in Figure 4.6, where C_a is attracting and $C_r^{\pm}$ are repelling. Notice that C_a is a graph $\hat{y} \in]-\delta, \delta[$ over Σ_s, while C_r^+ (C_r^-) is a graph $\hat{y} \in]\delta, 1[$

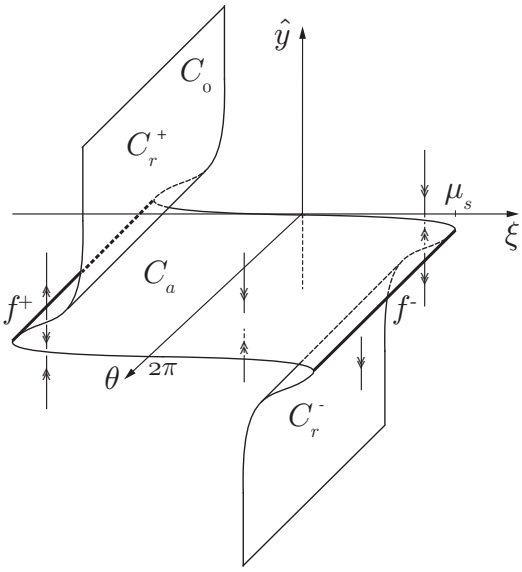

Figure 4.6: Critical manifold C_0 and its stability properties. In bold: $f^{\pm}$. The double arrow denotes dynamics in the fast time τ.

($\hat{y} \in]-1, -\delta[$) over $\Sigma^+_{s,\text{stiction}}$ ($\Sigma^-_{s,\text{stiction}}$). In terms of (x, y, θ), these sets collapse onto Σ_s and $\Sigma^{\pm}_{s,\text{stiction}}$, respectively, as $\varepsilon \to 0$ since $y = \varepsilon\hat{y}$. Similarly, $f^{\pm}$ collapse onto $\partial\Sigma^{\pm}_c$. This means that in the (x, y, θ)-space it is not possible to distinguish whether a trajectory belongs to C_a or to $C^{\pm}_r$ for $\varepsilon = 0$.

Proposition 4.11 *The reduced problem on C_0 coincides with the vector field $Z_s(z)$ on Σ_s.*

The proof is straightforward since the reduced problem, once constrained to C_0, is $(\dot{x}, \dot{\theta}) = (0, 1)$. From this proposition and the fact that $Z_\varepsilon(z) = Z^{\pm}(z)$ for $y \gtrless \pm\varepsilon$, it follows that the regularized problem (4.10) captures all the main features of the discontinuous vector field (4.4) for $\varepsilon \to 0$. Furthermore, when $0 < \varepsilon \ll 1$ the solutions of (4.10) are uniquely defined, so that the issue of nonuniqueness of (4.4) is eliminated. Proposition 4.11 also motivates the conditions (4.9) for the function $\phi(y)$, as explained in the following remark.

Remark 4.12 *The well-known Sotomayor–Teixeira (ST) regularization considers a regularization function $\phi^{ST}(y)$ that is monotonously increasing in $y \in]-1, 1[$ [ST96]. At the singular limit, the regularization $Z^{ST}_\varepsilon(z)$ has an attracting invariant manifold C^{ST}_a that is a graph of $\hat{y}$ over $\Sigma_{s,Filippov}$ [LdST08, KH15a]. In terms of (x, y, θ) this set collapses onto $\Sigma_{s,Filippov}$ instead of Σ_s, and hence*

$Z_\varepsilon^{ST}(z)$ does not tend to $Z(z)$ as $\varepsilon \to 0$. For this reason the ST regularization is inadequate for model (4.4).

The results of Fenichel [Fen74, Fen79] guarantee that when $\varepsilon > 0$ a normally hyperbolic, compact, and invariant manifold $S_0 \subset C_0$ perturbs into a nonunique and invariant *slow manifold* S_ε that is ε-close to S_0 for ε sufficiently small. Furthermore, system (4.12) has an invariant foliation with base on S_ε that is a perturbation of the foliation of the layer problem (4.13) with base on S_0.
Let $\varphi_t(z_0)$ be a regular stiction solution of model (4.4) with an initial condition in z_0, and let $\varphi_t^\varepsilon(z_0)$ be the solution of the regularized problem (4.10) for the same initial condition. The following statement relates these two solutions.

Proposition 4.13 *For any $T > 0$ there exists an $\varepsilon_0 > 0$ such that the distance between the two solutions $\varphi_t^\varepsilon(z_0)$ and $\varphi_t(z_0)$ is bounded by $|\varphi_t^\varepsilon(z_0) - \varphi_t(z_0)| \leq c(T)\varepsilon^{2/3}$ for $t \in [0, T]$, where $c(T)$ is a constant that depends upon T, and $0 < \varepsilon \leq \varepsilon_0$.*

Proof. Fenichel's theorems guarantee that, sufficiently far from the fold lines $f^\pm$, the orbit $\varphi_t^\varepsilon(z_0)$ of the slow-fast problem (4.11) is $\mathrm{O}(\varepsilon)$-close to the singular trajectory $\varphi_t(z_0)$. At the folds $f^\pm$, if at the singular level the solutions are unique, the result by Szmolyan and Wechselberger [SW04, Theorem 1] guarantees that the distance between the two trajectories is bounded by $\mathrm{O}(\varepsilon^{2/3})$ for a finite time interval T. This is the case of regular stiction solutions. □

The following proposition relates the family of sticking solutions of Corollary 4.4 with a family of trajectories on the slow manifold for the regularized problem. For this, define $S_a \subset C_a$ as the compact, invariant, normally hyperbolic set $S_a := \{(x, \hat{y}, \theta) \in \mathbb{R}^2 \times \mathbb{T}^1 \mid |\gamma^2 x| \leq \mu_s - 1 - c, \xi(x, \theta) + \mu_d \phi(\hat{y}) = 0\}$ for $\mu_s > 1$ and $c \in \mathbb{R}^+$ small. The set S_a is a graph over the set of invariant circles of Corollary 4.4 for $c \to 0$.

Proposition 4.14 *For $0 < \varepsilon \ll 1$ the set S_a perturbs into a slow manifold $S_{a,\varepsilon}$ and on it there exists a unique, attracting 2π-periodic limit cycle passing through $(x, \theta) = (0, 0) + \mathrm{O}(\varepsilon)$.*

Proof. From Proposition 4.11 and Corollary 4.4 it follows that S_a is filled by circular trajectories. By Fenichel's results, when $0 < \varepsilon \ll 1$ the set S_a perturbs into the graph $\hat{y} = \phi^{-1}(-\xi(x, \theta)/\mu_d) + \varepsilon h_1(x, \theta)$. On this graph the slow problem (4.11) is a 2π-periodic, nonautonomous ODE for $x(\theta)$, where θ has the meaning of time:

$$\dot{x}(\theta) = \varepsilon \phi^{-1}\left(\frac{-\xi(x, \theta)}{\mu_d}\right) + \varepsilon^2 h_1(x, \theta). \tag{4.16}$$

Fix a global Poincaré section at $\theta = 0$, and define the return map $P(x(0), \varepsilon) = x(2\pi)$. The fixed points of this map for $0 < \varepsilon \ll 1$ are the zeros of the function

$$Q(x(0), \varepsilon) := \frac{P(x(0), \varepsilon) - x(0)}{\varepsilon} = \int_0^{2\pi} \phi^{-1}\left(\frac{-\gamma^2 x(s) - \sin s}{\mu_d}\right) ds + \mathrm{O}(\varepsilon),$$

where the last equality is obtained by integrating (4.16). For $\varepsilon = 0$, (4.16) implies $x(\theta) = x(0)$. Both the functions ϕ^{-1} and $\sin s$ are symmetric with respect to the origin. This means that $Q(x(0), 0) = 0$ if and only if $x(0) = 0$. Furthermore, $(x(0), 0)$ is regular because

$$\partial_x Q(0, 0) = -\frac{\gamma^2}{\mu_d} \int_0^{2\pi} \frac{1}{\phi_y(-\sin s/\mu_d)}\, ds < 0 \tag{4.17}$$

and $\phi_y(\hat{y})$ is always positive in S_a, since $\hat{y} \in]-\delta, \delta[$. Then the Implicit Function Theorem guarantees that for $0 < \varepsilon \ll 1$ there exists $x(0) = m(\varepsilon)$ such that $Q(m(\varepsilon), \varepsilon) = 0$. Hence, $x(0) = m(\varepsilon)$ belongs to a stable periodic orbit since from (4.17) it follows that $|\partial_{x(0)} P(x(0), \varepsilon)| < 1$ for $0 < \varepsilon \ll 1$. □

Therefore, when $\mu_s > 1$ the family of invariant circles in Σ_s bifurcates into a single attracting limit cycle on the slow manifold $S_{a,\varepsilon}$. This result gives an upper bound of the time T of Proposition 4.13 as a function of ε since on the slow manifold $S_{a,\varepsilon}$, after a time $t = \mathrm{O}(1/\varepsilon)$, orbits are $\mathrm{O}(1)$ distant to the original family of circles in Σ_s. Furthermore, the regularization of regular stiction solutions does not necessarily remain uniformly close.

It is not possible to make a statement similar to Proposition 4.13 for singular stiction solutions, as they have nonunique forward solutions at the singular level. A further understanding can be obtained by studying the reduced problem (4.14). This differential algebraic equation is rewritten as a standard ODE by resolving the algebraic condition with respect to x and by differentiating it with respect to the time t:

$$\begin{aligned} -\mu_d \phi_y(\hat{y})\dot{\hat{y}} &= \cos\theta, \\ \dot{\theta} &= 1. \end{aligned} \tag{4.18}$$

Proposition 4.15 *The circles $f^{\pm} \subset \{\phi_y(\hat{y}) = 0\}$ are lines of singularities for the reduced problem (4.18), and solutions reach them in finite time. On $f^{\pm}$, the points $(\hat{y}, \theta) = (-\delta, \pi/2)$ and $(\hat{y}, \theta) = (\delta, 3\pi/2)$ are folded saddles, while $(\hat{y}, \theta) = (\delta, \pi/2)$ and $(\hat{y}, \theta) = (-\delta, 3\pi/2)$ are folded centres. Moreover, the intervals $\hat{I}^{\pm} \subset f^{\pm}$ defined as*

$$\begin{aligned} \hat{I}^{-} :=& \{(x, \hat{y}, \theta) \in \mathbb{R}^2 \times \mathbb{T}^1 \mid \xi = \mu_s, \quad \hat{y} = -\delta,\ \theta \in]\pi/2, 3\pi/2[\ \}, \\ \hat{I}^{+} :=& \{(x, \hat{y}, \theta) \in \mathbb{R}^2 \times \mathbb{T}^1 \mid \xi = -\mu_s, \hat{y} = \delta, \quad \theta \in [0, \pi/2[\cup]3\pi/2, 2\pi[\ \}, \end{aligned}$$

have nonunique forward solutions.

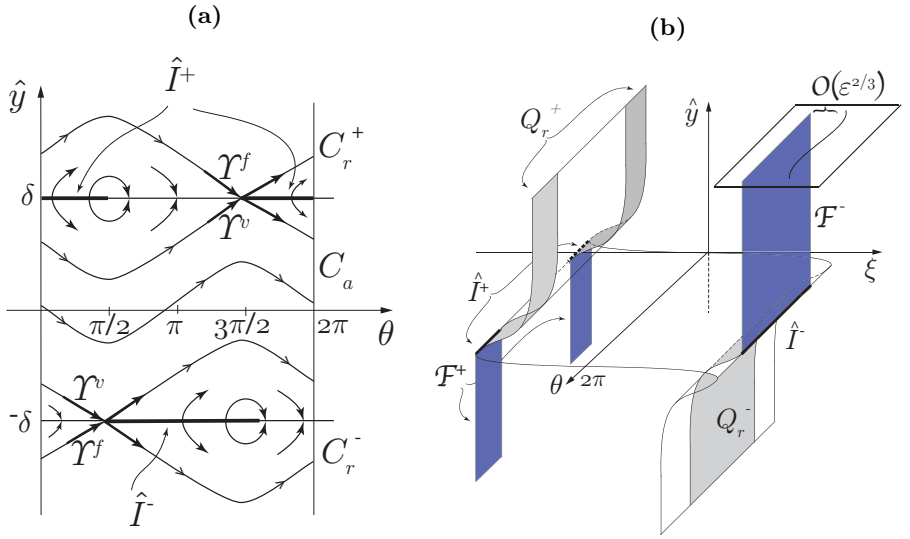

Figure 4.7: (a): Phase space of the reduced problem (4.18). (b): repelling invariant manifolds $Q_r^{\pm}$ in grey and foliations $\mathcal{F}^{\pm}$ in blue.

Proof. The time transformation $\mu_d \phi_y(\hat{y}) d\hat{t} = dt$ allows one to rewrite system (4.18) as the *desingularized problem*

$$\begin{aligned} \hat{y}' &= -\cos\theta, \\ \theta' &= \mu_d \phi_y(\hat{y}) \end{aligned} \tag{4.19}$$

in the new time $\hat{t}$. The difference between systems (4.18) and (4.19) is that $\hat{t}$ reverses the direction of time within $C_r^{\pm}$. Problem (4.19) has four equilibrium points in $\mathbb{R}^2 \times \mathbb{T}^1$. The points $(\delta, 3\pi/2)$ and $(-\delta, \pi/2)$ are hyperbolic saddles with eigenvalues $\pm\sqrt{\mu_d|\phi_{yy}(\delta)|}$ and eigenvectors $[1, \mp\sqrt{\mu_d|\phi_{yy}(\delta)|}]^T$ and $[1, \pm\sqrt{\mu_d|\phi_{yy}(\delta)|}]^T$, respectively. The remaining points $(\delta, \pi/2)$ and $(-\delta, 3\pi/2)$ are centers with eigenvalues $\pm i\sqrt{\mu_d|\phi_{yy}(\delta)|}$ and eigenvectors $[1, \pm i\sqrt{\mu_d|\phi_{yy}(\delta)|}]^T$ and $[1, \mp i\sqrt{\mu_d|\phi_{yy}(\delta)|}]^T$, respectively. The inversion of the time direction on $C_r^{\pm}$ gives the dynamics of the reduced problem (4.18). Thus a saddle in (4.19) is a folded saddle in (4.18), and similarly for the centres. Also, $f^{\pm}$ become lines of singularities with the time inversion, and the segments $\hat{I}^{\pm}$ have forward trajectories pointing inside both C_a and $C_r^{\pm}$; compare with Figure 4.7(a). Since $\dot{\theta} = 1$, orbits reach or leave $f^{\pm}$ in finite time. □

Figure 4.7 illustrates the results of Proposition 4.15. In the (x, y, θ) coordinates, the segments $\hat{I}^{\pm}$ collapse onto the lines of nonuniqueness $I^{\pm}$ for $\varepsilon = 0$. The layer problem (4.13) adds a further forward solution in $\hat{I}^{\pm}$ since orbits may

also leave a point of these lines by following a fast fibre for $\hat{y} \gtrless 0$.
Each folded saddle has two special solutions: the *singular vrai canard* Υ^v that connects C_a to $C_r^{\pm}$, and the *singular faux canard* Υ^f that does the opposite [BCDD81, DR96]. The vrai canard divides the critical manifold into regions with different types of forward dynamics: on one side of Υ^v, orbits *turn*, which means that they remain on C_a. On the other side of Υ^v, orbits reach $f^{\pm} \setminus \hat{I}^{\pm}$ and then *jump*; that is, they move away from C_0 by following a fast fibre. Each singular canard is a periodic orbit that visits both C_a and $C_r^{\pm}$; see Figure 4.7(a). The folded centres have no canard solutions [KW10], and for this reason they are not interesting for the analysis. Systems with $m \geq 2$ slow variables and one fast variable have robust canard solutions; i.e., the canards persist for small parameter variations. It follows that canard solutions are a generic feature of (4.12), where $m = 2$. Canards appear also in the Van der Pol oscillator [GHW05, VW15], in a model for global warming [WALC11], and in a model for transonic wind [CKW17].
When $0 < \varepsilon \ll 1$ the singular vrai canard Υ^v perturbs into a maximal canard [SW01]. This orbit corresponds to the intersection of $S_{a,\varepsilon}$ with $S_{r,\varepsilon}^{\pm}$. Hence, the maximal canard remains $\mathrm{O}(\varepsilon)$-close to $S_r^{\pm}$ for a time $t = \mathrm{O}(1)$. Furthermore, a family of orbits remains exponentially close to the maximal canard for some time before being repelled from $S_{r,\varepsilon}^{\pm}$ [Kue15, §8.1]. An orbit of this family is called a *canard*, and Figure 4.8(a) shows an example of it. Define $Q_r^{\pm}$ as the subsets of $C_r^{\pm}$ whose solutions, when flowed backwards in time, intersect the intervals of nonuniqueness $\hat{I}^{\pm}$. $Q_r^{\pm}$ are coloured in grey in Figure 4.7(b). The lines $\hat{I}^{\pm}$ are, backwards in time, the base of a foliation of fast (nonhyperbolic) fibres $\mathcal{F}^{\pm}$ that are coloured in blue in Figure 4.7(b). The following proposition describes the role of the repelling manifolds $Q_r^{\pm}$ for $0 < \varepsilon \ll 1$.

Proposition 4.16 *For $0 < \varepsilon \ll 1$, compact subsets $S_r^{\pm}$ of $Q_r^{\pm}$ perturb into the sets $S_{r,\varepsilon}^{\pm}$ that are $\mathrm{O}(\varepsilon)$-close to $S_r^{\pm}$. The slow problem on $S_{r,\varepsilon}^{\pm}$ is connected backwards in time to a family of fast trajectories $\mathcal{F}_{\varepsilon}^{\pm}$ that is $\mathrm{O}(\varepsilon^{2/3})$-close to $\mathcal{F}^{\pm}$. The orbits on $\mathcal{F}_{\varepsilon}^{\pm}$ and $S_{r,\varepsilon}^{\pm}$ separate the trajectories that, after possibly having been exponentially close to $S_{r,\varepsilon}^{\pm}$, are attracted to the slow manifold $S_{a,\varepsilon}$ from the ones that follow a fast trajectory away from the slow surface.*

Proof. By reversing the time orientation on the slow (4.11) and fast problem (4.12), the orbits on $Q_r^{\pm}$ satisfy the assumptions of Proposition 4.13. Hence, the distance of $\mathcal{F}^{\pm}$ to $\mathcal{F}_{\varepsilon}^{\pm}$ is $\mathrm{O}(\varepsilon^{2/3})$. Now consider again the true time direction, and take a set of initial conditions that is exponentially close to the fibres $\mathcal{F}_{\varepsilon}^{\pm}$. These orbits will follow the repelling slow manifolds $S_{r,\varepsilon}^{\pm}$ for a time $t = \mathrm{O}(1)$ [SW01]. The manifolds $S_{r,\varepsilon}^{\pm}$ act as separators of two different futures: on one side the orbits will get attracted to the slow attracting manifold $S_{a,\varepsilon}$, while on the other side they will jump away by following an escaping fast fibre; compare with Figure 4.8(b). □

It follows that around $\hat{I}^{\pm}$ and $\mathcal{F}^{\pm}$ there is a high sensitivity to the initial conditions. Even though the (x, θ)-dynamics on C_a coincides with the one on $C_r^{\pm}$, trajectories close to these two manifolds may have different futures. Orbits belonging to $S_{a,\varepsilon}$ will exit $S_{a,\varepsilon}$ in a predictable point. On the other hand, the orbits that follow $S_{r,\varepsilon}^{\pm}$ are very sensitive and may escape from it at any time. These two types of trajectories are coloured in blue and magenta, respectively, in Figures 4.8(b) and (d). The orbits that follow $S_{r,\varepsilon}^{\pm}$ for some time are canard-like in the forward behaviour. However, in backwards time they are connected to a family of fast fibres instead of to $S_{a,\varepsilon}$, and for this reason they are not typical canards like Υ^v.

In the original coordinates (x, y, θ), the canard trajectories of the folded saddles and the canard-like solutions of the lines $\hat{I}^{\pm}$ leave the slow manifold in a point inside $\Sigma_{s,stiction}^{\pm}$, as in Figures 4.8(c) and (d). In the piecewise smooth system these orbits satisfy the Carathéodory condition (4.7), but they are not stiction

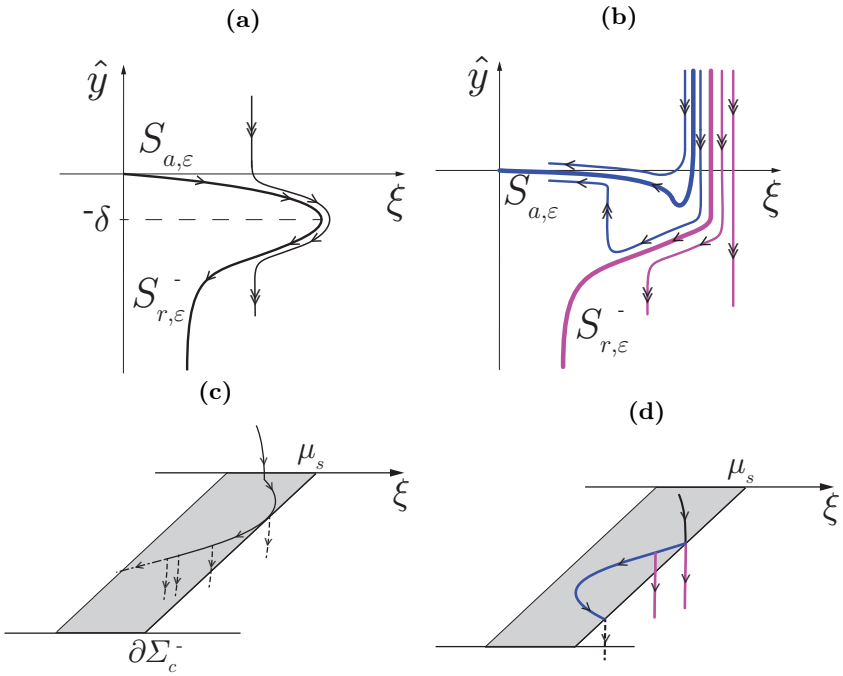

Figure 4.8: (a): A canard orbit at the intersection of $S_{a,\varepsilon}$ with $S_{r,\varepsilon}^{-}$. (b): Dynamics around a point of $\hat{I}^{-}$ for $0 < \varepsilon \ll 1$. (c) and (d): The same dynamics of Figures 4.8(a) and (b) in the (x, y, θ)-coordinates. The canard-like solutions leaving $\Sigma_{s,\text{stiction}}^{-}$ resemble Carathéodory solutions of model (4.4); compare with Figure 4.4(a).

solutions. It follows that some of the Carathéodory solutions of (4.4) appear upon regularization of the stiction model: these are the trajectories of Z_s that intersect $I^{\pm}$ backwards in time. All the other Carathédory solutions of model (4.4) do not have a corresponding solution in the regularized model. The interpretation of the solutions with canard is that the slip onset is delayed with respect to the time when the external forces have equalled the maximum static friction force. Figure 4.11(c) in subsection 4.6.1 will show a numerical solution having this delay.

4.6 Slip-stick periodic orbits

This section considers a family of periodic orbits of model (4.4) that interacts with the lines of nonuniqueness $I^{\pm}$. Then subsection 4.6.1 discusses how the family perturbs in the regularized system (4.10) for $0 < \varepsilon \ll 1$ by combining numerics and analysis.
Model (4.4) has several kinds of periodic motion: pure slip [Sha86, CS06], pure stick [HOP98], nonsymmetric slip-stick [OA01, GB99, AC01, OHP96, PS90], and symmetric slip-stick [OA01, HOP98]. This section focuses on the latter, as slip-stick orbits are likely to be affected by the nonuniqueness at $I^{\pm}$. Figure 4.9 shows an example of such a trajectory. The symmetric slip-stick trajectories can be found by solving a system of algebraic equations because system (4.4), in its nonautonomous form, is piecewise-linear in each region. Furthermore, it is sufficient to study only half the period, as ensured by Lemmas 4.17 and 4.18.

Lemma 4.17 *System (4.4) has a symmetry*

$$S(x, y, \theta) = (-x, -y, \theta + \pi). \tag{4.20}$$

Proof. The map (4.20) is a diffeomorphism $\mathbb{R}^2 \times \mathbb{T}^1 \to \mathbb{R}^2 \times \mathbb{T}^1$ that satisfies the condition for a symmetry $Z(S(z)) = S_z(z)Z(z)$, where $S_z(z)$ is the Jacobian of $S(z)$ and $z = (x, y, \theta)$ [Mei07, §6.4]. □

Lemma 4.18 *Let $\varphi_t(z)$ be the regular stiction orbit of system (4.4) at time t, with initial condition $z = (x, y, \theta)$. If $\varphi_\pi(z) = (-x, -y, \theta + \pi)$ then the orbit is symmetric and periodic with period $T = 2\pi$.*

Proof. Applying the symmetry map (4.20) to the point $\varphi_\pi(z)$, gives

$$S(-x, -y, \theta + \pi) = (x, y, \theta + 2\pi).$$

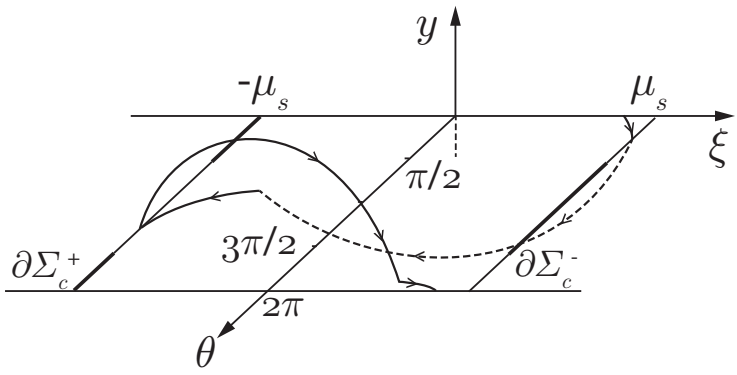

Figure 4.9: A symmetric, slip-stick, periodic orbit with $\theta \in \mathbb{T}^1$. The dashed line represents trajectories in Z^-. The interest is to study how such an orbit interacts with the intervals of nonuniqueness $I^{\pm}$ (in bold) under variation of a parameter.

Since $Z(x, y, \theta + 2\pi) \equiv Z(x, y, \theta)$ for any $\theta \in \mathbb{T}^1$, the flow $\varphi_t(z)$ is symmetric and periodic, with symmetry (4.20) and period $T = 2\pi$. □

The results of Lemma 4.18 have been used in [Sha86] even though the symmetry was not made explicit. Define $\varphi_t^{\text{slip}}(z_0)$ (resp., $\varphi_t^{\text{stick}}(z_1)$) as the slip (stick) solution of $Z^-(z)$ ($Z_s(z)$) with initial conditions in z_0 (z_1). The following lemma states when these two solutions, pieced together, belong to a symmetric slip-stick periodic orbit.

Lemma 4.19 *Necessary conditions for the slip and stick solutions $\varphi_t^{slip}(z_0)$ and $\varphi_t^{stick}(z_1)$ to form the lower half of a symmetric, slip-stick, periodic orbit are*

$$\varphi_{\pi-\theta^*}^{slip}(z_0) = \varphi_0^{stick}(z_1), \tag{4.21a}$$

$$\varphi_{\theta^*}^{stick}(z_1) = S(z_0), \tag{4.21b}$$

where $0 < \theta^* < \pi$ is the duration of one stick phase and $z_0 \in \partial\Sigma_c^-$, $z_1 \in \Sigma_s$.

Condition (4.21a) guarantees the continuity between the stick and slip phase, while (4.21b) guarantees the symmetry. The upper half-period of the orbit follows by applying the symmetry map (4.20) to φ_t^{slip} and φ_t^{stick}.

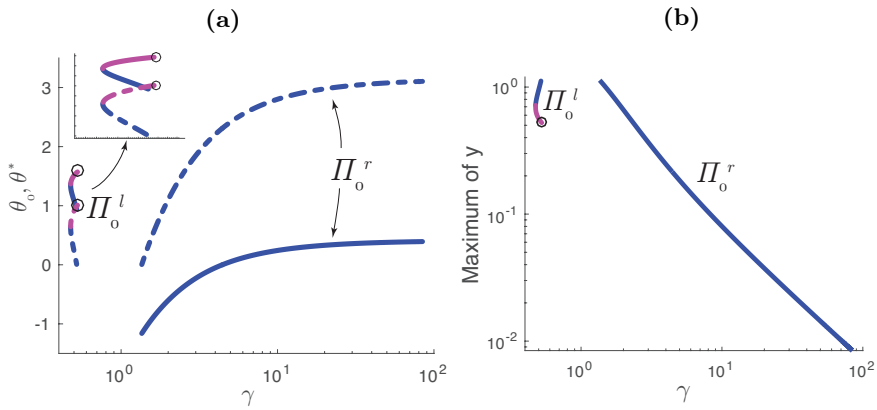

Figure 4.10: (a): Two families of slip-stick orbits $\Pi_0^{l,r}$ of (4.4) for $\mu_s = 1.1$, $\mu_d = 0.4$. The solid line is θ_0, while the dashed line is θ^*. The blue denotes a stable periodic orbit while the magenta a saddle periodic orbit. (b): Maximum amplitude of the orbits.

Corollary 4.20 *Conditions* (4.21) *are equivalent to*

$$x^{slip}(\pi - \theta^*) = -x_0, \tag{4.22a}$$
$$y^{slip}(\pi - \theta^*) = 0, \tag{4.22b}$$
$$\pi - \theta^* + \theta_0 = \theta_1, \tag{4.22c}$$

where $z_0 = (x_0, y_0, \theta_0) \in \Sigma_c^-$, $z_1 = (x_1, y_1, \theta_1) \in \Sigma_s$, *and* $\varphi_t^{slip}(z_0) = (x(t), y(t), \theta(t))^{slip}$.

Proof. The stick solution of (4.4) with initial condition $z_1 = (x_1, 0, \theta_1)$ is $(x, y, \theta)^{\text{stick}}(t) = (x_1, 0, t + \theta_1)$. Condition (4.21a) then implies that $x^{\text{slip}}(\pi - \theta^*) = x_1$ and $y^{\text{slip}}(\pi - \theta^*) = 0$, while $\theta^{\text{slip}}(\pi - \theta^*) = \pi - \theta^* + \theta_0 = \theta_1$. Condition (4.21b) adds, furthermore, that $x_1 = -x_0$. □

The stick-slip solutions of (4.4) are now investigated numerically. The system of conditions (4.22) has five unknown parameters: $\gamma, \theta_0, \theta^*, \mu_s$, and μ_d. It is reasonable to fix μ_s and μ_d, as these are related to the material used, and then find a family of solutions of (4.22) by varying the frequency ratio $\gamma = \Omega/\omega$. The values used in the computations are listed in Table 4.1. Notice that conditions (4.22) are necessary but not sufficient: further admissibility conditions may be needed. These are conditions that control that each piece of solution does not exit its region of definition; for example, the stick solution should not cross $\partial\Sigma_c^-$ before $t = \theta^*$, and should not cross $\partial\Sigma_c^+$ for any $t \in [0, \theta^*]$. A numerical computation shows that system (4.22) has two branches of solutions $\Pi_0^{l,r}$, as

Table 4.1: Parameters values used in the simulations.

System	μ_s	μ_d	ε	δ	a	b	c	d
Nonsmooth (4.4)	1.1	0.4						
Regularized (4.10)	1.1	0.4	10^{-3}	0.6	10.5766	–16.9937	1.7575	5.6595

shown in Figure 4.10: one for $\gamma < 1$ and one for $\gamma > 1$. The branches are disconnected around the resonance for $\gamma = 1$, where chaotic behaviour may appear [AC01, CS06, OHP96]. The branch Π_0^l for $\gamma < 1$ is bounded by pure slip orbits when $\theta^* \to 0$ and by the visible tangency on Σ_s when $\theta_0 \to \pi/2$. The latter is marked with a circle in Figure 4.10(a). The branch Π_0^r for $\gamma > 1$ is delimited by pure slip orbits when $\gamma \to 1$ since again $\theta^* \to 0$, while when $\gamma \gg 1$, which is the rigid body limit, the family is bounded by $\theta^* \to \pi$. Here periodic orbits have a very short slip phase and an almost π-long stick phase.
A slip-stick orbit of model (4.4) has three Floquet multipliers. Among these, one is trivially unitary, the second one is always zero, and the last indicates the stability of the periodic orbit. The zero multiplier is due to the interaction of the periodic orbit with the sticking manifold Σ_s: solutions lying on this surface are backwards nonunique. Figure 4.10 denotes in blue the attracting periodic solutions and in magenta the repelling ones. In particular, the family Π_o^l becomes unstable sufficiently close to the visible tangency at $\theta_0 = \pi/2$, which is marked with a circle in Figure 4.10. This is because the visible tangency acts as a separatrix of two very different behaviours: on one side orbits jump, while on the other side they turn; recall Figure 4.7(a).

4.6.1 Slip-stick periodic orbits in the regularized system

This section finds slip-stick periodic solutions of the regularized model (4.10) with a numerical continuation in AUTO [Doe07]. The solutions are then compared with the ones of the discontinuous system (4.4). The regularization function used is a polynomial

$$\phi(y) = y(ay^6 + by^4 + cy^2 + d),$$

within $y \in [-1, 1]$, where the coefficients a, b, c, d are determined by the conditions (4.9), and the specific values used in the simulations are listed in Table 4.1. Hence $\phi(y)$ is C^1 for $y \in \mathbb{R}$. Figure 4.11(a) shows the family of slip-stick periodic orbits Π_ε of system (4.10). This can be seen, loosely, as the union of three branches

$$\Pi_\varepsilon = \Pi_\varepsilon^l \cup \Pi_\varepsilon^c \cup \Pi_\varepsilon^r,$$

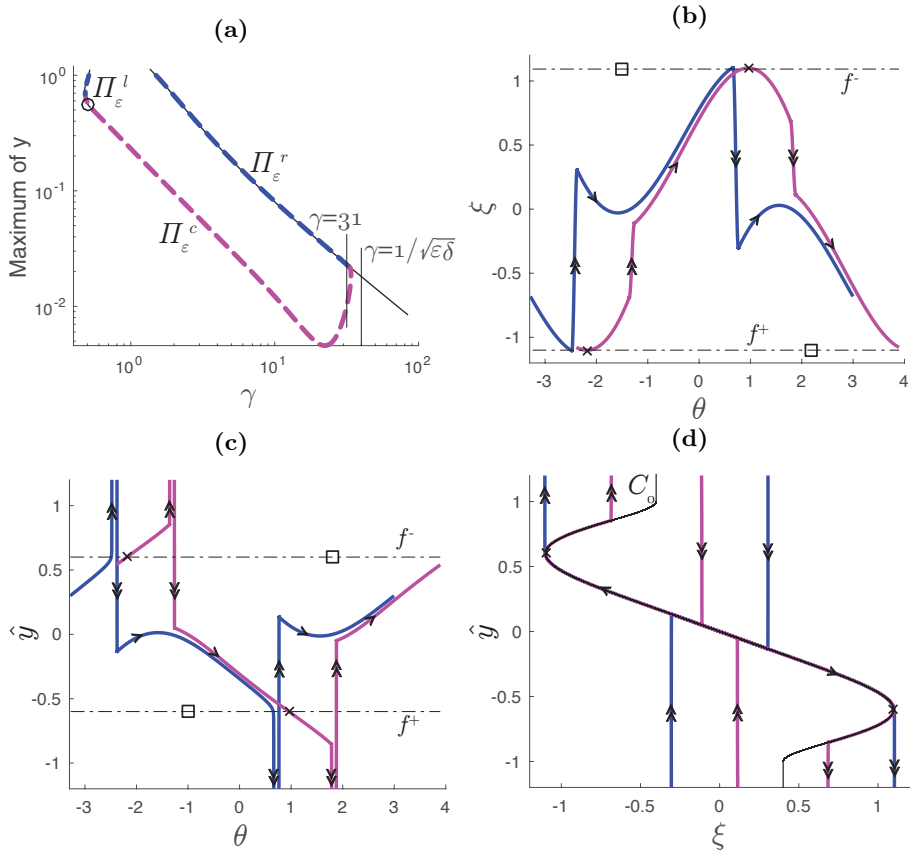

Figure 4.11: Numerical simulation in AUTO. (a): In dashed the family Π_ε. The repelling branch Π_ε^c connects the two regular branches $\Pi_\varepsilon^{l,r}$. Solid line: families $\Pi_0^{l,r}$. The colours denote the stability of the orbits, as in Figure 4.10.(b): Two periodic orbits coexisting for $\gamma = 31$: a regular slip-stick in blue and a slip-stick with canard segments in magenta. The x marks the folded saddle, while the □ denotes the folded node. (c) and (d): Projections of (b) in the $(\theta, \hat{y})$- and $(\xi, \hat{y})$-planes.

where $\Pi^{l,r}_\varepsilon$ are $O(\varepsilon^{2/3})$-close to the regular branches $\Pi^{l,r}_0$ [SW04]. The branch Π^c_ε connects Π^l_ε to Π^r_ε at the rigid body limit, which is $\gamma \gg 1$, and it consists of slip-stick periodic orbits each having two canard segments. Figures 4.11(b), (c) and (d) show for $\gamma = 31$ two coexisting periodic orbits: the magenta one belongs to Π^c_ε, and the blue one belongs to Π^r_ε. In particular, Figure 4.11(c) shows the delay in the slip onset, when the orbit follows the canard, since the slip happens after a time $t = O(1)$ with respect to when the orbit has intersected the fold lines $f^\pm$.

Remark 4.21 *Recall from* (4.15) *that trajectories on* C_0 *satisfy* $\xi(x,\theta) = -\mu_d\phi(\hat{y})$. *By Fenichel's results, a compact, normally hyperbolic submanifold* $S_0 \subset C_0$ *perturbs into a slow manifold* S_ε *for* $0 < \varepsilon \ll 1$, *and the flow on* S_ε *converges to the flow of* (4.14) *as* $\varepsilon \to 0$. *It follows that the time evolution of* $\xi(x,\theta)$ *is equivalent to evolution of the friction force up to* $O(\varepsilon)$ *terms; see Figures 4.11(b) and (d). In these figures, though, the vertical segments do not lie on* S_ε, *but they are the projections of the fast fibres onto* S_ε, *and these are denoted with a double arrow.*

The existence of the branch Π^c_ε is supported by Proposition 4.22 below. For this, let Σ_{out} be a cross-section orthogonal to the y-axis so that the fast fibres with base on the singular vrai canard on C^-_r intersect it on the line $L_{\text{out},0}$. Furthermore, define Σ_{in} as the cross-section orthogonal to the ξ-axis so that it intersects C_a on the line $L_{\text{in},0}$; see Figure 4.12(a).

Proposition 4.22 *Suppose that for* $\varepsilon = 0$ *there exists a smooth return mechanism* $R : \Sigma_{out} \to \Sigma_{in}$ *that maps* $L_{out,0} \subset \Sigma_{out}$ *onto* $L_{in,0} \subset \Sigma_{in}$. *Suppose, furthermore, that* $L_{in,0} = R(L_{out,0})$ *is transversal to the singular vrai canard* Υ^v. *Then for* $0 < \varepsilon \ll 1$ *there exists a unique, periodic orbit* $\varphi^\varepsilon_t(z)$ *that has a canard segment, and that tends to the singular canard for* $\varepsilon \to 0$. *Furthermore, this orbit has a saddle stability with Floquet multipliers:* $\{1, O(e^{-c_1/\varepsilon}), O(e^{c_2/\varepsilon})\}$, *with* $c_{1,2} \in \mathbb{R}^+$.

Proof. First notice that for $0 < \varepsilon \ll 1$ the singular vrai canard Υ^v on C^-_r perturbs into a maximal canard that is $O(\varepsilon^{2/3})$-close to it. This maximal canard is the base of a foliation of fibres that intersect Σ_{out} on a line $L_{\text{out},\varepsilon}$ that is $O(\varepsilon^{2/3})$-close to $L_{\text{out},0}$. The return map $R(z)$ is smooth so that $R(L_{\text{out},\varepsilon})$ intersects Σ_{in} in a line $L_{\text{in},\varepsilon}$ that is $O(\varepsilon^{2/3})$-close to $L_{\text{in},0}$. The line $L_{\text{in},\varepsilon}$ is transversal to the maximal canard for ε sufficiently small, since $L_{\text{in},0}$ was transversal to Υ^v, and the perturbation is $O(\varepsilon^{2/3})$.
Now consider the backward flow of $L_{\text{out},\varepsilon}$. This contracts to the maximal canard with an order $O(e^{-c/\varepsilon})$. Hence, it intersects $L_{\text{in},\varepsilon}$ in an exponentially small set that is centred around the maximal canard. This means that the reduced Poincaré map $P : L_{\text{in},\varepsilon} \to L_{\text{in},\varepsilon}$ is well defined and contracting in backwards

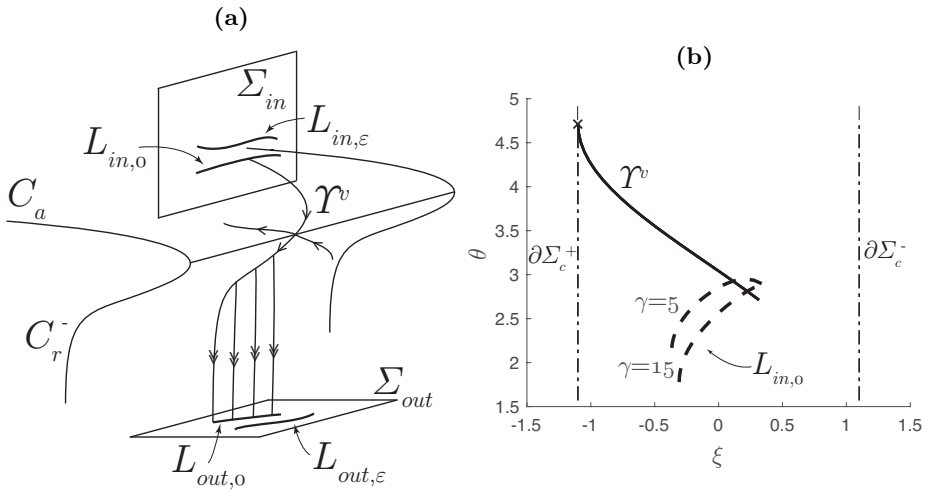

Figure 4.12: (a): Construction of the cross-sections $\Sigma_{\text{in,out}}$. (b): Numerical simulation showing that $R(L_{\text{out},0})$ (dashed line) is transversal to Υ^v (solid line) for $\varepsilon = 0$ and $\gamma = \{5, 15\}$. The visible tangency is marked with x. The dashed-dotted lines are $\partial\Sigma_c^{\pm}$.

time. Hence it has a unique fixed point. Such a fixed point corresponds to a periodic orbit with canard. It follows that the periodic orbit has an exponential contraction to the attracting slow manifold and an exponential repulsion forward in time around the maximal canard. This determines the Floquet multipliers and, consequently, the saddle stability. □

Figure 4.12(b) shows numerically that the discontinuous model (4.4) satisfies the assumptions of Proposition 4.22. This supports the existence of the branch Π_ε^c in the regularized model for ε sufficiently small. Because of the symmetry, the branch Π_ε^c has two canard segments for each period. A *canard explosion* may appear when a family of periodic orbits interacts with a canard. The explosion is defined as the transition from a small oscillation to a relaxation oscillation for an exponentially small variation in the parameter [KS01c]. However, system (4.10) has no canard explosion: Figure 4.11(a) shows that the maximum amplitude of the oscillations does not increase with the continuation from Π_ε^l to Π_ε^c. The effect of the canard is instead in the explosion of one of the Floquet multipliers as previously stated in Proposition 4.22 and observed numerically in AUTO. The saddle stability of the family Π_ε^c implies that the periodic orbits of Π_ε^c are always repelling, even with a time inversion. Hence, these periodic orbits are not visible in standard simulations. It could be interesting to make an experiment, with very high precision in the initial conditions, where the effects of

the canard are measurable. If canard solutions appear, then this would support the validity of the stiction model and of its regularization.

Proposition 4.23 *The branch Π^c_ε is bounded above by $\gamma = 1/\sqrt{\varepsilon\delta}$ for $0 < \varepsilon \ll 1$.*

Proof. Differentiate $\xi(x,\theta) = \gamma^2 x + \sin(\theta)$ with respect to time, and rewrite the slow problem (4.11) in the $(\xi, \hat{y}, \theta)$ variables

$$\begin{aligned} \dot{\xi} &= \gamma^2 \varepsilon \hat{y} + \cos\theta, \\ \varepsilon\dot{\hat{y}} &= -\xi - \mu_d \phi(\hat{y}), \\ \dot{\theta} &= 1. \end{aligned}$$

If $\gamma^2 = \mathrm{O}(1/\varepsilon)$, it makes sense to introduce the rescaling $\Gamma := \gamma^2\varepsilon$, so that the slow problem becomes

$$\begin{aligned} \dot{\xi} &= \Gamma \hat{y} + \cos\theta, \\ \varepsilon\dot{\hat{y}} &= -\xi - \mu_d \phi(\hat{y}), \\ \dot{\theta} &= 1. \end{aligned}$$

This system again has a multiple timescale with critical manifold (4.15). Its reduced problem in the time $\hat{t}$ is

$$\begin{aligned} \hat{y}' &= -\Gamma \hat{y} - \cos\theta, \\ \theta' &= \mu_d \phi_y(\hat{y}). \end{aligned} \tag{4.23}$$

Notice that (4.23) differs from the desingularized problem (4.19) only for the term $\Gamma\hat{y}$ in the $\hat{y}$ dynamics. The equilibrium points of (4.23) exist if $|\Gamma\delta| \leq 1$, and they have coordinates $\hat{y} = \pm\delta$, $\cos\theta = \mp\Gamma\delta$. The comparison of system (4.23) with the desingularized problem (4.19) shows that the equilibrium points have shifted along the θ-direction. In particular, the saddles have moved backwards while the centres have moved forward. Furthermore, the centres have become stable foci. For increasing values of Γ the stable foci turn into stable nodes. When $|\Gamma\delta| = 1$, pairs of saddles and nodes collide and disappear through a saddle-node bifurcation of type I [Kue15, Lemma 8.5.7]. Beyond this value canard solutions cease to exist. Such a condition is equivalent to $\gamma = 1/\sqrt{\varepsilon\delta}$. □

The bound $\gamma = 1/\sqrt{\varepsilon\delta}$, which is highlighted in Figure 4.11(b), is larger than the value of γ for which the family Π^c_ε folds. In particular, at the turning point, the folded foci have not turned into folded nodes yet. Thus the collision of the folded saddles with the folded foci is not a direct cause of the saddle-node bifurcation of Π^c_ε, but gives only an upper bound for the existence of the family. When the

folded nodes appear, there might exist further periodic orbits that exit the slow regime through the canard associated to the stable nodes.
Furthermore, the orbits of Π_ε^c interact with the folded saddle only, but they do not interact with the other points of $\hat{I}^\pm$. The regularized problem (4.10) may have other families of periodic orbits that interact with $\hat{I}^\pm$, for example, a family of pure slip periodic orbits that reaches $\hat{I}^\pm$ from a fast fibre and then jumps off through a canard-like solution. However, this family would also turn unstable when passing sufficiently close to the canards because of the high sensitivity to the initial conditions around $\mathcal{F}^\pm$. In particular, an explosion in the Floquet multipliers is again expected because of Proposition 4.22.

4.7 Conclusions

Stiction is a widely used formulation of the friction force because of its simplicity. However, this friction law has issues of nonuniqueness at the slip onset that in this chapter are highlighted in a friction oscillator model. This model is a discontinuous, non-Filippov system, with subregions having a nonunique forward flow. The forward nonuniqueness is problematic in numerical simulations: here a choice is required, and hence valid solutions may be discarded. A regularization of the model resolves the nonuniqueness by finding a repelling slow manifold that separates forward sticking to forward slipping solutions. Around the slow manifold there is a high sensitivity to the initial conditions. Some trajectories remain close to this slow manifold for some time before being repelled. These trajectories, which mathematically are known as canards, have the physical interpretation of delaying the slip onset when the external forces have equalled the maximum static friction force at stick. This result could potentially be verified experimentally, thus furthering the understanding of friction-related phenomena. Indeed, the appearance of the canard solutions is a feature of stiction friction rather than of the specific friction oscillator model. For example, the addition of a damping term on the friction oscillator or the problem of a mass on an oscillating belt would give rise to similar canard solutions.
The canard solutions of the regularized systems can be interpreted, in the discontinuous model, as Carathéodory trajectories that allow the slip onset in points inside the sticking region. These Carathéodory orbits are identified by being backwards transverse to the lines of nonuniqueness.
This chapter also shows that the regularized system has a family of periodic orbits Π_ε interacting with the folded saddles. The orbits with canard $\Pi_\varepsilon^c \subset \Pi_\varepsilon$ have a saddle stability, with Floquet multipliers $\mathrm{O}(\mathrm{e}^{\pm c\varepsilon^{-1}})$. Furthermore, the family Π_ε^c connects, at the rigid body limit, the two families of slip-stick periodic orbits $\Pi_0^{l,r}$ of the discontinuous problem. Further periodic orbits may interact with the canard segments.

Bibliography

[ABS08] F. Al-Bender and J. Swevers. Characterization of Friction Force Dynamics. *IEEE Control Systems*, 28(6):64–81, 2008.

[AC01] U. Andreaus and P. Casini. Dynamics of friction oscillators excited by a moving base and/or driving force. *Journal of Sound and Vibration*, 245(4):685–699, 2001.

[Aka02] A. Akay. Acoustics of friction. *The Journal of the Acoustical Society of America*, 111(4):1525–1548, 2002.

[And12] B Andreotti. Sonic sands. *Reports on Progress in Physics*, 75(2):026602, 2012.

[BB96] M. E. Belardinelli and E. Belardinelli. The quasi-static approximation of the spring-slider motion. *Nonlinear Processes in Geophysics*, 3(3):143–149, 1996.

[BBK17a] E. Bossolini, M. Brøns, and K. U. Kristiansen. Canards in stiction: On solutions of a friction oscillator by regularization. *SIAM Journal on Applied Dynamical Systems*, 16(4):2233–2258, 2017.

[BBK17b] E. Bossolini, M. Brøns, and K. U. Kristiansen. Singular limit analysis of a model for earthquake faulting. *Nonlinearity*, 30(7):2805–2834, 2017.

[BCDD81] E. Benoît, J. F. Callot, F. Diener, and M. Diener. Chasse au canard. *Collectanea Mathematica*, 31–32(1–3):37–119, 1981.

[BdST06] C. A. Buzzi, P. R. da Silva, and M. A. Teixeira. A singular approach to discontinuous vector fields on the plane. *Journal of Differential Equations*, 231(2):633–655, 2006.

[Ben83] E. Benoît. Systèmes lents-rapides dans $\mathbb{R}^3$ et leur canards. *Astérisque*, 109-110(2):159–191, 1983.

[Ben90] E. Benoît. Canards et enlacements. *Publications mathématiques de l'I.H.É.S.*, 72(1):63–91, 1990.

[Biz10] A. Bizzarri. On the recurrence of earthquakes: Role of wear in brittle faulting. *Geophysical Research Letters*, 37(20), 2010. L20315.

[BK67] R. Burridge and L. Knopoff. Model and theoretical seismicity. *Bulletin of the Seismological Society of America*, 57(3):341–371, 1967.

[BRMS16] C. Bonet-Revés and T. M-Seara. Regularization of sliding global bifurcations derived from the local fold singularity of Filippov systems. *Discrete and Continuous Dynamical Systems - Series A*, 36(7):3545–3601, 2016.

[BS95] P.-A. Bliman and M. Sorine. Easy-to-use realistic dry friction models for automatic control. In *Proceedings of the 3rd European Control Conference*, volume 4, pages 3778–3794, 1995.

[BZ08] Y. Ben-Zion. Collective behavior of earthquakes and faults: Continuum-discrete transitions, progressive evolutionary changes, and different dynamic regimes. *Reviews of Geophysics*, 46(4), 2008. RG4006.

[CCM+09] C. Cantoni, R. Cesarini, G. Mastinu, G. Rocca, and R. Sicigliano. Brake comfort - a review. *Vehicle System Dynamics*, 47(8):901–947, 2009.

[CGH+96] R. M. Corless, G. H. Gonnet, D. E. G. Hare, D. J. Jeffrey, and D. E. Knuth. On the LambertW Function. *Advances in Computational Mathematics*, 5(1):329–359, 1996.

[Chi06] C. Chicone. *Ordinary Differential Equations with Applications*, volume 34 of *Texts in Applied Mathematics*. Springer-Verlag New York, 2006.

[CJ11] A. Colombo and M. R. Jeffrey. Nondeterministic Chaos, and the Two-fold Singularity in Piecewise Smooth Flows. *SIAM Journal on Applied Dynamical Systems*, 10(2):423–451, 2011.

[CKW17] P. Carter, E. Knobloch, and M. Wechselberger. Transonic canards and stellar wind. *Nonlinearity*, 30(3):1006–1033, 2017.

[CL89] J. M. Carlson and J. S. Langer. Mechanical model of an earthquake fault. *Physical Review A*, 40(11):6470–6484, 1989.

[CLST91] J. M. Carlson, J. S. Langer, B. E. Shaw, and C. Tang. Intrinsic properties of a Burridge-Knopoff model of an earthquake fault. *Physical Review A*, 44(2):884–897, 1991.

[CLW94] S.-N. Chow, C. Li, and D. Wang. *Normal Forms and Bifurcation of Planar Vector Fields*. Cambridge University Press, 1994.

[Col17] A. Colombo. A Choice Between Smooth and Nonsmooth Models. *Trends in Mathematics, Extended Abstracts Spring 2016*, 8:43–47, 2017.

[Cor08] J. Cortés. Discontinuous Dynamical Systems. *IEEE Control Systems*, 28(3):36–73, 2008.

[CPW16] A. Cabboi, T. Putelat, and J. Woodhouse. The frequency response of dynamic friction: Enhanced rate-and-state models. *Journal of the Mechanics and Physics of Solids*, 92:210–236, 2016.

[CS06] G. Csernák and G. Stépán. On the periodic response of a harmonically excited dry friction oscillator. *Journal of Sound and Vibration*, 295(3–5):649–658, 2006.

[CSS07] G. Csernák, G. Stépán, and S. W. Shaw. Sub-harmonic resonant solutions of a harmonically excited dry friction oscillator. *Nonlinear Dynamics*, 50(1–2):93–109, 2007.

[dBBC01] M. di Bernardo, C. J. Budd, and A. R. Champneys. Corner collision implies border-collision bifurcation. *Physica D: Nonlinear Phenomena*, 154(3–4):171–194, 2001.

[DBBCK08] M. Di Bernardo, C. Budd, A. R. Champneys, and P. Kowalczyk. *Piecewise-smooth Dynamical Systems*. Applied Mathematical Sciences. Springer-Verlag London, 2008.

[DD95] F. Diener and M. Diener. *Nonstandard Analysis in Practice*. Universitext. Springer-Verlag Berlin Heidelberg, 1995.

[DGK+12] M. Desroches, J. Guckenheimer, B. Krauskopf, C. Kuehn, H. M. Osinga, and M. Wechselberger. Mixed-Mode Oscillations with Multiple Time Scales. *SIAM Review*, 54(2):211–288, 2012.

[Die72] J. H. Dieterich. Time-dependent friction in rocks. *Journal of Geophysical Research*, 77(20):3690–3697, 1972.

[Die78] J. H. Dieterich. Time-dependent friction and mechanics of stick-slip. *Pure and Applied Geophysics*, 116(4-5):790–806, 1978.

[Die79] J. H. Dieterich. Modeling of rock friction. 1. Experimental results and constitutive equations. *Journal of Geophysical Research: Solid Earth*, 84(B5):2161–2168, 1979.

[DKO08] M. Desroches, B. Krauskopf, and H. M. Osinga. The Geometry of Slow Manifolds near a Folded Node. *SIAM Journal on Applied Dynamical Systems*, 7(4):1131–1162, 2008.

[DMD06] P. De Maesschalck and F. Dumortier. Canard solutions at non-generic turning points. *Transactions of the American Mathematical Society*, 358(5):2291–2334, 2006.

[Doe07] E. J. Doedel. Lecture Notes on Numerical Analysis of Nonlinear Equations. In B. Krauskopf, H. M. Osinga, and J. Galán-Vioque, editors, *Numerical Continuation Methods for Dynamical Systems*, pages 1–49. Springer, Dordrecht, 2007.

[DR96] F. Dumortier and R. Roussarie. Canard Cycles and Center Manifolds. *Memoirs of the American Mathematical Society*, 121(577), 1996.

[EBL08] B. A. Erickson, B. Birnir, and D. Lavallée. A model for aperiodicity in earthquakes. *Nonlinear Processes in Geophysics*, 15(1):1–12, 2008.

[EBL11] B. A. Erickson, B. Birnir, and D. Lavallée. Periodicity, chaos and localization in a Burridge-Knopoff model of an earthquake with rate-and-state friction. *Geophysical Journal International*, 187(1):178–198, 2011.

[Eck73] W. Eckhaus. *Matched Asymptotic Expansions and Singular Perturbations*, volume 6 of *North-Holland Mathematics Studies*. Elsevier, 1973.

[Fen74] N. Fenichel. Asymptotic stability with rate conditions for dynamical systems. *Bulletin of the American Mathematical Society*, 80(2):346–349, 1974.

[Fen79] N. Fenichel. Geometric singular perturbation theory for ordinary differential equations. *Journal of Differential Equations*, 31(1):53–98, 1979.

[FGHP98] B. Feeny, A. Guran, N. Hinrichs, and K. Popp. A Historical Review on Dry Friction and Stick-Slip Phenomena. *Applied Mechanics Reviews*, 51(5):321–341, 1998.

[FHS09] E. Fossas, S. J. Hogan, and T. M. Seara. Two-parameter bifurcation curves in power electronic converters. *International Journal of Bifurcation and Chaos*, 19(1):349–357, 2009.

[Fil88] A. F. Filippov. *Differential Equations with Discontinuous Righthand Sides*. Mathematics and its Applications. Kluwer, 1988.

[FXN+14] Q. Fan, C. Xu, J. Niu, G. Jiang, and Y. Liu. Stability analyses and numerical simulations of the single degree of freedom spring-slider system obeying the revised rate- and state-dependent friction law. *Journal of Seismology*, 18(3):637–649, 2014.

[GB99] U. Galvanetto and S. R. Bishop. Dynamics of a Simple Damped Oscillator Undergoing Stick-Slip Vibrations. *Meccanica*, 34(5):337–347, 1999.

[GHS10] M. Guardia, S. J. Hogan, and T. M. Seara. An Analytical Approach to Codimension-2 Sliding Bifurcations in the Dry-Friction Oscillator. *SIAM Journal on Applied Dynamical Systems*, 9(3):769–798, 2010.

[GHW05] J. Guckenheimer, K. Hoffman, and W. Weckesser. Bifurcations of Relaxation Oscillations near Folded Saddles. *International Journal of Bifurcation and Chaos*, 15(11):3411–3421, 2005.

[GRRT84] J. C. Gu, J. R. Rice, A. L. Ruina, and S. T. Tse. Slip motion and stability of a single degree of freedom elastic system with rate and state dependent friction. *Journal of the Mechanics and Physics of Solids*, 32(3):167–196, 1984.

[GS09] I. Gucwa and P. Szmolyan. Geometric singular perturbation analysis of an autocatalator model. *Discrete and Continuous Dynamical Systems - Series S*, 2(4):783–806, 2009.

[GST11] M. Guardia, T. M. Seara, and M. A. Teixeira. Generic bifurcations of low codimension of planar Filippov systems. *Journal of Differential Equations*, 250(4):1967–2023, 2011.

[Gu86] J. C. Gu. Friction constitutive law with rate and state dependences. *Pure and Applied Geophysics*, 124(4-5):773–791, 1986.

[HA00] M. A. Heckl and I. D. Abrahams. Curve squeal of train wheels, Part 1: Mathematical model for its generation. *Journal of Sound and Vibration*, 229(3):669–693, 2000.

[Har04] R. A. Harris. Numerical Simulations of Large Earthquakes: Dynamic Rupture Propagation on Heterogeneous Faults. *Pure and Applied Geophysics*, 161(11–12):2171–2181, 2004.

[HB03] W. P. M. H. Heemels and B. Brogliato. The Complementarity Class of Hybrid Dynamical Systems. *European Journal of Control*, 9(2–3):322–360, 2003.

[HBP+94] F. Heslot, T. Baumberger, B. Perrin, B. Caroli, and C. Caroli. Creep, stick-slip and dry-friction dynamics: Experiments and a heuristic model. *Physical Review E*, 49(6):4973–4988, 1994.

[Hea90] T. H. Heaton. Evidence for and implications of self-healing pulses of slip in earthquake rupture. *Physics of the Earth and Planetary Interiors*, 64(1):1–20, 1990.

[Hol13] M. H. Holmes. *Introduction to Perturbation Methods*, volume 20 of *Texts in Applied Mathematics*. Springer-Verlag New York, 2013.

[HOP96] N. Hinrichs, M. Oestreich, and K. Popp. Experimental and numerical investigation of a friction oscillator. *ASME, Design Engineering Division*, 90:57–62, 1996.

[HOP98] N. Hinrichs, M. Oestreich, and K. Popp. On the modelling of friction oscillators. *Journal of Sound and Vibration*, 216(3):435–459, 1998.

[Ibr94] R. A. Ibrahim. Friction-Induced Vibration, Chatter, Squeal, and Chaos – Part II: Dynamics and Modeling. *Applied Mechanics Reviews*, 47(7):227–253, 1994.

[Jef14] M. R. Jeffrey. Hidden dynamics in models of discontinuity and switching. *Physica D: Nonlinear Phenomena*, 273–274:34–45, 2014.

[Jef15] M. R. Jeffrey. On the mathematical basis of solid friction. *Nonlinear Dynamics*, 81(4):1699–1716, 2015.

[Jon95] C. K. R. T. Jones. Geometric Singular Perturbation Theory. In R. Johnson, editor, *Dynamical Systems*, volume 1609 of *Lecture Notes in Mathematics*, pages 44–118. Springer, Berlin, Heidelberg, 1995.

[Kap99] T. J. Kaper. An Introduction to Geometric Methods and Dynamical Systems Theory for Singular Perturbation Problems. In *Proceedings of Symposia in Applied Mathematics*, volume 56, pages 85–132. American Mathematical Society, 1999.

[KH15a] K. U. Kristiansen and S. J. Hogan. On the Use of Blowup to Study Regularizations of Singularities of Piecewise Smooth Dynamical Systems in $\mathbb{R}^3$. *SIAM Journal on Applied Dynamical Systems*, 14(1):382–422, 2015.

[KH15b] K. U. Kristiansen and S. J. Hogan. Regularizations of Two-Fold Bifurcations in Planar Piecewise Smooth Systems Using Blowup. *SIAM Journal on Applied Dynamical Systems*, 14(4):1731–1786, 2015.

[Kos12] I. Kosiuk. *Relaxation oscillations in slow-fast systems beyond the standard form*. PhD thesis, University of Leipzig, 2012.

[KP08] P. Kowalczyk and P. T. Piiroinen. Two-parameter sliding bifurcations of periodic solutions in a dry-friction oscillator. *Physica D: Nonlinear Phenomena*, 237(8):1053–1073, 2008.

[KPK08] M. Krupa, N. Popović, and N. Kopell. Mixed-Mode Oscillations in Three Time-Scale Systems: A Prototypical Example. *SIAM Journal on Applied Dynamical Systems*, 7(2):361–420, 2008.

[KPKR08] M. Krupa, N. Popović, N. Kopell, and H. G. Rotstein. Mixed-Mode Oscillations in a Three Time-Scale Model for the Dopaminergic Neuron. *Chaos: An Interdisciplinary Journal of Nonlinear Science*, 18(1):015106, 2008.

[Kri17] K. U. Kristiansen. Blowup for flat slow manifolds. *Nonlinearity*, 30(5):2138–2184, 2017.

[KS01a] M. Krupa and P. Szmolyan. Extending Geometric Singular Perturbation Theory to Nonhyperbolic Points–Fold and Canard Points in Two Dimensions. *Siam Journal on Mathematical Analysis*, 33(2):286–314, 2001.

[KS01b] M. Krupa and P. Szmolyan. Extending Slow Manifolds near Transcritical and Pitchfork Singularities. *Nonlinearity*, 14(6):1473–1491, 2001.

[KS01c] M. Krupa and P. Szmolyan. Relaxation Oscillation and Canard Explosion. *Journal of Differential Equations*, 174(2):312–368, 2001.

[KS11] I. Kosiuk and P. Szmolyan. Scaling in Singular Perturbation Problems: Blowing Up a Relaxation Oscillator. *SIAM Journal on Applied Dynamical Systems*, 10(4):1307–1343, 2011.

[KS16] I. Kosiuk and P. Szmolyan. Geometric analysis of the Goldbeter minimal model for the embryonic cell cycle. *Journal of Mathematical Biology*, 72(5):1337–1368, 2016.

[Kue14] C. Kuehn. Normal hyperbolicity and unbounded critical manifolds. *Nonlinearity*, 27(6):1351–1366, 2014.

[Kue15] C. Kuehn. *Multiple Time Scale Dynamics*, volume 191 of *Applied Mathematical Sciences*. Springer International Publishing, 2015.

[KW10] M. Krupa and M. Wechselberger. Local analysis near a folded saddle-node singularity. *Journal of Differential Equations*, 248(12):2841–2888, 2010.

[LC14] G. Licskó and G. Csernák. On the chaotic behaviour of a simple dry-friction oscillator. *Mathematics and Computers in Simulation*, 95:55–62, 2014.

[LdST08] J. Llibre, P. R. da Silva, and M. A. Teixeira. Sliding Vector Fields via Slow-Fast Systems. *Bulletin of the Belgian Mathematical Society, Simon Stevin*, 15(5):851–869, 2008.

[LRBZZ00] N. Lapusta, J. R. Rice, Y. Ben-Zion, and G. Zheng. Elastodynamic analysis for slow tectonic loading with spontaneous rupture episodes on faults with rate-and-state dependent friction. *Journal of Geophysical Research*, 105(B10):23765–23789, 2000.

[LT97] J. Llibre and M. A. Teixeira. Regularization of discontinuous vector fields in dimension three. *Discrete and Continuous Dynamical Systems - Series A*, 3(2):235–241, 1997.

[Mad98] R. Madariaga. Complex Heterogeneous Faulting Models. Unpublished lecture notes. *Fourth Workshop on three dimensional modelling of seismic waves generation. Propagation and their inversion*, 1998.

[Mar98a] C. Marone. The effect of loading rate on static friction and the rate of fault healing during the earthquake cycle. *Nature*, 391(6662):69–72, 1998.

[Mar98b] C. Marone. Laboratory-derived friction laws and their application to seismic faulting. *Annual Review of Earth and Planetary Sciences*, 26:643–696, 1998.

[MC96] R. Madariaga and A. Cochard. Dynamic friction and the origin of the complexity of earthquake sources. *Proceedings of the National Academy of Sciences of the United States of America*, 93(9):3819–3824, 1996.

[Mei07] J. D. Meiss. *Differential Dynamical Systems*. Mathematical Modeling and Computation. SIAM, 2007.

[Moe06] J. Moehlis. Canards for a reduction of the Hodgkin-Huxley equations. *Journal of Mathematical Biology*, 52(2):141–153, 2006.

[MSLG98] A. Milik, P. Szmolyan, H. Loffelmann, and E. Groller. Geometry of Mixed-Mode Oscillations in the 3-D Autocatalator. *International Journal of Bifurcation and Chaos*, 8(3):505–519, 1998.

[MVE95] C. Marone, J. E. Vidale, and W. L. Ellsworth. Fault healing inferred from time dependent variations in source properties of repeating earthquakes. *Geophysical Research Letters*, 22(22):3095–3098, 1995.

[Nak01] M. Nakatani. Conceptual and physical clarification of rate and state friction: Frictional sliding as a thermally activated rheology. *Journal of Geophysical Research: Solid Earth*, 106(B7):13347–13380, 2001.

[NM99] R. M. Nadeau and T. V. McEvilly. Fault Slip Rates at Depth from Recurrence Intervals of Repeating Microearthquakes. *Science*, 285(5428):718–721, 1999.

[Nor91] A. B. Nordmark. Non-periodic motion caused by grazing incidence in an impact oscillator. *Journal of Sound and Vibration*, 145(2):279–297, 1991.

[OA01] H. Olsson and K. J. Åström. Friction Generated Limit Cycles. *IEEE Transactions on Control Systems Technology*, 9(4):629–636, 2001.

[OACdW+98] H. Olsson, K. J. Åström, C. Canudas de Wit, M. Gäfvert, and P. Lischinsky. Friction Models and Friction Compensation. *European Journal of Control*, 4(3):176–195, 1998.

[OHP96] M. Oestreich, N. Hinrichs, and K. Popp. Bifurcation and stability analysis for a non-smooth friction oscillator. *Archive of Applied Mechanics*, 66(5):301–314, 1996.

[PB11] Y. Pomeau and M. Le Berre. Critical speed-up vs critical slow-down: a new kind of relaxation oscillation with application to stick-slip phenomena. *ArXiv e-prints arXiv:1107.3331 [physics.geo-ph]*, 2011.

[PD15] T. Putelat and J. H. P. Dawes. Steady and transient sliding under rate-and-state friction. *Journal of the Mechanics and Physics of Solids*, 78:70–93, 2015.

[PDC17] T. Putelat, J. H. P. Dawes, and A. R. Champneys. A phase-plane analysis of localized frictional waves. *Proceedings of the Royal Society A*, 473(2203):20160606, 2017.

[PDW07] T. Putelat, J. H. P. Dawes, and J. R. Willis. Sliding modes of two interacting frictional interfaces. *Journal of the Mechanics and Physics of Solids*, 55(10):2073–2105, 2007.

[PDW10] T. Putelat, J. H. P. Dawes, and J. R. Willis. Regimes of frictional sliding of a spring-block system. *Journal of the Mechanics and Physics of Solids*, 58(1):27–53, 2010.

[PRSV16] E. Pennestrì, V. Rossi, P. Salvini, and P. P. Valentini. Review and comparison of dry friction force models. *Nonlinear Dynamics*, 83(4):1785–1801, 2016.

[PS90] K. Popp and P. Stelter. Stick-Slip Vibrations and Chaos. *Philosophical Transactions of the Royal Society A*, 332(1624):89–105, 1990.

[PW81] T. K. Pratt and R. Williams. Non-linear analysis of stick/slip motion. *Journal of Sound and Vibration*, 74(4):531–542, 1981.

[PWD08] T. Putelat, J. R. Willis, and J. H. P. Dawes. On the seismic cycle seen as a relaxation oscillation. *Philosophical Magazine*, 88(28–29):3219–3243, 2008.

[Rab51] E. Rabinowicz. The Nature of the Static and Kinetic Coefficients of Friction. *Journal of Applied Physics*, 22(11):1373–1379, 1951.

[RDKL11] J. Rankin, M. Desroches, B. Krauskopf, and M. Lowenberg. Canard cycles in aircraft ground dynamics. *Nonlinear Dynamics*, 66(4):681–688, 2011.

[RM13] A. P. Rathbun and C. Marone. Symmetry and the critical slip distance in rate and state friction laws. *Journal of Geophysical Research: Solid Earth*, 118(7):3728–3741, 2013.

[RR83] J. R. Rice and A. L. Ruina. Stability of Steady Frictional Slipping. *Journal of Applied Mechanics*, 50(2):343–349, 1983.

[RR99] K. Ranjith and J. R. Rice. Stability of quasi-static slip in a single degree of freedom elastic system with rate and state dependent friction. *Journal of the Mechanics and Physics of Solids*, 47(6):1207–1218, 1999.

[RT86] J. R. Rice and S. T. Tse. Dynamic motion of a single degree of freedom system following a rate and state dependent friction law. *Journal of Geophysical Research: Solid Earth*, 91(B1):521–530, 1986.

[Rui83] A. Ruina. Slip instability and state variable friction laws. *Journal of Geophysical Research: Solid Earth*, 88(B12):10359–10370, 1983.

[RW07] J. Rubin and M. Wechselberger. Giant squid-hidden canard: the 3D geometry of the Hodgkin-Huxley model. *Biological Cybernetics*, 97(1):5–32, 2007.

[Sch73] J. C. Schelleng. The bowed string and the player. *The Journal of the Acoustical Society of America*, 53(1):26–41, 1973.

[Sha86] S. W. Shaw. On the dynamic response of a system with dry friction. *Journal of Sound and Vibration*, 108(2):305–325, 1986.

[Shc05] E. Shchepakina. Canards and black swans in a model of a 3-D autocatalator. *Journal of Physics: Conference Series*, 22(1):194–207, 2005.

[Sho02] C. Sholtz. *The Mechanics of Earthquakes and Faulting*. Cambridge University Press, 2002.

[ST96] J. Sotomayor and M. A. Teixeira. Regularization of discontinuous vector fields. In *International Conference on Differential Equations (Lisboa)*, pages 207–223, 1996.

[Ste00] D. E. Stewart. Rigid-Body Dynamics with Friction and Impact. *SIAM Review*, 42(1):3–39, 2000.

[SW01] P. Szmolyan and M. Wechselberger. Canards in $\mathbb{R}^3$. *Journal of Differential Equations*, 177(2):419–453, 2001.

[SW04] P. Szmolyan and M. Wechselberger. Relaxation oscillations in $\mathbb{R}^3$. *Journal of Differential Equations*, 200(1):69–104, 2004.

[Tei93] M. A. Teixeira. Generic Bifurcation of Sliding Vector Fields. *Journal of Mathematical Analysis and Applications*, 176(2):436–457, 1993.

[VECM94] J. E. Vidale, W. L. Ellsworth, A. Cole, and C. Marone. Variations in rupture process with recurrence interval in a repeated small earthquake. *Nature*, 368(6472):624–626, 1994.

[vGKS05] S. van Gils, M. Krupa, and P. Szmolyan. Asymptotic expansions using blow-up. *Zeitschrift für angewandte Mathematik und Physik*, 56(3):369–397, 2005.

[VKK16] T. Vo, M. A. Kramer, and T. J. Kaper. Amplitude-Modulated Bursting: A Novel Class of Bursting Rhythms. *Physical Review Letters*, 117(26):268101, 2016.

[VW15] T. Vo and M. Wechselberger. Canards of Folded Saddle-Node Type I. *SIAM Journal on Mathematical Analysis*, 47(4):3235–3283, 2015.

[WALC11] S. Wieczorek, P. Ashwin, C. M. Luke, and P. M. Cox. Excitability in ramped systems: the compost-bomb instability. *Proceedings of the Royal Society A*, 467(2129):1243–1269, 2011.

[Wec12] M. Wechselberger. À propos de canards (Apropos canards). *Transactions of the American Mathematical Society*, 364(6):3289–3309, 2012.

[WPM15] J. Woodhouse, T. Putelat, and A. McKay. Are there reliable constitutive laws for dynamic friction? *Philosophical Transactions of the Royal Society A*, 373(2051):20140401, 2015.

[WSWK08] J. Wojewoda, A. Stefański, M. Wiercigroch, and T. Kapitaniak. Hysteretic effects of dry friction: modelling and experimental studies. *Philosophical Transactions of the Royal Society A*, 366(1866):747–765, 2008.

[ZN12] J. D. Zechar and R. M. Nadeau. Predictability of repeating earthquakes near Parkfield, California. *Geophysical Journal International*, 190(1):457–462, 2012.